

AD-A083 140

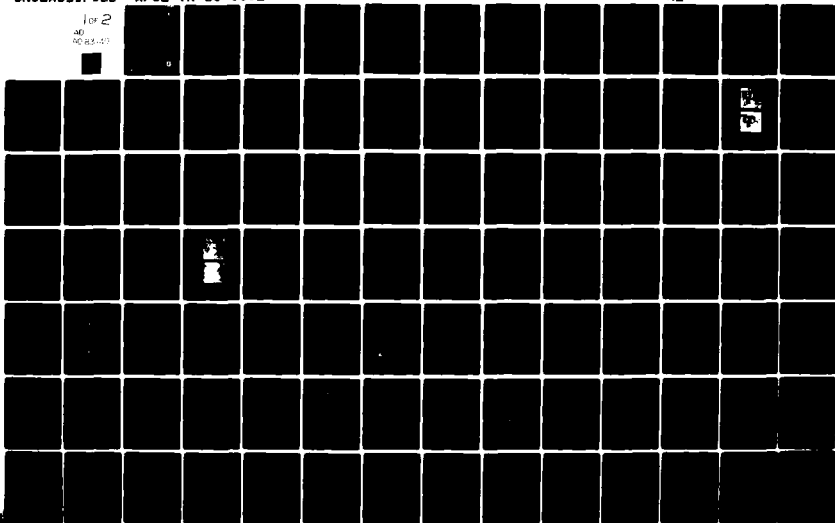
AIR FORCE GEOPHYSICS LAB HANSCOM AFB MA F/G 4/2  
MICROPHYSICAL PROPERTIES OF A LARGE SCALE CLOUD SYSTEM, 1-3 MAR--ETC(U)  
JAN 80 D J VARLEY

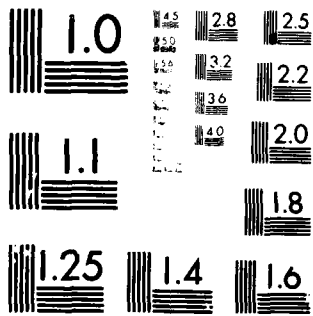
UNCLASSIFIED

AFGL-TR-80-0002

NL

for 2  
30  
40 85-97





MICROCOPY RESOLUTION TEST CHART  
 NATIONAL BUREAU OF STANDARDS-1963-A

ADA 0831 40

AFGL-TR-80-0002  
ENVIRONMENTAL RESEARCH PAPERS, NO. 000

12  
B.S.

LEVEL



**Microphysical Properties of a Large  
Scale Cloud System, 1-3 March 1978**

**DONALD J. VARLEY, Lt Col, USAF**

7 January 1980

Approved for public release; distribution unlimited.

DTIC  
ELECTE  
APR 17 1980

A

METEOROLOGY DIVISION PROJECT 2310  
**AIR FORCE GEOPHYSICS LABORATORY**  
HANSCOM AFB, MASSACHUSETTS 01731

**AIR FORCE SYSTEMS COMMAND, USAF**



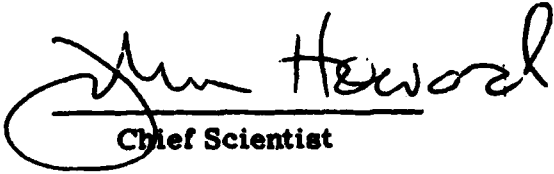
DDC FILE COPY

80 4 17 0 19

This report has been reviewed by the ESD Information Office (OI) and is releasable to the National Technical Information Service (NTIS).

This technical report has been reviewed and is approved for publication.

FOR THE COMMANDER

  
Chief Scientist

Qualified requestors may obtain additional copies from the Defense Documentation Center. All others should apply to the National Technical Information Service.

Accession For	
NTIS G&I	<input checked="" type="checkbox"/>
DDC TAB	<input type="checkbox"/>
Unannounced	
Justification	
By _____	
Distribution/	
Availability Codes	
Dist	Avail and/or special
A	

Unclassified

SECURITY CLASSIFICATION OF THIS PAGE (When Data Entered)

REPORT DOCUMENTATION PAGE		READ INSTRUCTIONS BEFORE COMPLETING FORM
1. REPORT NUMBER 14 AFGL-TR-80-0002, AFGL-ERP-690	2. GOVT ACCESSION NO.	3. RECIPIENT'S CATALOG NUMBER
4. TITLE (and Subtitle) 6 MICROPHYSICAL PROPERTIES OF A LARGE SCALE CLOUD SYSTEM, 1-3 MARCH 1978	5. TYPE OF REPORT & PERIOD COVERED Scientific. Interim.	
7. AUTHOR(s) 10 Donald J. Varley, Lt Col, USAF	6. PERFORMING ORG. REPORT NUMBER ERP No. 690	
9. PERFORMING ORGANIZATION NAME AND ADDRESS Air Force Geophysics Laboratory (LYC) Hanscom AFB Massachusetts 01731	10. PROGRAM ELEMENT, PROJECT, TASK AREA & WORK UNIT NUMBERS 61102F 23100501 17 G5	
11. CONTROLLING OFFICE NAME AND ADDRESS Air Force Geophysics Laboratory (LYC) Hanscom AFB Massachusetts 01731	12. REPORT DATE 7 January 1980	
14. MONITORING AGENCY NAME & ADDRESS (if different from Controlling Office) 12 101	13. NUMBER OF PAGES 100	
	15. SECURITY CLASS. (of this report) Unclassified	
16. DISTRIBUTION STATEMENT (of this Report) Approved for public release; distribution unlimited. 9 Environmental research papers		
17. DISTRIBUTION STATEMENT (of the abstract entered in Block 20, if different from Report)		
18. SUPPLEMENTARY NOTES		
19. KEY WORDS (Continue on reverse side if necessary and identify by block number) Cloud microphysics Cloud particle spectra Liquid water content Ice water content		
20. ABSTRACT (Continue on reverse side if necessary and identify by block number) This report describes the microphysical properties observed by a specially instrumented C-130 while flying in portions of a large cloud system on 3 successive days in March 1978. Each of the flights was made slightly east of an upper level trough as it moved across the U.S. Horizontal sampling passes of 50 to 100 nm (93 to 186 km) in length were made at various levels from approximately 2 to 9 km above ground in portions of the cloud system that were relatively homogeneous horizontally and vertically. Particle spectra data from		

DD FORM 1473 1 JAN 73 EDITION OF 1 NOV 65 IS OBSOLETE

Unclassified

SECURITY CLASSIFICATION OF THIS PAGE (When Data Entered)

409578

JP

## 20. Abstract (Continued)

PMS 1-D spectrometers were averaged for consecutive 20-sec periods. On each of the 3 days the particles having the smallest mean size were observed at the highest levels flown and had median diameters near  $100 \mu\text{m}$ . The calculated equivalent liquid water content from 7 to 9 km was near  $0.01 \text{ g m}^{-3}$ . The total particle count was between 8,000 and 18,000  $\text{m}^{-3}$  over Arkansas and coastal Delaware, but was near 25,000  $\text{m}^{-3}$  over the mountains of New Mexico. Values of mass and particle size increased with particle distance fallen, indicating growth by collective means. The largest equivalent liquid water content values were near  $1 \text{ g m}^{-3}$  and were recorded in the large snow just above the freezing level. The form factor, a mathematical parameter, was found useful in studying particle spectra. Certain maxima and minima observed in several plotted spectra, especially those from 7-km altitude data, are suggested as being due to an aggregation mechanism.

## Preface

This report is the culmination of efforts by many individuals to acquire, process and present the best and most accurate data possible on the microphysical characteristics found in a portion of a large winter storm. The aid of the pilots and crews of the 4950th Test Wing at Wright-Patterson AFB who flew the MC-130E aircraft, instrumented by AFGL, was particularly noteworthy. The AFGL personnel who flew the 3 mission days described here were Captain Leandro Delgado, mission director; SMSgt Thomas Moraski and MSgt Stephen Crist, equipment technicians; and Mr. Anthony Matthews, engineer. These individuals worked closely with the aircraft crew to help insure that sampling was performed in cloud-rich locations, and that the many pieces of instrumentation functioned optimally. Other assistance in determining sampling locations came from Mr. Robert Myers, Mr. John Powers and Dr. Arnold Barnes who interpreted satellite data from AFGL's McIDAS (Man-Computer Interactive Data Access System). Several helpful suggestions on report content were made by Dr. Barnes, Dr. Robert Cunningham and Mr. Vernon Plank. The assistance of Mr. Michael Francis and Mr. James Lally, both of Digital Programming Services, Incorporated, was invaluable in developing necessary computer programs and in processing the large volume of cloud data available. The aid of Mrs. Patricia Sheehy and Ms. Barbara Main in preparing the manuscript was also indispensable and is greatly appreciated.

## Contents

1. INTRODUCTION	9
2. RELATED STUDIES	10
3. DATA CALCULATIONS	14
3.1 Cloud Mass	14
3.2 Form Factor	16
3.3 $N_0$ and $\Lambda$	17
3.4 Departure of Cloud Probe Data from Calculated Slope	18
3.5 Data Presentation Format	19
4. WEATHER AND FLIGHT DATA - 1 MARCH 1978	21
4.1 Synoptic Situation	21
4.2 The Flight	25
4.3 Sampling Data: 1 March	27
4.3.1 Temporal Variations During Flight	27
4.3.2 Class Values of Data From Four Passes	31
4.3.3 Observed Particle Distributions	34
5. WEATHER AND FLIGHT DATA - 2 MARCH 1978	41
5.1 Synoptic Situation	41
5.2 The Flight	45
5.3 Sampling Data: 2 March	47
5.3.1 Temporal Variations During Flight	47
5.3.2 Class Values of Data From Three Passes	49
5.3.3 Observed Particle Distributions	51
6. WEATHER AND FLIGHT DATA - 3 MARCH 1978	56
6.1 Synoptic Situation	56
6.2 The Flight	59
6.3 Sampling Data: 3 March	64

## Contents

6.3.1 Temporal Variations During Flight	64
6.3.2 Class Values of Data From Six Passes	66
6.3.3 Observed Particle Distributions	68
7. FURTHER OBSERVATIONS	77
7.1 Particle Concentration	77
7.2 Median Diameter and Form Factor	79
7.3 Liquid Water Content	80
7.4 Maxima and Minima in Particle Spectra	81
7.5 Suppressed and Enhanced Spectra	83
7.6 Reflectivity Values	85
8. SUMMARY	86
REFERENCES	89
APPENDIX A: Mission Director Comments (1 March 1978)	93
APPENDIX B: Mission Director Comments (2 March 1978)	95
APPENDIX C: Mission Director Comments (3 March 1978)	97
APPENDIX D: List of Abbreviations	99

## Illustrations

1. Schematic Examples of Heavy and Light Precipitation Spectra	13
2. Schematic Views of Representative Spectra and Their Approximate Form Factor Values	17
3. Sample and Explanation of Data Format	20
4. Synoptic Weather Charts for Approximate Time of 1 March Flight	22
5. Satellite Visible (a) and Infrared (b) Photos of Western U.S. and Mexico at 1815Z 1 March 1978	24
6. Albuquerque, NM, Sounding Data for Times Prior to and After Data Flight	25
7. Generalized View of Clouds Along Sampling Tracks on 1 March 1978	26
8. Variation With Time During 1 March 1978 Flight of Several Measured and Calculated Elements Based on Values of Consecutive 20-Second Averages	28
9. Percent Frequency By Class of Six Measured or Calculated Variables Based on Total Number of 20-sec Mean Values During Each Pass on 1 March 1978	32

## Illustrations

10. Representative Cloud Data for 11, 000 ft (3.3 km) MSL Sample on 1 March 1978	35
11. Representative Cloud Data for 19, 000 ft (5.8 km) MSL Sample on 1 March 1978	37
12. Representative Cloud Data for 25, 000 ft (7.7 km) MSL Sample on 1 March 1978	39
13. Representative Cloud Data for 29, 000 ft (9.0 km) MSL Sample on 1 March 1978	40
14. Synoptic Weather Charts for Approximate Time of 2 March Flight	42
15. Satellite Visible (a) and Infrared (b) Photos of South-Central U.S. about 1800Z 2 March 1978	43
16. Little Rock, Arkansas, Sounding Data for Times Just Prior to and After Data Flight	44
17. Generalized View of Clouds Along Sampling Tracks on 2 March 1978	45
18. Variation With Time During 2 March 1978 Flight of Several Measured and Calculated Elements Based on Values of Consecutive 20-Second Averages	48
19. Percent Frequency by Class of Six Measured or Calculated Variables on 2 March 1978 Based on Total Number of 20-sec Mean Values in Overall Pass	50
20. Representative Cloud Data for 5, 000 ft (1.5 km) MSL Samples on 2 March 1978	52
21. Representative Cloud Data for Light Precipitation Portion of 10, 000 ft (3.0 km) MSL Pass on 2 March 1978	54
22. Representative Cloud Data for Heavy Precipitation Portion of 10, 000 ft (3.0 km) MSL Pass on 2 March 1978	55
23. Representative Cloud Data for 25, 000 ft (7.7 km) MSL Sample on 2 March 1978	57
24. Synoptic Weather Charts for Approximate Time of 3 March Flight	58
25. GOES-East Satellite Visible (a) and Infrared (b) Photos of East Coast of U.S. on 3 March 1978	60
26. Wallops Island, Virginia, Soundings for Times Prior to and After 3 March Sampling Flight	61
27. Generalized View of Clouds and Sampling Tracks on 3 March 1978	61
28. Variation With Time During 3 March 1978 Flight of Several Measured and Calculated Elements Based on Values of Consecutive 20-Second Averages	63
29. Percent Frequency by Class of Six Measured or Calculated Variables, 3 March 1978 Based on Total Number of 20-sec Mean Values in Overall Pass	67

## Illustrations

30. Representative Cloud Data for 25,000 ft (7.7 km) MSL, Sampling Pass on 3 March 1978	69
31. Representative Cloud Data for 23,500 ft. (7.2 km) MSL Sampling Pass on 3 March 1978	71
32. Representative Cloud Data for Large LWC Pass at 18,500 ft (5.6 km) MSL on 3 March 1978	72
33. Representative Cloud Data for Small LWC Pass at 18,500 ft (5.6 km) MSL on 3 March 1978	73
34. Representative Cloud Data for Large LWC Pass at 9,800 ft (2.9 km) MSL on 3 March 1978	75
35. Representative Cloud Data for Small LWC Pass at 9,800 ft (2.9 km) MSL on 3 March 1978	76
36. Mean Pass Values of NT (Particle Number Total) as Function of Temperature	77
37. Mean Pass Values of Median Volume Diameter as Function of Temperature	79
38. Mean Pass Values of Form Factor as Function of Temperature	79
39. Mean Pass Values of Liquid Water Content as Function of Temperature	80
40. Suggested Changes of Particle Spectra with Temperature Due to Aggregation in Large Cloud Systems	82
41. Generalized Examples of Enhanced (a) and Suppressed (b) Particle Distributions	83
42. Four 1 March Spectra for 100-sec Periods Replotted From Figures 10 to 13	84
43. Values of N-Axis Intercept vs Temperature for 14 Data Figures in This Report	85

## Tables

1. Values Used to Obtain Adjusted Channel Number	15
2. Values Used to Obtain Equivalent Melted Diameter	15
3. Predominant Particle Types During Periods Indicated on 1 March	29
4. Sampling Passes - 1 March	31
5. Predominant Particle Types During Periods Indicated on 2 March	47
6. Sampling Passes - 2 March	51
7. Predominant Particle Types During Periods Indicated on 3 March	65
8. Sampling Passes - 3 March	66

## Microphysical Properties of a Large Scale Cloud System, 1-3 March 1978

### 1. INTRODUCTION

The purpose of this report is to describe the particle distributions and other microphysical properties observed by an instrumented C-130 aircraft that flew in portions of a large cloud system on 3 successive days, 1, 2 and 3 March 1978.

During this time the storm and the airplane moved from New Mexico to coastal Delaware. While changes in synoptic conditions and storm dynamics were anticipated before the flight program, the main emphasis in the current work was to obtain data on "typical" cloud particle number, size and size range in large cloud systems. Increased knowledge of such systems will help to better determine their composition and will contribute information needed to better forecast their meteorological consequences.

Previous airborne examinations have been made of the nature of particulates in frontal systems and clouds of rather limited horizontal extent, but less study has been devoted to the distribution of ice particles and water droplets found in more extensive cloud systems.

---

(Received for publication 7 January 1980)

## 2. RELATED STUDIES

Work somewhat similar to that to be described has been done in the University of Washington's Cyclonic Extratropical Storms (CYCLES) program. The CYCLES program primarily has concentrated on storms passing by or through the Pacific Northwest while the present study has examined portions of a storm as it crossed the United States. Several papers have described results of the CYCLES study, and an overview of the program that examined storms over the Pacific Northwest has been given by Hobbs.<sup>1</sup>

In their study of rainbands in an occluded frontal system Houze et al<sup>2</sup> found that vapor deposition caused rapid growth of particles as they settled below the convective layer. This growth of the particles continued just above the melting layer and was a result of riming and aggregation. Their finding of very little precipitation growth below the melting layer was previously mentioned by Harper,<sup>3</sup> Hardy<sup>4</sup> and Ohtake<sup>5, 6</sup> among others. On the other hand, Cunningham<sup>7</sup> found that in certain portions of storms, considerable growth occurs in lower cloud layers. Ohtake<sup>6</sup> has pointed out that the size distribution of raindrops is often dependent on the size distribution of the precursor snow flakes or ice crystals above the melting layer. The distributions of these hydrometeors are in turn controlled by the temperature, ice nuclei and humidity at levels higher aloft.

Marwitz and Stewart<sup>8</sup> found that atmospheric stability was one of the determinants of droplet-size distribution and particle habit. In convection, distributions were frequently bimodal with peaks near 5 and 30  $\mu\text{m}$  while stable conditions resulted

1. Hobbs, P. V. (1978) The University of Washington's CYCLES Project: An Overview, Preprints of Conference on Cloud Physics and Atmospheric Electricity, Issaquah, WA, 271-276.
2. Houze, R. A. Jr., Locatelli, J. D. and Hobbs, P. V. (1976) Dynamics and cloud microphysics of the rainbands in an occluded frontal system, J. of Atmos. Sci. 33:1921-1936.
3. Harper, W. G. (1957) Variation with height of rainfall below the melting level, Quart. J. Roy. Meteor. Soc. 83:368-371.
4. Hardy, K. R. (1963) The development of raindrop-size distributions and implications related to the physics of precipitation, J. of Atmos. Sci. 20:299-312.
5. Ohtake, T. (1969) Observations of size distributions of hydrometeors through the melting layer, J. of Atmos. Sci. 26:545-557.
6. Ohtake, T. (1970) Factors affecting the size distribution of raindrops and snowflakes, J. of Atmos. Sci. 27:804-813.
7. Cunningham, R. M. (1952) The Distribution and Growth of Hydrometeors Around a Deep Cyclone. Ph. D Thesis, Mass. Institute of Techn., pp 59. Also M. I. T. Dept. of Meteor. Tech. Report No. 18.
8. Marwitz, J. D. and Stewart, R. E. (1978) Dynamical and microphysical characteristics of winter storms over the Sierra Nevadas, Preprints of Conf. on Cloud Physics and Atmospheric Electr., Issaquah, WA, 244-246.

in a single maximum near 10  $\mu\text{m}$ . Instability produced rimed crystals, and sometimes aggregates and graupel, while stable air resulted in less riming and more dendrites. These results are generally in accord with other measurements in mountainous areas by Lamb et al,<sup>9</sup> Hobbs<sup>10</sup> and Marwitz.<sup>11</sup> In Switzerland, Waldvogel<sup>12</sup> reported large-drop spectra during stable conditions, and graupel or a small-drop spectrum when the atmosphere was unstable.

Browning<sup>13</sup> has similarly pointed out the importance of stability in the atmosphere in his study of rain systems over the British Isles. He believes that the main regions of potential instability are generated at the surface cold front. This instability is realized when convective lifting occurs over the frontal surface.

As discussed by Hobbs and Locatelli<sup>14</sup> cirrus uncinus, or "mares tales," have been thought for some time to be generating cells of ice crystals. Plank et al<sup>15</sup> were among the first to suggest that generating cells might be important in the development of stratiform precipitation. In aircraft experiments Braham<sup>16</sup> observed the development of a major precipitation system due to ice fallout from cirrus. He believed the cirrus provided sufficient crystals to ice-out the super-cooled middle cloud. The released heat of fusion then enhances the convective motions and provides a stimulus for organizing the instability over wider areas. Contrails may also have the capability of seeding lower clouds since Knollenberg<sup>17</sup> found particle concentrations and mass in contrails are similar to those in natural cirrus.

9. Lamb, D., Nielson, K.W., Klieforth, H.E. and Hallett, J. (1976) Measurements of liquid water content in winter cloud systems over the Sierra Nevada, J. Appl. Meteor. 15:763-775.
10. Hobbs, P.V. (1975) The nature of winter clouds and precipitation in the Cascade Mountains and their modification by artificial seeding. Part 1: Natural conditions, J. Meteor. 14:783-804.
11. Marwitz, J.D. (1974) An airflow case study over the San Juan Mountains of Colorado, J. of Meteor. 13:450-458.
12. Waldvogel, A. (1974) The  $N_o$  jump of raindrop spectra, J. of Atmos. Sci. 31:1067-1078.
13. Browning, K.A. (1974) Mesoscale structure of rain systems in the British Isles, J. of Meteor. Soc. Japan 52:314-327.
14. Hobbs, P.V. and Locatelli, J.D. (1978) Rainbands, precipitation cores and generating cells in a cyclonic storm, Jour. Atmos. Sci. 35:230-241.
15. Plank, V.G., Atlas, D. and Paulsen, W.H. (1955) The nature and detectability of clouds and precipitation as determined by 1.25 cm radar, J. Meteor. 12:358-377.
16. Braham, R.R. Jr. (1967) Cirrus cloud seeding as a trigger for storm development, J. Atmos. Sci. 24:311-312.
17. Knollenberg, R.G. (1972) Measurements of the growth of the ice budget in a persisting contrail, J. Atmos. Sci. 29:1367-1374.

Much has been written during the last several years on the subject of ice and droplet distributions by size. For droplets larger than about 1 mm Marshall and Palmer<sup>18</sup> approximated a rain droplet number-size relationship using an exponential function of the form

$$N_D = N_0 e^{-\Lambda D} \quad (1)$$

where  $N_D$  represents the number of drops per millimeter-diameter interval and per cubic meter of air,  $N_0$  is the N-axis intercept and  $\Lambda$  is a parameter depending on the rainfall rate. Marshall and Palmer considered  $N_0$  to be a constant; however, it was soon realized it varies considerably according to rain type.

Gunn and Marshall<sup>19</sup> found the snowflake number-size relationship to also be an exponential of the same form as Eq. (1); however, they stipulated that size values be those of melted flakes or crystals. Since then several investigators, including Douglas,<sup>20</sup> Smith et al<sup>21</sup> and Houze et al,<sup>22</sup> have also implicitly or explicitly assumed the size distribution of frozen crystals or snowflakes is approximated by an exponential line.

Knowledge of  $N_0$  and  $\Lambda$  values of given particle spectra is useful in determining the intensity and size of typical particles. A very generalized view of the  $N_0$  and  $\Lambda$  during heavy and light periods of precipitation is given in Figure 1.

When the precipitation is mostly rain, Hardy<sup>23</sup> has indicated the light precipitation case in Figure 1 is often affected by considerable evaporation. Strong evaporation is probably common in spectra obtained in tropical locations. Blanchard<sup>24</sup> found very few drops larger than 2 mm in Hawaiian rains, although concentrations of drops less than 0.5 mm were often in excess of 40,000/m<sup>3</sup>.

18. Marshall, J.S. and Palmer, W. McK. (1948) The distribution of raindrops with size, J. Meteor. 5:165-166.
19. Gunn, K.L.S. and Marshall, J.S. (1958) The distribution with size of aggregate snowflakes, J. of Meteor. 15:452-461.
20. Douglas, R.H. (1964) Hail size distribution, Preprints of World Conf on Radio Meteor. and Eleventh Weath. Radar Conf., Boulder, CO, 147-149.
21. Smith, P.L. Jr., Musil, D.J., Weber, S.F., Spahn, J.F., Johnson, G.N., and Sand, W.R. (1967) Raindrop and hailstone size distributions inside hailstorms, Preprints Intnatl. Conf. on Cld. Physics, Boulder, CO, 252-257.
22. Houze, R.A. Jr., Hobbs, P.V., Herzegh, P.H., and Parsons, D.B. (1979) Size distributions of precipitation particles in frontal clouds, J. Atmos. Sci. 36:156-162.
23. Hardy, K.R. (1963) The development of raindrop-size distributions and implications related to the physics of precipitation, J. Atmos. Sci. 20:299-312.
24. Blanchard, D.C. (1953) Raindrop size distributions in Hawaiian rains. J. of Meteor. 10:457-473.

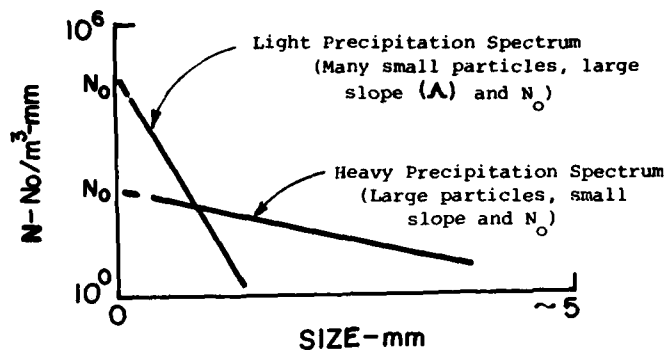


Figure 1. Schematic Examples of Heavy and Light Precipitation Spectra

The heavy precipitation slope in Figure 1 is most common in or near clouds having many and large ice crystals and/or snowflakes. At cirrus levels, however, where most ice crystals are smaller than 2 mm, Varley and Barnes<sup>25</sup> found the light precipitation slope in Figure 1 to be approximately representative.

Joss et al<sup>26</sup> could find no characteristic development of  $N_0$  and  $\Lambda$  values over short intervals during extended periods of rain. After an hour or more of droplet data had been obtained, however, they found the overall spectrum to be very close to an exponential distribution. The  $N_0$  just prior to a cold front passage was calculated by Waldvogel and Joss<sup>27</sup> to be 6887 while during the frontal passage 16, 220, and afterward, 3, 300.

In a multicell storm in Switzerland, Federer and Waldvogel<sup>28</sup> found the total liquid water content was due to equal contributions of rain and hail and that it totaled  $5 \text{ g/m}^3$  or less. The size-distribution curve appeared to be in two parts: the smaller rain drops had a steep curve while the portion due to hail was much flatter.

25. Varley, D.J. and Barnes, A.A. Jr. (1979) Cirrus Particle Distribution Study, Part 4, Air Force Geophysics Lab TR-79-0134, Air Force Surveys in Geophysics, No. 413, 91 pp.
26. Joss, J., Thams, J.C. and Waldvogel, A. (1968) The variation of raindrop size distributions at Locarno, Proceedings Intnatl. Conf. on Cld. Phy., Toronto, Ontario, 369-373.
27. Waldvogel, A. and Joss, J. (1970) The influence of a cold front on the drop size distribution, Preprints Conf. on Cld. Physics, Ft Collins, Amer. Meteor. Soc., 195-196.
28. Federer, B. and Waldvogel, A. (1975) Hail and raindrop size distributions from a Swiss multicell storm, J. Appl. Meteor. 14:91-97.

### 3. DATA CALCULATIONS

Before presenting the data obtained in our specialized sampling flights it is useful to discuss some AFGL processing techniques so that the results may be more understandable and meaningful.

#### 3.1 Cloud Mass

One of the most useful physical values in the study of clouds is their mass or water content. In this report the terms "water content" and "liquid water content" will apply to information obtained from ice and snow particles as well as from rain or cloud droplets. Our method of determining mass involves first a determination of particle-equivalent melted diameters (assuming an original frozen state) and then the use of simple equations to calculate total liquid water content (LWC). The calculation of equivalent melted diameter using PMS spectrometer particle size-number data is a three-step procedure.

The first step, spectrometer channel number adjustment, is a function of particle type and channel number. A study of the corrections needed to convert from recorded channel (diode) number to maximum particle size was supported by AFGL and made by Knollenberg.<sup>29</sup>

As described by Cunningham<sup>30</sup> the adjusted channel number is given by

$$\text{adj ch. no. (H)} = M \times \text{indicated ch no.} + B.$$

The AFGL values of M (slope) and B (intercept) for some types of particles are given in Table 1.

The second step in determining equivalent melted-particle sizes involves a determination of their actual physical size (L). This is found by multiplying values derived from the first step by the spectrometer probe diode width:

$$\text{physical size (L)} = (\text{adjusted ch no. (H)}) \times (\text{probe diode width})$$

Finally, the equivalent melted diameter of each channel for each probe is given by

$$\text{diameter (D)} = a \cdot L^b \text{ (mm)}$$

29. Knollenberg, R. G. (1975) The response of optical array spectrometers to ice and snow: A study of probe size to crystal mass relations, AFCRL-TR-75-0494. Air Force Cambridge Research Laboratories, 69 pp.

30. Cunningham, R. M. (1978) Analysis of particle spectral data from optical array (PMS) 1-D and 2-D sensors, Preprints of Fourth Symposium on Meteorological Observations and Instrumentation. Amer. Meteor. Soc., 345-350. Also, AFGL-TR-78-0102.

where the values of a and b (after Cunningham<sup>30</sup>) for the particle types in Table 1 are given in Table 2.

Table 1. Values Used to Obtain Adjusted Channel Number

Particle Type	M	B	Breakpoint (L) (mm)
Rain	0.990	0.180	
Wet Snow	0.990	0.180	LE 2
Wet Snow	1.150	0.180	GT 2
Large Snow	1.150	0.180	
Small Snow	1.150	0.180	
Bullet Rosettes	1.018	0.318	
Columns	1.302	0.761	
Needles	0.200	3.040	LE 1
Needles	1.280	1.080	GT 1

Table 2. Values Used to Obtain Equivalent Melted Diameter

Particle Type	a	b	Breakpoint (mm)
Rain	1.00	1.00	
Wet Snow	1.00	1.00	LE 1.0 mm
Wet Snow	1.00	0.653	GT 1.0 mm
Large Snow	0.40	0.782	
Small Snow	0.40	0.782	LE 0.5 mm
Small Snow	0.37	0.670	GT 0.5 mm
Bullet Rosettes	0.256	0.667	LE 0.2 mm
Bullet Rosettes	0.438	1.000	GT 0.2 mm
Columns	0.438	1.000	
Needles	0.256	0.670	

Once particle-equivalent melted diameters are known the LWC is easily determined when density is assumed to be  $1 \text{ g cm}^{-3}$ .

The 1-D precipitation probe measured particles in 15 size classes, the largest of which was about  $5300 \mu\text{m}$  (depending on particle type). In some cases of extremely heavy precipitation, which we believe are few, particle-size spectra will be

truncated at the large-size end. A capability of determining the number of particles exceeding the size of the fifteenth channel has recently been developed, but this was not available at the time of the three flights discussed in this report.

### 3.2 Form Factor

Another calculated variable that has proven useful in studying particle spectra is the "form factor" described by Plank<sup>31</sup> and Plank and Barnes.<sup>32</sup>

The form factor (FF) essentially describes in a decimal number between 0 and 1 the manner in which the concentrations of the particles in the different diameter classes are apportioned relative to each other and to the total number concentration value of a given sample. The FF is a bi-product of AFGL PMS 1-D data processing and, as experience has been gained in its use, it has enabled analysts to obtain a rough mental view of the particle spectrum without plotting.

Plank<sup>31</sup> defines the form factor mathematically as

$$FF = \frac{\sum_{i=2}^{i=n} (2i - 1)^3 \alpha_i}{\left[ \sum_{i=2}^{i=n} (2i - 1)^6 \alpha_i \right]^{0.5}} \quad (2)$$

where  $i$  is the specific channel of data being considered (from 2 to 15 for the PMS cloud probe and from 1 to 15 for the precipitation probe) and  $\alpha_i$  is the ratio of the number of particles in channel  $i$  to the total number of particles in all channels (for sizes from  $\sim 50$  to  $5300 \mu\text{m}$ ).

In the early use of the form factor with limited data, Plank and Barnes<sup>32</sup> believed that values below 0.20 would be very rare. With more and varied data, however, it has been found that spectra represented by FFs less than 0.10 are not unusual, particularly in very moist low-level clouds.

Figure 2 shows schematic and generalized views of spectra frequently observed in this study and their approximate form factors.

Experience indicates that spectra most closely approaching exponential distributions are represented by form factors between approximately 0.25 and 0.35. Plank has shown FF values for such distributions will never be smaller than 0.22.

As previously indicated, the form factor depends on the relative concentrations of various size classes to each other. Since these factors change almost continually

31. Plank, V.G. (1977) Hydrometeor Data and Analytical-Theoretical Investigations Pertaining to the SAMS Rain Erosion Program of the 1972-73 Season at Wallops Island, Virginia, Air Force Geophysics Laboratory TR-77-0149, pp 239.

32. Plank, V.G. and Barnes, A.A. Jr. (1978) An improvement in obtaining real-time water content values from radar reflectivity, Preprints of 18th Conf. Radar Meteor., Atlanta, Amer. Meteor. Soc., 426-431.

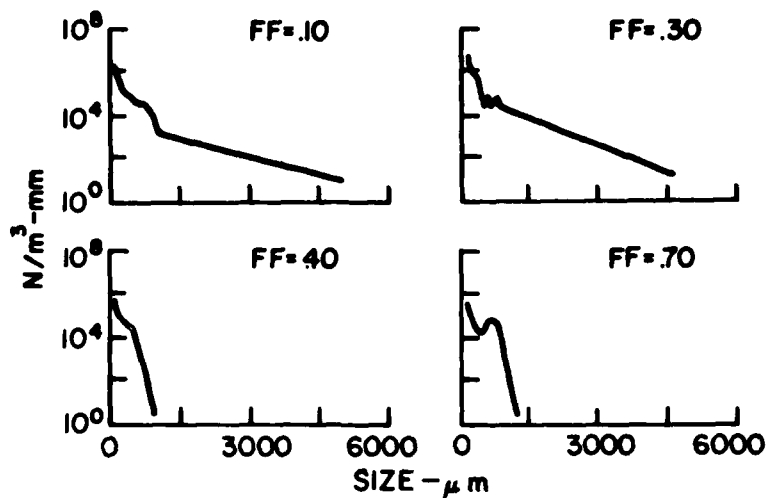


Figure 2. Schematic Views of Representative Spectra and Their Approximate Form Factor Values

during sampling through a cloud the resulting spectra also change. However, while two or more different spectra may have the same form factor, the general resemblance of their shapes is ordinarily very close. This subject and the possibility of ambiguity in a form factor will be further discussed in Section 7.

In this report calculations of form factor and total particle counts per  $m^3$  are based on measurements made over the approximate 50 to 5300  $\mu m$  range observed by the PMS cloud and precipitation probes.

### 3.3 $N_0$ and $\Lambda$

As previously indicated, the early work of Marshall and Palmer, Gunn and Marshall and others found the size distribution of raindrops and ice crystals of precipitable size can be reasonably described by a distribution function of exponential type. In this relation,  $N_0$ , the N-axis intercept, and  $\Lambda$ , the slope function, vary according to the type and category of hydrometeors being considered.

In this report values of  $N_0$  and  $\Lambda$  have been computed for specified sampling times based on particle data in the precipitation-probe range. Specifically, the slope is based on a best-fit straight line using the second and all higher channel data in the precipitation probe, but excluding data from channels where the number concentration is computed to be less than  $10 m^{-3} mm^{-1}$ . Thus, only particle sizes greater than approximately 650  $\mu m$  (depending on particle type) were considered in the slope computation. If sufficient numbers of particles did not extend

to at least the fifth channel (approximately 1780  $\mu\text{m}$ ) then neither a slope nor  $N_0$  was calculated.

The 650  $\mu\text{m}$  lower value, upon which the slope is based, was determined from experience that has shown exponential straight-line decreases (on log-linear plots) in number density from approximately that point to larger sizes are common. For particle sizes smaller than  $\sim 650 \mu\text{m}$  the departure from exponential distributions is often significant.

The spectra of particle data in the figures similar to Figure 3 that follow are plotted using a base 10 logarithm scale for the y-axis, although slope calculations must be based on "natural" log scales. When manually checking the computed slope figures on the forms similar to Figure 3 it is necessary to multiply y-axis differences over a specified x-axis distance by 2.30. This is a factor that converts base 10 logarithms to natural logarithms, which are required by Eq. (1).

The goodness-of-fit of the calculated best-fit straight-line slope to the actual data has been addressed by Smith and Laco.<sup>33</sup> They failed to prove the hypothesis that precipitation particles follow an exponential distribution, but they found the coefficient of determination,  $r^2$ , a reasonably good measure of the goodness-of-fit of the calculated slope to the initial data from which it was derived. A perfect fit of the derived slope to the initial data would result in an  $r^2$  score of 1. Most of the actual values in this report were slightly greater than 0.90 reflecting generally good fits. Houze et al<sup>22</sup> used a similar measure, the correlation coefficient,  $r$ , in determining goodness-of-fit of the calculated slope values. Their values, as would be expected, were slightly higher.

In subsequent pages where data are presented the values of coefficient of determination are under the heading "C.O.D.". These are not calculated when data are insufficient to calculate  $N_0$  and  $\Lambda$ .

#### 3.4 Departure of Cloud Probe Data from Calculated Slope

The portion of the particle spectrum in the cloud probe range (25-350  $\mu\text{m}$ ) and even larger sizes frequently departs from an extrapolated extension of the slope derived from the precipitation probe data. Such departures do not occur where the distribution is exponential through very small particle sizes, however, this is rarely the case. Houze et al<sup>22</sup> have used the terms "enhanced" and "suppressed" for distributions that depart in the smallest sizes toward greater or lesser concentrations, respectively, than what would be expected from an extension of the slope line to  $N_0$ . These distributions will be further discussed in Section 7.5.

33. Smith, P. L. Jr. and Laco, C. P. (1978) Techniques for fitting size distribution functions to observed particle size data, Preprints of 18th Conf. on Radar Meteor., Atlanta, GA, 129-133.

As a measure of how much the data in the cloud probe range depart from an (imaginary) extension of the slope line, it has been useful to calculate a value on the data sheets that follow which is termed Average Departure and is shown as AVE DEPT. This is derived by subtracting the logarithm of the population values for each cloud probe channel from the corresponding population number value each channel would have if the calculated slope line were extrapolated into the cloud probe range.

Such average departure values are useful in comparing spectra. When they are small ( $\sim 0.5$  to  $1.0$ ) there is general agreement with an exponential distribution into the cloud probe range. When values are as large as  $3.5$  to  $4.5$ , the data in the cloud probe range often have a distinctive slope that is much greater than the calculated one for the precipitation probe data.

Since the "average departure" value is partially derived from the slope line it is not calculated when data do not allow a calculation of the slope.

### 3.5 Data Presentation Format

In some of the figures that follow data representative of conditions during a sampling pass are given in a format similar to that in Figure 3. The meanings of most of the data there are either evident or are described in the accompanying or following notes.

The numerical values of the particle populations in each of the 15 channels of the three measuring probes are given in the bottom-left portion of the data in Figure 3 while the same data are shown in plotted form in the curve at the right. The solid lines in the spectrum represent normalized (per mm) population figures plotted against the physical size of the particles. The longest portion of the solid line is from the precipitation probe data while the shorter portion to the left is from the cloud probe. Scatter probe data (particles  $\sim <30 \mu\text{m}$ ) are not discernable on the plot, although numerical values for each of the scatter probe channels are given on the figure.

The dashed line on the Figure 3 graph reflects normalized values of liquid water content for the spectrum of particle sizes. They show the effective contribution to total measured LWC that various sizes of particles (and their associated number) make. While the number concentration of particles normally decreases with increasing size, the smaller number of larger particles often results in as great an LWC as a larger number of smaller particles. In the Figure 3 example the decrease of number with increased size results in a roughly constant contribution to total LWC (horizontal dashed line) across the spectrum of sizes.

The data presented numerically and graphically at the bottom of the data portion of Figure 3, and ensuing similar ones, are the averages of those recorded during the five consecutive 20-second periods beginning at the times indicated at

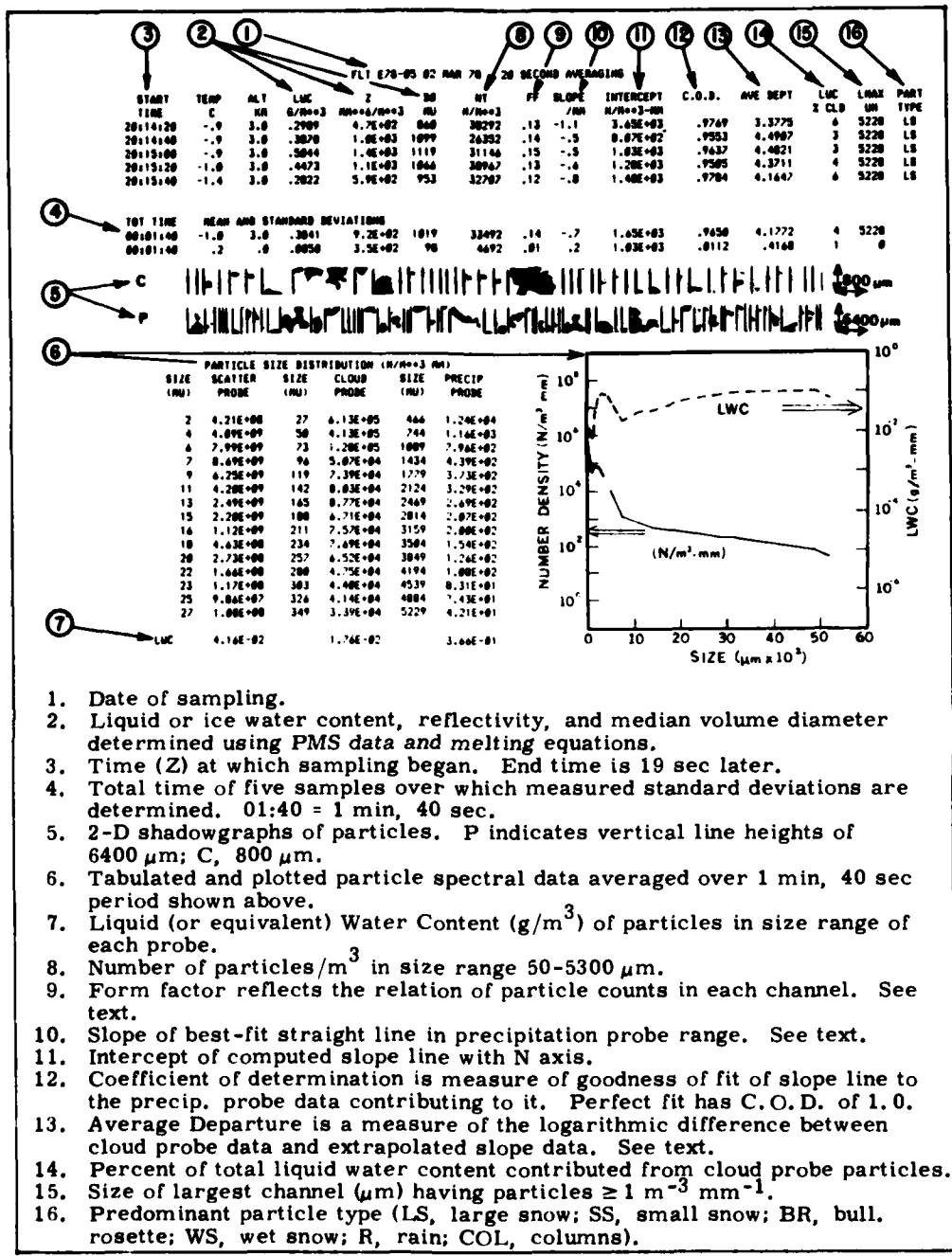


Figure 3. Sample and Explanation of Data Format

the upper left of the figure. Average values of temperature, altitude and other recorded or calculated data are given for each of the 20-second periods that contribute to the spectral data in the lower portion of the figure.

The purpose in presenting data at the top of Figure 3 for five consecutive periods rather than one overall period of 100 seconds is to provide the reader a feel for the variations in data that may or may not have occurred during the overall period. Another measure of the variations that occurred is given in the mean and standard deviations for each column of data. Samples from the thousands of PMS (Particles Measuring Systems, Inc) 2-D probe particle shadowgraphs acquired are also given on Figure 3. In that and ensuing figures the broad assortment of particle types and sizes is amply shown, although in the type clouds examined most particles appeared to be irregular-shaped agglomerates of smaller crystals.

The 2-D shadowgraph rows on Figure 3 preceded by "P" indicate precipitation probe data. The size of individual particles in both horizontal and vertical directions may be estimated from knowledge that the height of the vertical lines in that row is 6400  $\mu\text{m}$ . Similarly, a "C" reflects PMS 2-D cloud probe data. The height of the vertical lines in these rows is 800  $\mu\text{m}$ .

The first day on which cloud sampling was conducted to acquire the type data discussed above was 1 March 1978. A description of the sampling flight and the data obtained is given in the following section.

#### 4. WEATHER AND FLIGHT DATA -- 1 MARCH 1978

##### 4.1 Synoptic Situation

Aircraft sampling on the first day of this flight program, 1 March 1978, was conducted between Albuquerque and Farmington, in the northwestern part of New Mexico. The following discussion refers to the central and western parts of the U.S. with emphasis on the New Mexico area.

The general surface and upper-air weather situation occurring during the 3 days of this program has been described in a contract report by Chin and Hamilton.<sup>34</sup> The diagrams in Figure 4 are reproduced from that report, and most of the comments that follow are from material in it.

Essentially, a large area of high pressure dominated the central U.S. on 1 March. A quasi-stationary front along the Rocky Mountains delineated the western boundary of the cold-air mass over the central U.S. A low pressure area along the California coast caused widespread rainfall in the southwest corner of the

34. Chin, D. and Hamilton, H. D. (1978) Synoptic Analysis Case 1, 1 March 1978-4 March 1978, Systems and Applied Sciences Corporation Scientific Report No. 1, AFGL-TR-78-0294, AD A065 486.



U.S. This low remained nearly stationary, but an associated frontal system shown in part a of Figure 4 moved into the Colorado-New Mexico area where a low developed on 2 March.

As indicated in parts b and c of Figure 4, the two frontal systems over New Mexico on 1 March resulted in widespread fog, cloudiness and considerable precipitation. Most stations in New Mexico reported rain, while those farther north reported snow. Nephanalyses on Figure 4 and others indicated one of the main cloud forms was stratocumulus, but aircraft, sounding and satellite data also indicated the presence of cumulus and cirrus clouds in the northwestern part of New Mexico, where sampling was conducted.

The flow aloft was generally from the southwest to west over the flight area as shown in the d part of Figure 4. The 700 mb analysis at 2 March, 00Z (not shown) indicated a minor short-wave trough over the eastern parts of Colorado and New Mexico. This could have earlier triggered convective development that was observed in the sampling area.

Figures 5a and b are Defense Meteorological Satellite Program (DMSP) visual and infrared pictures showing the area that was sampled on 1 March. The visual picture shows extensive cloudiness over most of the area portrayed, but only in the whitest portions of the infrared photo do the clouds reach cirrus altitudes ( $\geq \sim 7$  km). Most of the cloud mass east of the  $100^{\circ}\text{W}$  is relatively low and warm.

In the satellite photos, cumulus clouds can be seen forming near the Gulf of California and enlarging as they move northeast. Cirrus and cirrocumulus occurred over much of the area between  $100$  and  $110^{\circ}\text{W}$ . Near the Farmington-Albuquerque area, where sampling was conducted, the clouds did not have a predominant orientation, but were widespread and composed of both cirriform and cumuliform types.

Albuquerque sounding data are shown in Figure 6 for the two soundings immediately prior to, and after, the sampling flight. A significant feature of both of these is the small temperature-dewpoint spread (and consequent high humidity) to relatively high atmospheric levels. This spread is 3C degrees or less to nearly 23,000 ft (7.0 km) MSL on both soundings. The spread was only slightly greater near 28,000 ft (8.5 km), the highest level for which dewpoint data were reported.

Lapse rates for the soundings in Figure 6 are less than adiabatic (more stable) except for small thicknesses near the 6000 to 9000 ft (1.8 to 2.7 km) MSL level where they approach that rate. Both soundings, however, are close to being potentially unstable over thicknesses of several thousand feet. Such instability occurs when wet-bulb potential temperatures decrease with height (AWS-USAF).<sup>35</sup> In the cases of the 12Z and 00Z soundings these potential temperatures are indicated to

35. AWS-USAF (1969) Use of the Skew T, Log p Diagram in Analysis and Forecasting, Air Weather Service Manual, 105-124.

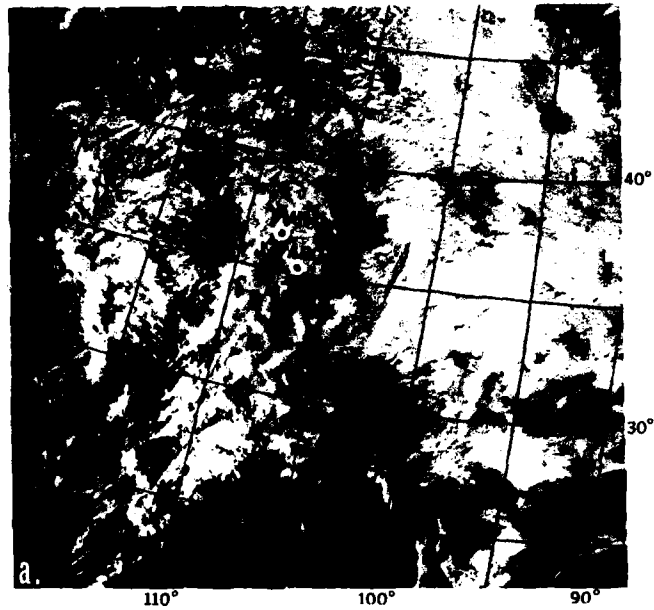


Figure 5. Satellite Visible (a) and Infrared (b) Photos of Western U. S. and Mexico at 1815Z 1 March 1978. Sampling was conducted between Farmington (FMN) and Albuquerque (ABQ), New Mexico

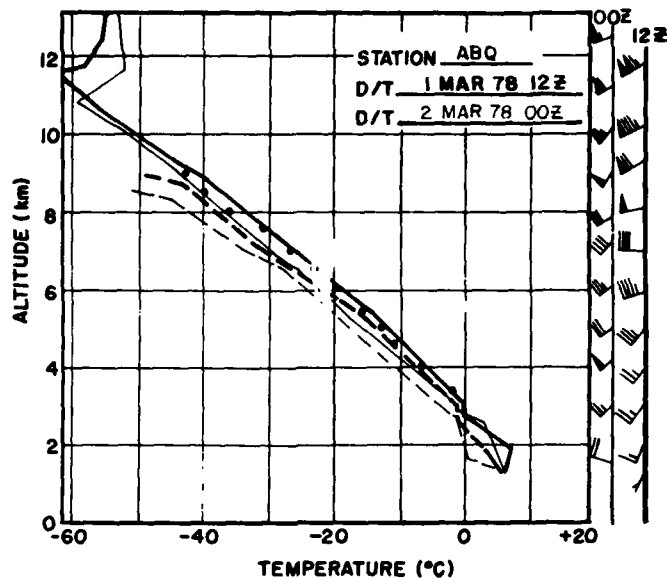


Figure 6. Albuquerque, NM, Sounding Data for Times Prior to and After Data Flight. Dots are aircraft-measured temperatures

be constant from approximately 700 mb (~3.0 km MSL) to above 500 mb (~5.6 km MSL). Slight temperature changes could have resulted in large layers of potential instability amenable to triggering by the aforementioned minor trough.

While no dewpoint data were reported in the soundings above 28,000 ft, some thin cirrus was seen above this level. The tops on this cloud are not known, but were undoubtedly at or below tropopause altitude, which was 38,000 ft (11.6 km) on 1 March, 12Z, and 36,000 ft (10.9 km) MSL on 2 March, 00Z.

The freezing level at the time of both soundings was near 9000 ft (2.7 km) MSL, about 2000 ft below the lowest sampling level.

#### 4.2 The Flight

The C-130 sampling flight departed Kirtland AFB at Albuquerque at 1740Z (1040L) 1 March and flew northeast into an area of ragged, uneven but generally overcast clouds. Bases of a cumuliform cloud layer were encountered at 7000 ft (2.1 km) MSL. By 1751Z the aircraft reached 11,000 ft (3.3 km) MSL and leveled off to continue northwestward. Mountains in this area reach 5000 to 7000 ft (1.5 to 2.1 km) MSL, so this portion of the flight was at approximately 4000 to 6000 ft above ground level (AGL). A schematic view of the cloud areas penetrated on this flight is given in Figure 7.

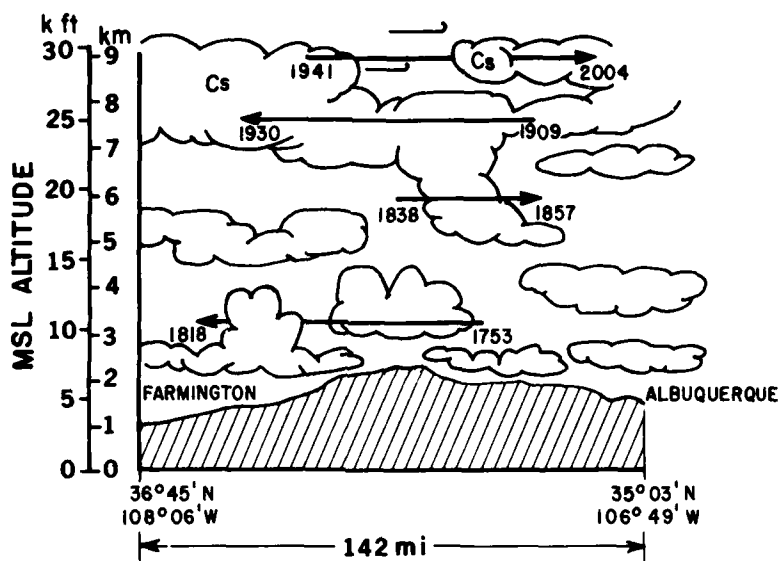


Figure 7. Generalized View of Clouds Along Sampling Tracks on 1 March 1978. The main data acquisition was along the passes having the starting and ending times indicated

The aircraft was in generally heavy clouds from 1753 until 1811Z although there were occasional breaks when lower clouds could be seen. Crystals seen on the windshield and snow stick were relatively large, and some icing occurred on the nose and propeller spinners. The aircraft mission director commented during this time that it was necessary to keep moving the snow stick so that it would not ice up.

At 14 miles southwest of Farmington, NM the 11,000 ft pass was concluded and the aircraft began climbing and turning southeast toward Albuquerque. Rising through 16,000 ft (4.9 km) the sun could be seen fairly brightly through thin higher clouds. Cloud bases were entered at 17,000 ft (5.2 km); however, occasional openings in the clouds were found near this level.

The second horizontal pass was made at 19,000 ft (5.8 km) MSL beginning at 1838Z while flying southeast. During the first part of this pass the sun was bright through cirrus above and the ground could be seen below; however, uniform clouds were penetrated for several minutes when the ground was only dimly visible and cloud tops could not be estimated. At 1857Z, 7 miles northwest of Albuquerque, the aircraft began a climbing turn back toward Farmington, NM.

At 25,000 ft (7.7 km) at 1907Z the aircraft again leveled off to acquire more data while flying northwestward. The cirrus at this level was uniform and had a

thin hazy appearance. The sun was sometimes bright above, but heavier cirriform clouds occasionally darkened it. The cloud tops at this time were estimated to be 4000 to 5000 ft above flight level, but this later proved to be lower than actual top heights. No optical phenomena (halos, sun dogs, etc.) were seen at any time during this flight. Light turbulence was reported at this altitude as the aircraft flew on a heading of 300°.

Approximately 32 miles southeast of Farmington a climbing turn was made to return to Albuquerque on a southeasterly heading. The cirrus remained quite uniform during this ascent, although it became slightly thinner with altitude. By about 1941Z, 29,000 ft MSL (9.0 km) had been attained and the aircraft leveled off. This was the highest altitude at which data were acquired during the flight. There were brief periods when the aircraft was not in the cirrus, but most of the time at this level the sun shown through a thin uniform veil that had no structure. In contrast, the clouds below appeared to be of a cumuliform nature that topped several thousand feet lower.

The data pass at 29,000 ft was concluded at 2004Z and the aircraft returned to Kirtland AFB to land at 2024Z. A more comprehensive description of the flight from the aircraft mission director's notes is given in Appendix A.

#### 4.3 Sampling Data: 1 March

##### 4.3.1 TEMPORAL VARIATIONS DURING FLIGHT

The data recorded by the PMS (Particle Measuring Systems) spectrometers and the other meteorological and aircraft data are averaged over 20-second periods in this study. Each data sample therefore represents conditions averaged over a distance interval of approximately 2 km since the aircraft was flying at about 100 m/sec. This averaging interval is adequate to properly represent conditions in the large and relatively homogeneous cloud conditions that were sampled in this storm system.

A graphical depiction of the temporal variation of some of the values recorded or computed from flight measurements on 1 March is given in Figure 8. Part a shows both the variation in altitude and temperature with time. The flat plateaus indicate times when the aircraft had leveled off at the four main data-acquisition levels of 11,000, 19,000, 25,000 and 29,000 ft (3.3, 5.8, 7.7 and 9.0 km) MSL. The correlation and variation of temperature with altitude is very close.

The b and c portions of Figure 8 demonstrate the variation of the calculated liquid water content (LWC) and of the median volume diameter of particles recorded in the overall range of the cloud and precipitation probes (~25-5300  $\mu\text{m}$ ). After studying extensive PMS 2-D "shadowgraph" records of observed particles the 1-D data were processed using AFGL equations for times and predominant particle types given in Table 3.

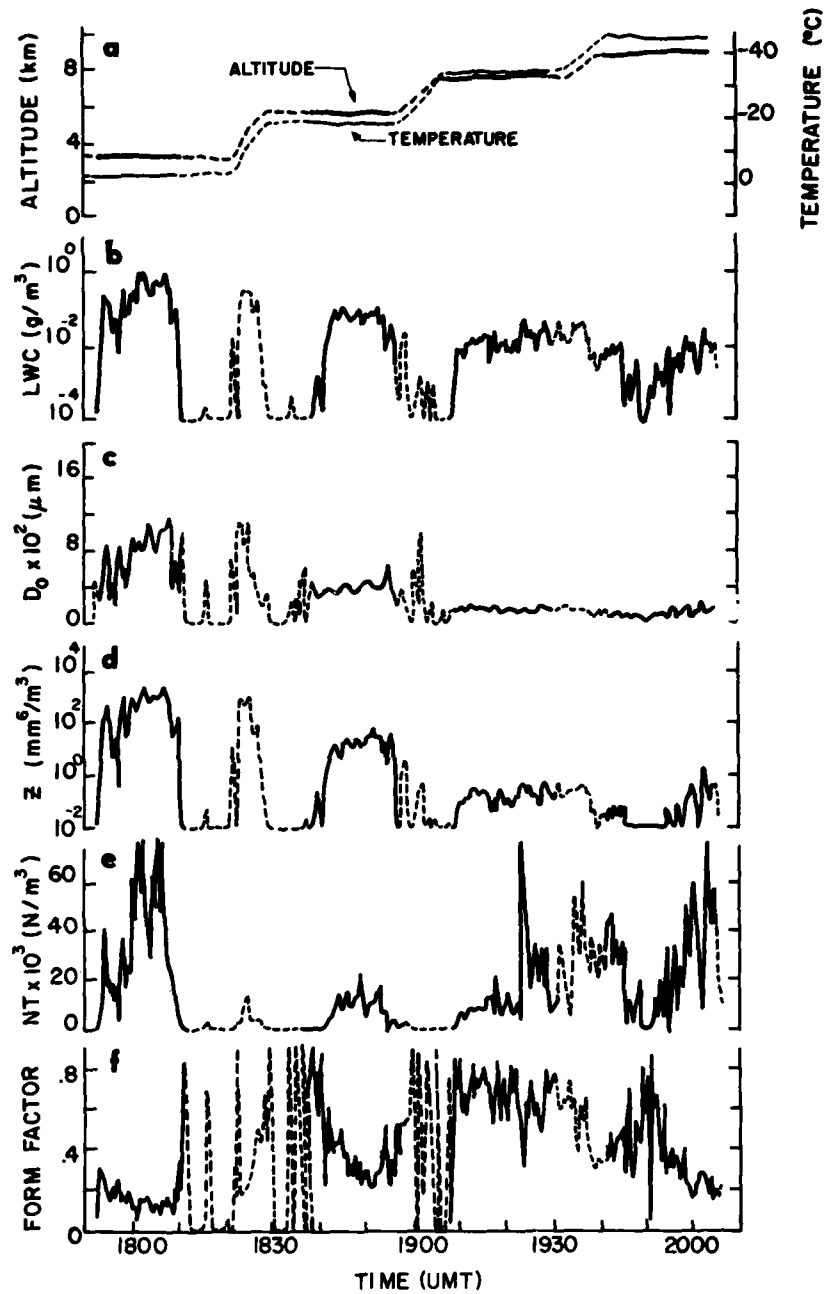


Figure 8. Variation With Time During 1 March 1978 Flight of Several Measured and Calculated Elements Based on Values of Consecutive 20-Second Averages. Solid lines indicate portions of flight for which data on Figure 9 were prepared

Table 3. Predominant Particle Types During Periods Indicated on 1 March

Time	Type
1750:00 to 1825:59Z	Large Snow
1826:00 to 1937:59Z	Small Snow
1938:00 to 2004:59Z	Bullet Rosettes

The shadowgraphs varied extensively in size and shape from one sampling level to another, but the majority of particles seemed to be irregular aggregates. Hobbs and Atkinson<sup>36</sup> have reported that more than 95 percent of the ice particles they collected in orographic clouds and cyclonic storms were irregular in shape.

The general agreement in the temporal variation of LWC and mean volume diameter,  $D_o$ , can be seen in Figure 8. The largest values of LWC were calculated to occur while the aircraft was flying at the lowest sampling altitude, 11,000 ft (3.3 km) MSL, where the temperature was approximately  $-3^{\circ}\text{C}$ . The highest value was  $1.1 \text{ g/m}^3$  at 1802:20Z, but for several minutes before and after that time the LWC was near or greater than  $0.5 \text{ g/m}^3$ .

Cloud density was variable throughout the flight so that particle counts rose and fell frequently. While still at 3.3 km the LWC fell to less than  $10^{-4} \text{ g/m}^3$  at 1809Z, but rose above  $0.1 \text{ g/m}^3$  again at 1820Z.

At the next higher sampling level of 19,000 ft (5.8 km) typical LWC values, while flying in clouds, were near  $0.1 \text{ g/m}^3$ , and the temperature was  $-19^{\circ}\text{C}$ . Corresponding typical values at the 25,000 ft (7.7 km) level were near  $0.01 \text{ g/m}^3$  and  $-33^{\circ}\text{C}$ , while at 29,000 ft (9.0 km) they were between 0.001 and  $0.01 \text{ g/m}^3$  and the temperature was  $-43^{\circ}\text{C}$ .

The median volume diameter,  $D_o$ , is the diameter of a particle having a mass at the median of the combined cloud and precipitation probes' total LWC value. It is the equivalent size of a melted particle, not that of the frozen particle. As shown in part c of Figure 8 the value of  $D_o$  was approximately 800-900  $\mu\text{m}$  in the cloud at 3.3 km.

At 5.8 km the typical value of  $D_o$  fell to 300-450  $\mu\text{m}$ , and at 7.7 km to 150-250  $\mu\text{m}$ . At the highest sampling altitude, 9.0 km, values of  $D_o$  were generally between 50 and 150  $\mu\text{m}$ . These values would have been less if the smaller particles measured by the scatter probe had been included in the calculations.

36. Hobbs, P. V. and Atkinson, D. G. (1976) The concentrations of ice particles in orographic clouds and cyclonic storms over the Cascade Mountains, *J. Atmos. Sci.* 33:1362-1374.

The variation of reflectivity,  $Z$ , with units of  $\text{mm}^6/\text{m}^3$ , that is shown in part d of Figure 8, is somewhat correlated with changes in LWC. Plank,<sup>37</sup> among others, has pointed out that the largest hydrometeors do not contribute significantly to LWC, which is essentially a function of  $D^3$ , ( $D$  being diameter), but they do contribute importantly to the reflectivity factor which is dependent on  $D^6$ . Reflectivity values are commonly determined with radar sets, but the values on Figure 8 are derived from the sixth moment of equivalent melted diameters of spectrometer data. These values varied from near  $10^3$  at 11,000 ft to less than  $10^{-1}$  at 29,000 ft.

The number of all sized particles (in the 50-5300  $\mu\text{m}$  range), NT, varied from 0 to more than 100,000/ $\text{m}^3$ . Its variation during sampling on 1 March is shown in part e of Figure 8. A few of the highest values in both parts e and f are off the ordinate scale. The differences between the amplitudes shown on part e and those for LWC on part b are of interest. For example, the peak in the LWC curve at 1825Z is barely reflected in the NT curve, even though the preceding LWC values at about 1800Z were of similar magnitude and accompanied by large NT counts. Since the LWC decreased only slightly from the 1800Z data epoch to that of 1825, while the NT decreased significantly, there is an indication that the mean particle size increased. This, in fact, was the case, although the  $D_0$  increase in part c of Figure 8 is barely noticeable on the logarithmic scale.

The consistently highest numbers of particles over a 5 to 10-minute period were measured at the 11,000 ft (3.3 km) MSL level as shown in part e of Figure 8. The NT figure dropped off significantly at the 19,000 ft (5.8 km) level, but increased again at 25,000 ft (7.7 km) and 29,000 ft (9.0). The variation of NT with time was much more erratic at the two higher levels than the lower ones indicating more continuous, homogeneous cloud conditions at the lower levels.

The form factor calculations varied considerably with time as shown in part f of Figure 8. However, in considering the primary longer periods when the aircraft was in representative clouds, the form factor increased from approximately 0.05-0.15 at 3.3 km to 0.20-0.50 at 5.8 km to 0.60-0.75 at 7.7 km. At the highest sampling altitude, 9.0 km, the form factor decreased to the 0.20-0.45 range.

The occasional radical changes in form factor from high to low values in part f are a result of insufficient data to provide stable measurements. Fluctuations in these values are much less extreme when NT values are of the order of 500/ $\text{m}^3$  or greater.

37. Plank, V.G. (1974) Hydrometeor Parameters Determined From the Radar Data of the SAMS Rain Erosion Program, AFCRL/SAMS Report No. 2. AFCRL-TR-74-0249, pp 86.

#### 4.3.2 CLASS VALUES OF DATA FROM FOUR PASSES

The various plots on Figure 8 and in ensuing similar figures were developed from instruments that recorded continuously during a flight. Other instruments, such as the formvar replicator, however, were used only during certain periods, frequently termed "passes," when special efforts were made to obtain all possible data. These pass times were usually determined by the mission director beforehand when the aircraft was flying a straight course at an optimum sampling speed of 150 kt ( $77 \text{ m sec}^{-1}$ ) indicated air speed.

The data for the six sets of variables on Figure 9 were acquired during passes at four particular altitudes and in relatively homogeneous cloud conditions. The times of the four samples, their duration, altitude, and temperature are given in Table 4.

Table 4. Sampling Passes - 1 March

Time (Z)	Duration (min)	Altitude (ft/km)	Ave. Temp ( $^{\circ}\text{C}$ )
1941-2004	23	29,000/9.0	-43.4
1909-1930	21	25,000/7.7	-33.2
1838-1857	19	19,000/5.8	-18.7
1753-1811	18	11,000/3.3	- 2.8

Averaged data for each of the pass levels in Table 4 were calculated for each consecutive 20-second period during the pass; therefore, a 23-minute period, for example, contains 69 individual data samples. The first of the 10 classes for each of the variables on each histogram reflects the percent of time the aircraft was in clear or nearly clear air. Since emphasis was on cloud conditions the percentage in this first range is small or zero in most cases.

The histograms are useful in showing the predominant (modal) ranges of the data while the aircraft was flying on a steady heading and at a constant altitude. The histograms also show the general spread of data and facilitate a judgment of the representativeness of the mean values. In all cases the mean figures given with each histogram are based on non-zero values, that is, they do not reflect the usually short periods when the aircraft may have been between two cloud masses.

As an example of the use of Figure 9, the four histograms in the column on the far left reflect the liquid water content calculations that were made from 11,000 ft (3.3 km), at the bottom of Figure 9, to 29,000 ft (9.0 km) at the top.

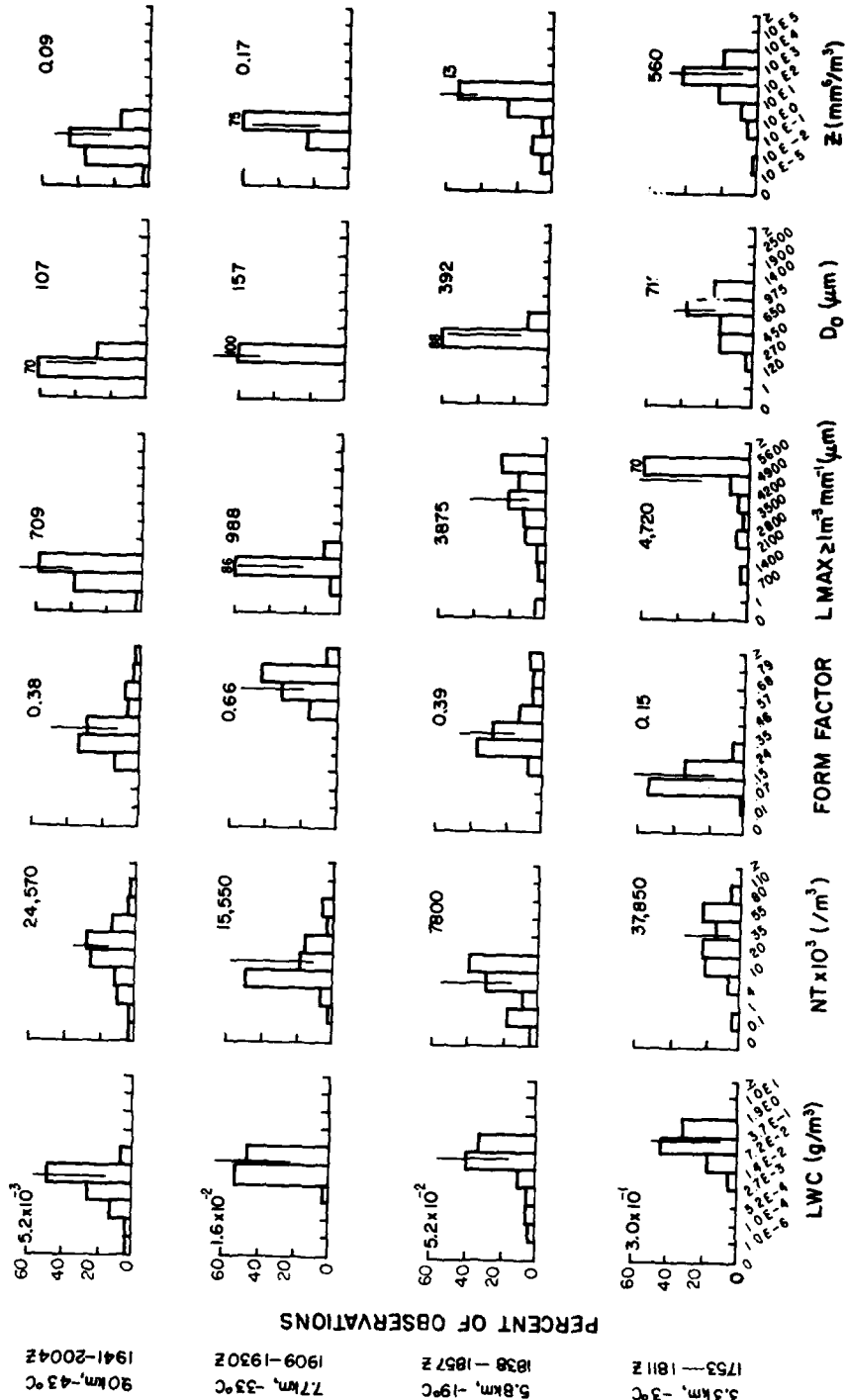


Figure 9. Percent Frequency By Class of Six Measured or Calculated Variables Based on Total Number of 20-sec Mean Values During Each Pass on 1 March 1978. Printed numbers and vertical lines are at 50 percentile values. These do not consider data in cloud-free areas

At the lowest measuring level slightly more than 40 percent of the LWC calculations were in the class between 0.07 and 0.37 g/m<sup>3</sup>. Lesser percentages are in adjoining range classes. At the next higher level, 5.8 km, approximately 33 percent of the LWC values are also in the same 0.07 to 0.37 class, but the modal class, representing 40 percent of the values, is smaller. At 7.7 km almost all LWC values are equally spread in two classes that extend from 0.0027 to 0.07 g/m<sup>3</sup>. The histogram for the 9.0 km level shows that predominant LWC values are between 0.0005 and 0.014 and that there is a slight skew toward lower values. As previously indicated, these values would have been slightly less if data for the small particles measured by the scattering probe had been considered.

The histograms of particle number totals, NT, for the same four sampling levels show a fairly even distribution of total counts over an extended range. At 3.3 km there were a few samples of more than 80,000/m<sup>3</sup>, but at 19,000 ft there were none greater than 20,000/m<sup>3</sup>. Some higher values of NT were measured at higher altitudes; approximately 5 percent of the time at 9.0 km particle counts in excess of 80,000/m<sup>3</sup> were recorded.

The graphs of form factor on Figure 9 show that these values are relatively low at lowest levels, that they reach peak values near 7.7 km and then decrease at 9.0 km. The apparent cause of this will be discussed in a later section.

The histograms labeled L<sub>max</sub> reflect the percent of time that the maximum physical size of measured particles (with concentration  $\geq 1 \text{ m}^{-3} \text{ mm}^{-1}$ ) were in the classes indicated. This information is of significance to modelers, weather modifiers and radar personnel because of the frequently great effect the largest particles have on liquid water content and even more so on reflectivity values.

The L<sub>max</sub> diagrams in Figure 9 indicate that 70 percent of the largest particles at 3.3 km were in the 4900-5600  $\mu\text{m}$  class. As previously indicated we had no capability for measuring larger sized particles during these flights. There was a much broader distribution at 5.8 km, while at 7.7 km more than 80 percent were between 700 and 1400  $\mu\text{m}$ . This was also the predominant class at 9.0 km, though the maximum size of many particles at that altitude was even smaller.

The diagrams reflecting medium-volume diameter, D<sub>o</sub>, on Figure 9 show that typical values were broadly spread at 3.3 km, but that at 7.7 km they were all between 120 and 270  $\mu\text{m}$ . At 9.0 km the mean value of D<sub>o</sub> was the smallest during this flight. Some 70 percent of the values were less than 120  $\mu\text{m}$ .

The calculated values of reflectivity on Figure 9 decrease fairly smoothly with altitude. The greatest concentration of values in single classes are 54 percent at 5.8 km and 75 percent at 7.7 km. The smallest values of Z are at the highest level sampled, which is consistent with the smaller size particles and lower LWC values there.

#### 4.3.3 OBSERVED PARTICLE DISTRIBUTIONS

The foregoing sections have outlined the large amplitudinal changes several variables underwent during a 2-hour flight and also showed the most frequently observed classes for these variables at four levels in an extensive cloud mass. Based on the modal classes and mean values it is now possible to determine times during sampling periods when particle spectra were recorded that were "representative" of conditions at a given level over a fairly large area.

An approximation to the length of this area may be estimated from a knowledge that the sampling aircraft moved at  $\sim 100$  m/sec. During a 10-minute pass (for example) the aircraft moved 60 km. Modal values on Figure 9 indicated typically that 30 percent or more of the time during the passes at various altitudes certain classes of LWC,  $D_0$ , NT, etc., were recorded or calculated. This indicates that approximately the same values of data were recorded over at least 18 of the total 60-mile pass length. In many cases higher percentages of data were nested in single classes, indicating even more homogeneous cloud conditions.

The data presented on Figure 10 follow the same format as the example described in Figure 3. They reflect cloud and particle conditions that were "common" during the horizontal pass at 3.3 km MSL on 1 March, although the specific averaged data were acquired during the 100-second period beginning at 1803:20Z.

How representative or typical the Figure 10 data are may be judged by comparing some of the various mean values at the top of the figure to the mean and predominant values given in the histograms at the bottom of Figure 9. The histograms reflect conditions over the longer 1753-1811Z time period when the aircraft was at 3.3 km. The mean short-term values on Figure 10 are generally quite close to the longer term values. For example, the longer period mean LWC value on the bottom of Figure 9 is 0.300, while that for the Figure 10 data is  $0.367 \text{ g/m}^{-3}$ .

The clouds sampled at 3.3 km were relatively rich in large particles and in liquid water content. The largest spectrometer channel, about  $5300 \mu\text{m}$ , recorded particles during most of the pass. The LWC values occasionally neared  $1 \text{ g/m}^3$ , which may be compared to the  $4 \text{ g/m}^3$  Marwitz and Stewart<sup>8</sup> found in post-frontal convection and to the  $0.5 \text{ g/m}^3$  they found in more stable pre-frontal clouds in the Sierra Nevadas in winter.

The number of particles of all sizes, NT, was also greater at the 3.3 km level than at higher levels. In comparing the Figure 10 spectrum to others it appears this is due to large numbers of particles in both the cloud and the precipitation probe ranges.

The low form factor of 0.12 for the spectrum shown on Figure 10 was common in cases where large particles were numerous. The small slope of  $-0.8/\text{mm}$  also reflected the presence of many large particles in the heavy cloud that was sampled.

FLT E78-84 1 MAR 76 20 SECOND AVERAGING

START TIME	TEMP C	ALT KM	LWC G/M <sup>3</sup>	Z M	MW/M <sup>3</sup>	NU	NU	NT M/M <sup>3</sup>	FF /MM	SLOPE /MM	INTERCEPT N/M <sup>3</sup> -MM	C.O.D.	AVE DEPT	LWC X CLB	LMAX UM	PART TYPE
18:03:26	-2.6	3.3	.4114	7.9E+02	42283	852	42283		.14	-.9	3.84E+03	.9322	3.5086	5	5228	LS
18:03:40	-2.8	3.3	.2741	6.4E+02	1937	852	26123		.13	-.6	8.85E+02	.8827	4.5641	6	5228	LS
18:04:00	-2.7	3.3	.2671	6.4E+02	1928	852	43662		.10	-.7	1.01E+03	.8853	4.3468	4	5228	LS
18:04:20	-2.8	3.3	.3893	9.4E+02	1638	852	68831		.16	-.7	1.67E+03	.8683	4.2857	5	5228	LS
18:04:40	-2.9	3.3	.4928	9.7E+02	923	852	56227		.13	-.9	3.95E+03	.9735	3.5476	4	5228	LS

TOT TIME MEAN AND STANDARD DEVIATIONS

04:01:40	-2.8	3.3	.3668	8.0E+02	975	45825	975		.12	-.8	2.27E+03	.8824	4.6584	5	5228	
06:01:40	.1	.8	.0657	1.4E+02	75	12155	75		.02	-.1	1.35E+03	.0580	.4366	0	0	



PARTICLE SIZE DISTRIBUTION (N/M<sup>3</sup>-MM)

SIZE (UM)	SCATTER PROBE (NU)	SIZE (UM)	CLOUD PROBE (NU)	SIZE (UM)	PRECIP PROBE (NU)
2	3.97E+07	27	8.86E+05	466	1.64E+04
4	2.17E+06	58	7.67E+05	744	2.66E+03
6	5.14E+08	73	1.34E+05	1089	1.13E+03
7	7.85E+08	94	8.54E+04	1434	5.46E+02
9	8.46E+08	119	8.93E+04	1779	4.63E+02
11	8.22E+08	142	1.62E+05	2124	2.99E+02
13	6.24E+08	145	1.62E+05	2469	2.63E+02
15	5.89E+08	188	7.76E+04	2814	2.15E+02
16	4.80E+08	211	9.37E+04	3159	1.61E+02
18	2.94E+08	234	7.24E+04	3504	1.33E+02
20	2.43E+08	257	6.23E+04	3849	9.20E+01
22	1.89E+08	288	4.70E+04	4194	8.01E+01
23	1.66E+08	303	4.44E+04	4539	6.16E+01
25	1.24E+08	326	4.13E+04	4884	5.99E+01
27	1.10E+08	349	3.53E+04	5229	4.84E+01

LWC	1.80E-02	1.69E-02	3.48E-01
-----	----------	----------	----------

Figure 10. Representative Cloud Data for 11, 000 ft (3.3 km) MSL Sample on 1 March 1978. See Figure 3 for explanation of values

The straight line in the plotted spectrum for sizes greater than  $1400\ \mu\text{m}$  attests to an exponential distribution; however, at smaller particle sizes there is a significant departure from exponential. This is reflected in the relatively low C.O.D. value of 0.89. The C.O.D. is based on the slope computation, which includes population figures for sizes as small as approximately  $650\ \mu\text{m}$ , a size smaller than the  $1400\ \mu\text{m}$  where the initial departure from the straight-line distribution begins. The high "average departure" value of 4.05 of the cloud probe data from the extrapolated slope line also attests that the distribution is not exponential at small particle sizes ( $\sim 1400\ \mu\text{m}$ ). The reason for the large departure from an exponential slope in the small-particle sizes is not fully understood, but examination of other plotted spectra for the same level indicated it was common.

Data at the upper-right portion of Figure 10 indicates about 5 percent of the total LWC was contributed by particles in the cloud probe range. The largest particle sizes recorded during the pass were near  $5300\ \mu\text{m}$ , although larger sizes were undoubtedly present.

The dashed horizontal line in the spectrum plot shows that particles of all sizes from  $300$  through  $5300\ \mu\text{m}$  made roughly comparable contributions to the total liquid water content.

The 2-D cloud probe was not functioning correctly during most of the flight so only 2-D precipitation probe images could be displayed on Figure 10. Since the height of the vertical lines is  $6400\ \mu\text{m}$  it can be seen that a few of the images are  $5000$  to  $6000\ \mu\text{m}$  in their maximum dimension. The irregular shapes of the particles are also to be noted.

Typical cloud conditions at  $19,000\ \text{ft}$  ( $5.8\ \text{km}$ ) on 1 March are shown on Figure 11. The number of both large and small particles at this altitude is considerably less than at  $11,000\ \text{ft}$ , and the largest are approximately  $3400\ \mu\text{m}$ . The calculated LWC dropped to  $0.076\ \text{g/m}^3$  and the  $D_0$  to  $377\ \mu\text{m}$ .

Mean number total, NT, at  $5.8\ \text{km}$  was the lowest of any levels sampled. The numerous particles recorded at higher levels apparently aggregated in their fall to form fewer but larger particles. The finding of both more and larger particles at  $3.3\ \text{km}$  than at  $5.8\ \text{km}$  seems an indication that many of the minute particles that escaped detection at the higher level had grown sufficiently to be recorded after falling to the  $3.3\ \text{km}$  level.

Overall particle distributions approach the exponential at  $5.8\ \text{km}$ . The sample form factor average of 0.42 on Figure 11 is quite close to the pass average of 0.39 on Figure 9, which has been seen to be associated with near-exponential distributions. The small "average departure" of  $-0.34$  of the actual cloud probe data from the extrapolated slope also indicates the overall distribution approaches the exponential. Only about 4 percent of the LWC is from cloud probe particles.

FLT E78-84 1 MAR 78 20 SECOND AVERAGING

START TIME	TEMP C	ALT KM	LUC G/H <sub>2</sub> O	Z M/H <sub>2</sub> O	D <sub>0</sub> M	NT M/H <sub>2</sub> O	FF SLOPE /MM	INTERCEPT M/H <sub>2</sub> O <sup>3</sup> -MM	C.O.D.	AVE DEPT	LUC % CLD	LMAX UM	PART TYPE
18:42:48	-18.7	5.8	.8551	8.2E+08	374	7727	.42 -2.8	2.67E+04	.9963	-2.292	4	3158	SS
18:43:00	-18.7	5.8	.8618	9.5E+08	388	9625	.39 -2.9	3.81E+04	.9961	-1.685	5	3848	SS
18:43:28	-18.8	5.8	.8855	1.4E+01	391	16913	.42 -2.8	3.91E+04	.9942	-3.558	4	3583	SS
18:43:48	-18.8	5.8	.1897	1.5E+01	379	13238	.43 -2.9	5.13E+04	.9952	-2.963	5	3583	SS
18:44:00	-18.8	5.8	.8881	1.8E+01	364	12539	.43 -3.2	6.14E+04	.9952	-6.688	3	2813	SS

TOT TIME MEAN AND STANDARD DEVIATIONS

TOT TIME	MEAN	STANDARD DEVIATIONS
00:01:48	-18.8	5.8
00:01:48	.1	.8

SIZE (MU)	SCATTER PROBE (MU)	SIZE (MU)	PRECIP PROBE (MU)	NUMBER DENSITY (N/H <sub>2</sub> O <sup>3</sup> -MM)	LWC (G/M <sup>3</sup> -MM)
2	2.51E+07	27	3.34E+04	466	5.51E+03
4	6.45E+07	58	5.98E+04	744	4.24E+03
6	1.88E+08	73	5.14E+04	1889	1.93E+03
7	1.18E+08	96	1.98E+04	1434	6.67E+02
9	1.84E+08	119	3.54E+04	1779	2.83E+02
11	7.93E+07	142	3.48E+04	2124	7.72E+01
13	5.77E+07	165	2.85E+04	2469	3.24E+01
15	5.97E+07	188	2.85E+04	2814	5.28E+00
16	4.88E+07	211	1.73E+04	3159	3.68E+00
18	3.14E+07	234	1.24E+04	3584	5.54E-01
20	2.68E+07	257	8.39E+03	3849	3.81E-01
22	2.28E+07	288	6.22E+03	4194	8.
23	2.38E+07	303	6.24E+03	4539	8.
25	1.95E+07	326	6.44E+03	4884	8.
27	1.66E+07	349	6.28E+03	5229	8.
LUC	2.28E-03		3.51E-03		7.38E-02

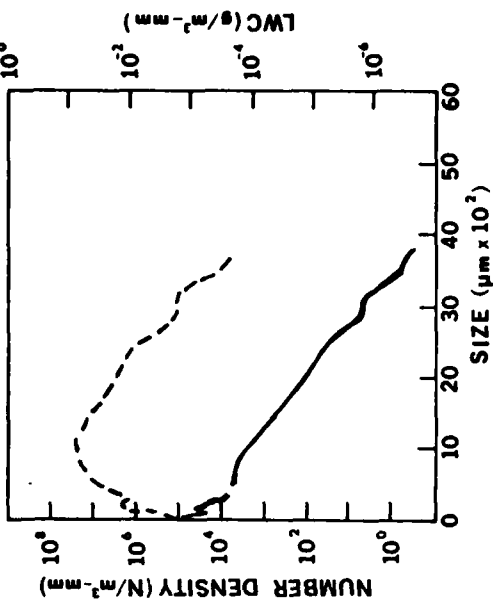


Figure 11. Representative Cloud Data for 19,000 ft (5.8 km) MSL Sample on 1 March 1978

The 2-D shadowgraphs of particles on Figure 11 indicate much smaller particles than recorded at the lower level. Most, in fact, are near the smallest sizes that can be resolved by the precipitation probe. Smaller particles could have been displayed if the cloud probe had been functioning properly.

A representative particle spectrum for the cirrus clouds at 25,000 ft (7.7 km) is given in Figure 12. Mean particle size and calculated liquid water content were both considerably less than at lower levels, but form factors increased to the 0.60-0.70 range.

The mean NT value for the Figure 12 data is  $6618 \text{ m}^{-3}$  which is in the modal class shown for this level on Figure 9, although the 50 percentile value is 15,550. The largest particles at this level were generally slightly less than  $1000 \mu\text{m}$ . Since there were fewer large particles the percent of total LWC contributed by the cloud probe increased at this level to 67 percent for the Figure 12 data. There were insufficient data in the precipitation probe range to permit the computations of a slope figure. For this reason there were also no computations made of intercept, C.O.D. and average departure.

Two features to be noted in the plotted spectral data of Figure 12 are the minimum near  $120 \mu\text{m}$  and the maximum at  $230 \mu\text{m}$ . This small valley-hill feature was seen at the same general spectral location in several other plotted spectra for 7.7 km,  $-33^\circ\text{C}$  data. The precise point where the minimum and maximum values occurred varied in time by one or two spectrometer channel widths. The significance of this feature is not entirely clear, but will be discussed in Section 7.

A representative (as deduced from Figure 9) particle spectrum for the highest level sampled, 29,000 ft (9.0 km), is shown in Figure 13. The cirrus was uniform but thin at this level and the sun was fairly bright above. The largest particles sampled according to the  $L_{\text{max}}$  column on Figure 13 were near or slightly less than  $1000 \mu\text{m}$ , while 69 percent of the total LWC was determined from measurements in the cloud probe range.

The average particle median volume diameter decreased slightly in ascending from 7.7 to 9.0 km; however, the total number of particles of all sizes increased. In comparing numerical values of particle concentration on Figures 12 and 13 for the two levels, it can be seen that the main increase in concentration at the higher level is in the smallest sizes, from 27 through  $\sim 165 \mu\text{m}$ . This increase resulted in a filling of the minimum spectral valley that was seen on Figure 12 at about  $120 \mu\text{m}$ . The filling of this valley resulted in a closer approximation to an exponential, straight-line spectral distribution of particles at 9.0 km. The form factor on Figure 13 also dropped to 0.33, a figure in the range where exponential distributions are most closely approximated.

The 2-D cloud probe was repaired in flight and began obtaining data during the 9.0 km pass. Sample shadowgraphs of some of the irregular particle shapes

FLI E78-04 1 MAR 78 20 SECOND AVERAGING

START TIME	TEMP C	ALT KM	LUC G/M**3	Z MN**6/M**3	D0 MU	NT N/M**3	FF SLOPE /MM	INTERCEPT N/M**3-MM	C.O.D.	AVE DEPT	LUC % CLD	LMAX UH	PART TYPE
19:17:40	-33.4	7.7	.0095	5.2E-02	131	9337	.82	I	I	I	94	743	SS
19:18:00	-33.2	7.7	.0070	6.8E-02	157	4793	.74	I	I	I	77	743	SS
19:18:20	-33.3	7.7	.0070	1.4E-01	184	4483	.54	I	I	I	48	1433	SS
19:18:40	-33.3	7.7	.0126	2.5E-01	191	7358	.56	I	I	I	44	1088	SS
19:19:00	-33.1	7.7	.0095	9.9E-02	164	7122	.68	I	I	I	73	743	SS

TOT TIME MEAN AND STANDARD DEVIATIONS

00:01:40	-33.3	7.7	.0091	1.2E-01	165	6618	.67	I	I	I	67	950
00:01:40	.1	.0	.0021	7.1E-02	21	1793	.11	I	I	I	19	275

2-D IMAGES NOT AVAILABLE

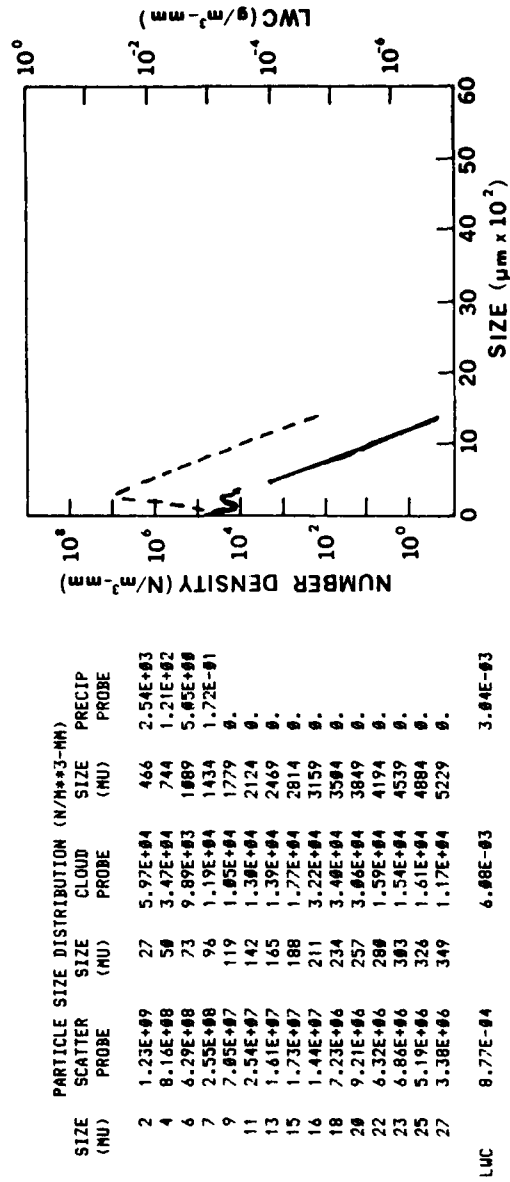


Figure 12. Representative Cloud Data for 25,000 ft (7.7 km) MSI. Sample on 1 March 1978

FLT E78-84 1 MAR 78 29 SECOND AVERAGING

START TIME	TEMP C	ALT KM	LWC G/M <sup>3</sup>	Z MM	DW MU	NT M/M <sup>3</sup>	FF /MM	INTERCEPT N/M <sup>3</sup> -MM	C.O.D.	AVE DEPT	LUC X CLD	LMAX UM	PART TYPE
19:55:28	-43.2	9.8	.0026	1.3E-02	113	18611	.33	I	I	I	78	766	BR
19:55:48	-43.1	9.8	.0044	1.7E-02	182	32478	.36	I	I	I	84	766	BR
19:56:08	-43.2	9.8	.0029	6.7E-02	168	6828	.26	I	I	I	38	1314	BR
19:56:28	-43.2	9.8	.0055	6.8E-02	135	17135	.33	I	I	I	55	1811	BR
19:56:48	-43.2	9.8	.0031	9.6E-03	93	22926	.48	I	I	I	88	766	BR

TOT TIME MEAN AND STANDARD DEVIATIONS

00:01:48	-43.2	9.8	.0037	3.3E-02	122	19593	.33	I	I	I	49	889	
00:01:48	.1	.8	.0011	2.5E-02	26	8329	.85	I	I	I	19	244	



PARTICLE SIZE DISTRIBUTION (N/M<sup>3</sup>-MM)

SIZE (MU)	SCATTER PROBE (MU)	SIZE (MU)	CLOUD PROBE (MU)	PRECIP PROBE (MU)
2	2.15E+09	27	1.15E+05	438
4	1.14E+08	47	6.27E+05	766
6	4.44E+07	67	2.83E+04	1812
7	3.78E+07	88	3.38E+04	1317
9	2.48E+07	108	3.44E+04	1622
11	2.84E+07	129	3.13E+04	1928
13	1.13E+07	149	2.62E+04	2233
15	1.78E+07	169	1.78E+04	2539
16	1.28E+07	190	3.72E+04	2844
18	6.98E+06	210	3.32E+04	3149
20	6.74E+06	230	2.41E+04	3455
22	5.59E+06	251	1.77E+04	3760
23	5.81E+06	271	1.53E+04	4066
25	5.67E+06	291	1.33E+04	4371
27	4.83E+06	312	9.34E+03	4676
LUC	5.78E-04		2.54E-03	1.14E-03

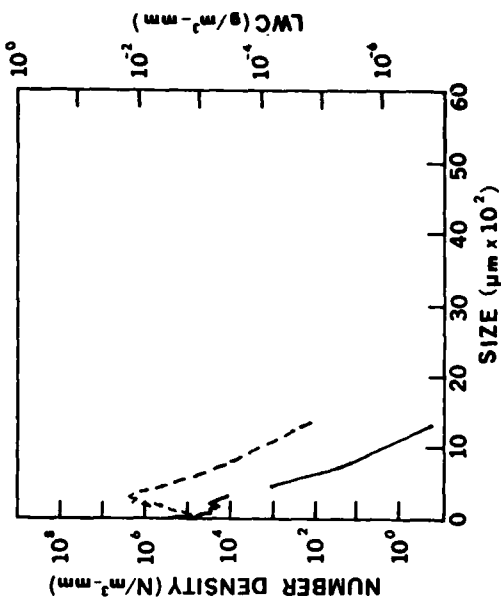


Figure 13. Representative Cloud Data for 29,000 ft (9.0 km) MSL Sample on 1 March 1978

are shown on Figure 13. Since the height of the vertical lines is  $800 \mu\text{m}$  it can be seen that the few particles have maximum sizes of 200 to  $400 \mu\text{m}$ . Most are smaller.

## 5. WEATHER AND FLIGHT DATA -- 2 MARCH 1978

### 5.1 Synoptic Situation

After reviewing synoptic analyses and forecasts and satellite data from AFGL's McIDAS (Man-Computer Interactive Data Access System) it was decided to sample on 2 March over the Arkansas-Tennessee area. Specifically, the sampling was conducted from Little Rock, Arkansas eastward 110 nm to Memphis, Tennessee.

By midday on 2 March, a low center wave had formed over central Texas on the extension of the quasi-stationary Rocky Mountain front. A front, shown in part a of Figure 14, which extended from this wave southwestward into Mexico, was the remnant of the one that had passed through New Mexico the previous day.

Prior to the time the flight was made the Little Rock-Memphis area had been under the influence of a moist southerly flow as a result of the circulation around the high over Ohio and the Texas low. As a result, overcast conditions prevailed over much of the south and central parts of the U.S. with stratocumulus clouds at lower levels, layers of stratiform clouds above, and cumuliform clouds scattered throughout the area.

The local area surface chart in Figure 14, part b shows the widespread precipitation and fog over Arkansas, Tennessee and adjoining states. In the flight area most of the precipitation at the surface was reported to be rain or drizzle, but within 150 miles north moderate snow was reported. A measure of the extensiveness of the cloud cover on 2 March can be seen in the nephanalysis in the part c of Figure 14.

At higher levels over the Oklahoma Panhandle there was a closed low at 850 mb ( $\sim 1.4$  km MSL) which was a reflection of the Texas surface low. At 700 mb ( $\sim 3.0$  km) and 500 mb ( $\sim 5.5$  km), however, only a trough of low pressure extended from Wisconsin southward through eastern Texas (see Figure 14, part d). As on the previous day the flight was made in an area of southwesterly to westerly winds before the trough. Other synoptic charts (not shown) indicated that sampling was conducted in an area of generally upward motion as the trough moved eastward toward Memphis; however, 3 hours after the sampling was completed, subsiding air reached the area.

The DMSP photos in Figures 15a and b show that although most of the Central Rocky Mountain portions of the U.S. were cloud covered, only the area east of



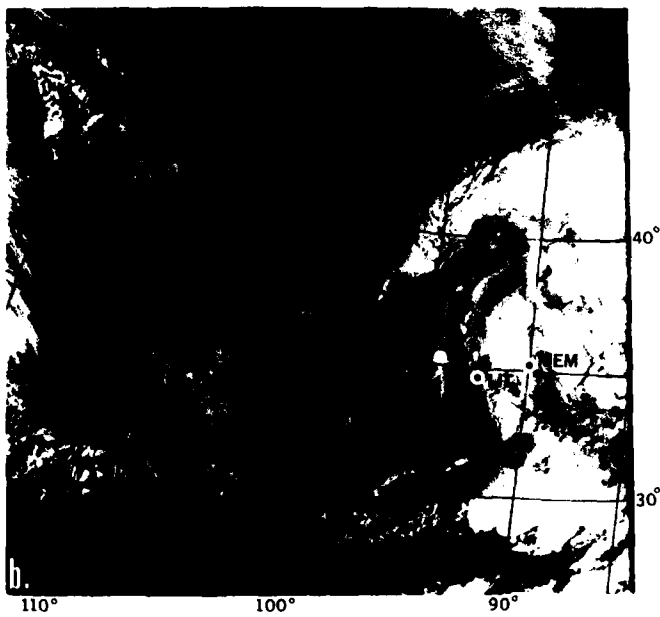
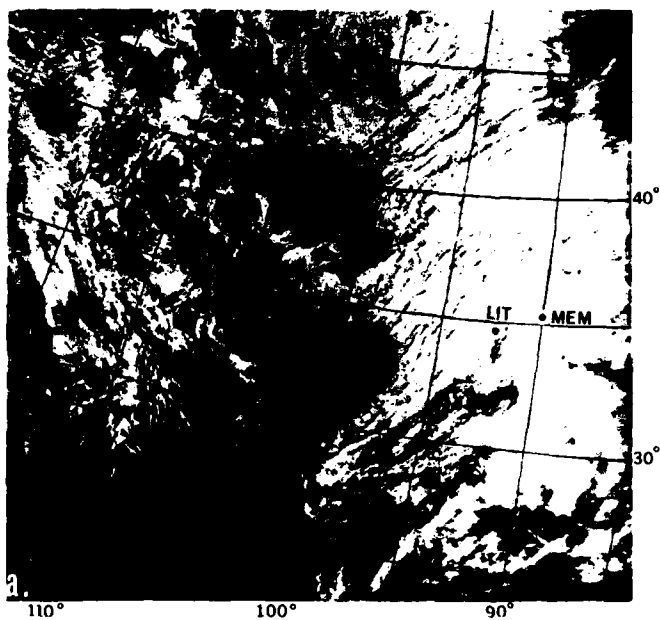


Figure 15. Satellite Visible (a) and Infrared (b) Photos of South-Central U. S. about 1800Z 2 March 1978. Sampling was conducted between Little Rock (LIT) and Memphis (MEM)

95°W had extensive high, cold clouds. This longitude was the approximate location of the 500-mb trough.

The Little Rock-Memphis area is shown on Figure 15b to be near the western edge of the highest clouds. The cloudiness appeared to have a cumulus origin. Slightly further south, near 30°N, the high clouds were due to cirrus blowoff from the large cumuli.

The two Little Rock soundings on Figure 16 both display strong inversions extending from approximately 1000 ft to 4000 ft (0.3 to 1.2 km) MSL. At 2 March 12Z the 850-mb temperature was 6°C warmer than at the surface. Such stable conditions were conducive to fog, drizzle and continuous light rain. This earliest sounding was also marked by small temperature-dewpoint differences from the surface to the highest level for which dewpoint data were available, approximately 27,000 ft (8.2 km) MSL. The difference was 3°C or less up to about 23,000 ft (7.2 km).

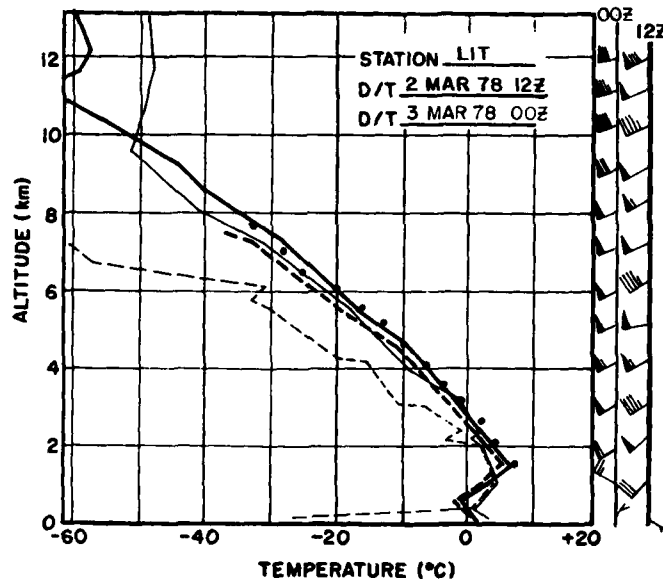


Figure 16. Little Rock, Arkansas Sounding Data for Times Just Prior To and After Data Flight. Dots are aircraft-measured temperatures

The 3 March 00Z sounding was similarly saturated or very moist from the surface up to about 7000 ft (2.1 km) MSL. Above a small frontal inversion at that level, the atmosphere became considerably dryer. Above the surface inversion

the lapse rate of both soundings was near the moist-adiabatic rate. Considering the related dewpoint data, the wet-bulb potential temperatures were nearly constant with height indicating a neutral potential for convective development. Yet, convective activity in the form of cumulus buildups and light turbulence was observed so that at least a slight potential for unstable conditions did exist and was realized. This potential is believed to have been triggered by an overriding front or trough. The main freezing level for both Little Rock soundings was near the 9000 ft (2.7 km) MSL level. The tropopause lowered from 37,000 ft (11.3 km) at 2 March 12Z to 32,000 ft (9.7 km) 12 hours later.

## 5.2 The Flight

The aircraft departed Kirtland AFB, New Mexico at 1634Z and was over Arkansas at 1900Z (1300L). A sampling pass was begun at 1902Z over Little Rock at about 25,000 ft (7.7 km) MSL. As the aircraft flew east there were numerous cloud buildups below that rose to about 18,000 ft. A schematic view of the flight profile and the type clouds encountered between Little Rock and Memphis is shown in Figure 17.

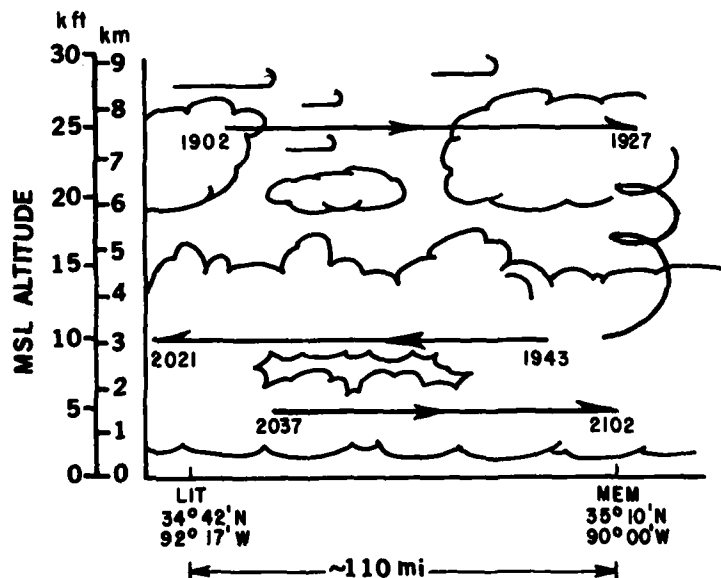


Figure 17. Generalized View of Clouds Along Sampling Tracks on 2 March 1978. Main data acquisition was along the passes having the starting and ending times indicated

At sampling altitude the aircraft moved in and out of thin cirrus through which the sun could be clearly seen. Wind was measured to be from 240 degrees at 54 kt at 1904Z.

At 1905Z, when the aircraft was temporarily in clear air, the base of a cirrus deck above was estimated to be near 34,000 ft. At 1915Z the mission director noted that the cirrus at flight level was thin, hard to locate and that probably little good data had been acquired up to that time. But at approximately 1920Z heavier altocumulus or cirrocumulus was penetrated. This provided large numbers of small particles. Still, the mission director determined there was very little widespread cloud to sample at 25,000 ft and at 1929Z, 15 nm east of Memphis requested the pilot of the C-130 to turn west and descend to a lower level.

During descent, the aircraft passed through occasional thicker clouds, but the larger scale, more widespread cloudiness was not encountered until the approximate 13,500-ft level was reached. At 1940Z, 96 nm east of Little Rock the clouds were reported to be heavy and to extend from at least 9000 to 13,000 ft. There was some light turbulence at that time.

An extended period of sampling at 3.0 km was begun at 1943Z as the C-130 was flying westward near Memphis. The mission director considered this a heavy cloud form and reported seeing many large snowflakes and occasional indications of rain on the snow stick. At 1952Z he indicated there was no turbulence.

Sampling at the 3.0 km level was concluded at 2021Z when the aircraft was 3 miles west of Little Rock. The winds at that time were 252<sup>0</sup>/40 kt. As the C-130 began a descent and a 180<sup>0</sup> turn it was noted that the base of one large cloud was near 9000 ft (2.7 km) MSL; however, there were widespread clouds elsewhere that extended from approximately 1000 ft through 13,000 ft MSL. The cloud ceiling at about this time at Little Rock was 600 ft.

A horizontal sampling pass at 5000 ft (1.5 km) through light to moderate rain was begun at 2038Z as the aircraft was flying eastward 35 nm east of Little Rock. Wind at this level was measured as 240<sup>0</sup>/55 kt. Clouds were widespread and dense and there was seldom anything to be seen in any direction. The ground was never visible.

After completing the 1.5 km sampling pass at 2102Z, the aircraft began to ascend. The tops of most of the heavier cumuliform clouds were reached at about 12,500 ft (3.8 km), although there was a higher layer based near 16,000 ft (4.9 km) and cirrus at a higher level.

At 2141Z, the aircraft landed at Little Rock, AFB, Arkansas. A more thorough listing of mission director comments during the flight is given in Appendix B.

### 5.3 Sampling Data: 2 March

#### 5.3.1 TEMPORAL VARIATIONS DURING FLIGHT

In contrast to the 1 March flight, which began sampling at the lower levels, the 2 March sampling began at a higher level and moved down. The flight profile, with reference to altitude and outside air temperature, is shown in part a of Figure 18.

After reviewing the mission director's comments, the 16mm movie film from the nose camera, and the PMS 2-D shadowgraph data it was decided to make LWC calculations based on the AFGL "length to diameter" particle-type equations in Table 5. The method of making these calculations and the empirical values used are as outlined in Section 3.

Table 5. Predominant Particle Types During Periods Indicated on 2 March

Time	Type
1900:00 to 1928:59	Bullet Rosettes
1929:00 to 1935:59	Small Snow
1936:00 to 1924:59	Large Snow
2025:00 to 2059:59	Rain

As shown in the b portion of Figure 18, the LWC values between approximately 1910 and 1912Z were near or slightly less than  $5 \times 10^{-3} \text{ g/m}^3$  while hazy cirrus was being recorded at 25,000 ft (7.7 km). This value increased about one order of magnitude at 1924Z when heavier altocumulus or cirrocumulus was being recorded.

In the heavier cloud penetrated at 10,000 ft (3.0 km) the LWC varied extensively for the first 20 minutes, but averaged slightly less than  $10^{-1} \text{ g/m}^3$ . During the period from approximately 2012 to 2021Z the mean was approximately  $0.5 \text{ g/m}^3$  and the maximum for a 20-sec sample at 2017Z was slightly more than  $0.9 \text{ g/m}^3$ . At the lowest level sampled, 5000 ft (1.5 km) the LWC in the continuous rain was found to vary about a mean near  $3 \times 10^{-1} \text{ g/m}^3$ .

The values of median volume diameter shown in Figure 18, part c varied from approximately  $150 \mu\text{m}$  at 25,000 ft to more than  $1800 \mu\text{m}$  in the large-snow regime near 3.0 km. A value of  $2500 \mu\text{m}$  was calculated for one 20-sec average at 2026Z in rain. The LWC at that time was not extraordinarily high, however, which indicates there were not a large number of these large-size snowflakes. In the rain at the 1.5 km level the  $D_0$  values varied considerably between 300 and  $1500 \mu\text{m}$ .

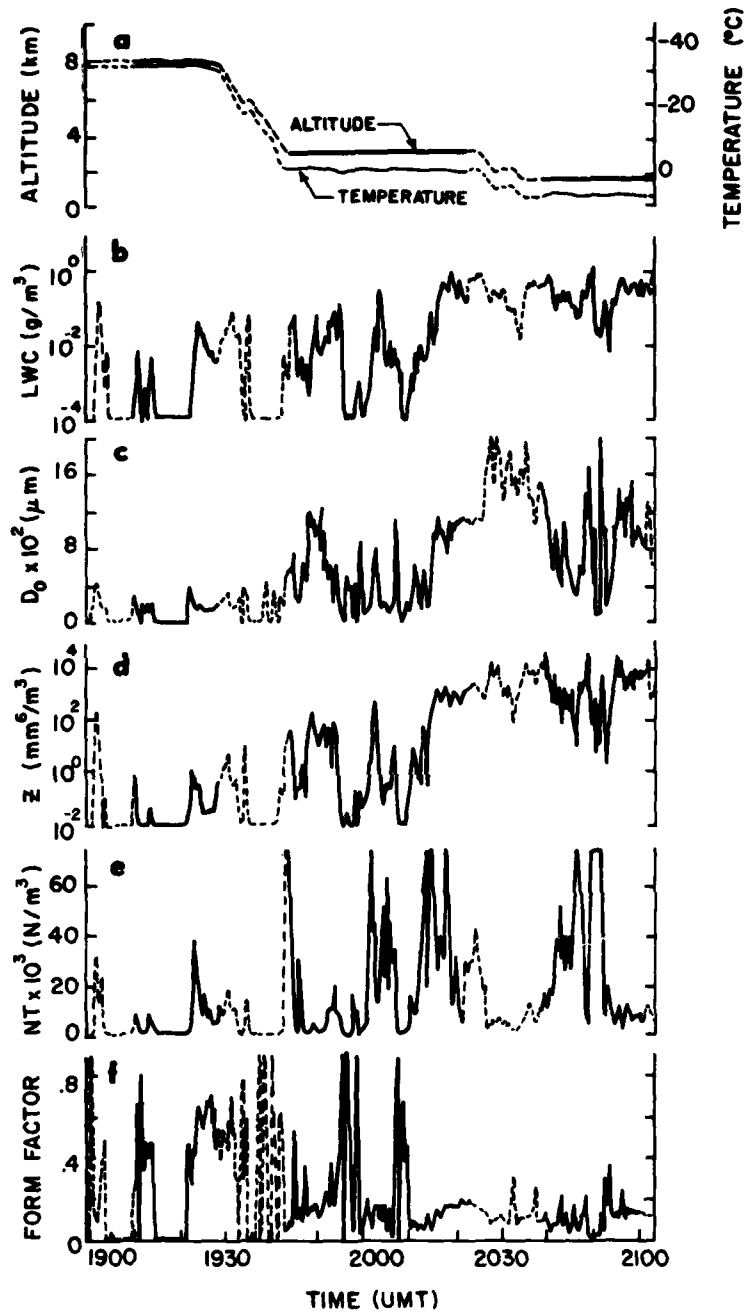


Figure 18. Variation With Time During 2 March 1978 Flight of Several Measured and Calculated Elements Based on Values of Consecutive 20-Second Averages. Solid lines indicate portions of flight for which Data on Figure 19 were prepared

The reflectivity ( $Z$ ) values in part d of Figure 18 varied from  $10^{-2}$  at 7.7 km to near  $10^4 \text{ mm}^6/\text{m}^3$  in the large snow at 3.0 km and the rain at 1.5 km. Values between 100 and 10,000 were common at the lower level.

In the mostly cloud-free air at 7.7 km the total number of particles counted was usually small. In the relatively thin clouds that were encountered values of NT were generally less than  $10^4/\text{m}^3$ . The part e of Figure 18 shows the great variation in the number of particles that were counted throughout this flight. At both 3.0 and 1.5 km NT occasionally jumped to values in excess of  $75,000/\text{m}^3$ , the highest values shown in part e. However, more common values were near  $25,000/\text{m}^3$ .

During the relatively brief periods when heavier cirrostratus or altostratus cloud particles were recorded at 7.7 km, the form factor reached values between 0.50 and 0.65 as shown in the part f of Figure 18. It was noted, however, that at about 1912Z, when very thin, wispy cirrus filaments were sampled, that the form factor was near 0.45. The difference in the spectra was that the heavier cirrus clouds had a few more larger particles (max size  $1100 \mu\text{m}$ , vs  $470 \mu\text{m}$ ) and they also had the valley-peak feature for sizes less than  $300 \mu\text{m}$  that was seen in the 1 March spectra for the same altitude. The thin cirrus did not display this anomaly and the spectra were closer to having straight-line exponential distribution.

At the two lower levels, the form factor was generally less than 0.20 (excluding short times when NT was small and the data, therefore, less representative). Experience indicates these small values are correlated with spectra showing many particles as large as 4000 to 5300  $\mu\text{m}$ .

### 5.3.2 CLASS VALUES OF DATA FROM THREE PASSES

Histograms similar to those in Section 4.3.2 were prepared for 2 March for periods when the aircraft was in relatively homogeneous, continuous cloud conditions at the three main sampling altitudes. Selection of extended time periods was not difficult at the two lower levels, 3.0 and 1.5 km, but at 7.7 km there was a slight problem because the aircraft was in clear air for much of the overall pass. The 18-minute period selected at 7.7 km includes considerable data for zero- or near-zero values when the sampling was being done outside any clouds. The times chosen for further examination of the three levels are given in Table 6.

The problem with lack of widespread cloud at 25,000 ft is shown in the high percentages in each of the extreme left-hand classes of the row on Figure 19 that reflect 7.7 km data. It should be repeated that the mean values printed and shown as vertical lines on each graph reflect only non-zero data, that is, times when the aircraft was in at least thin cloud.

Computed liquid water content is shown on Figure 19 to be slightly greater in the rain at 1.5 km than at 3.0 km in the region of large snowflakes. The LWC

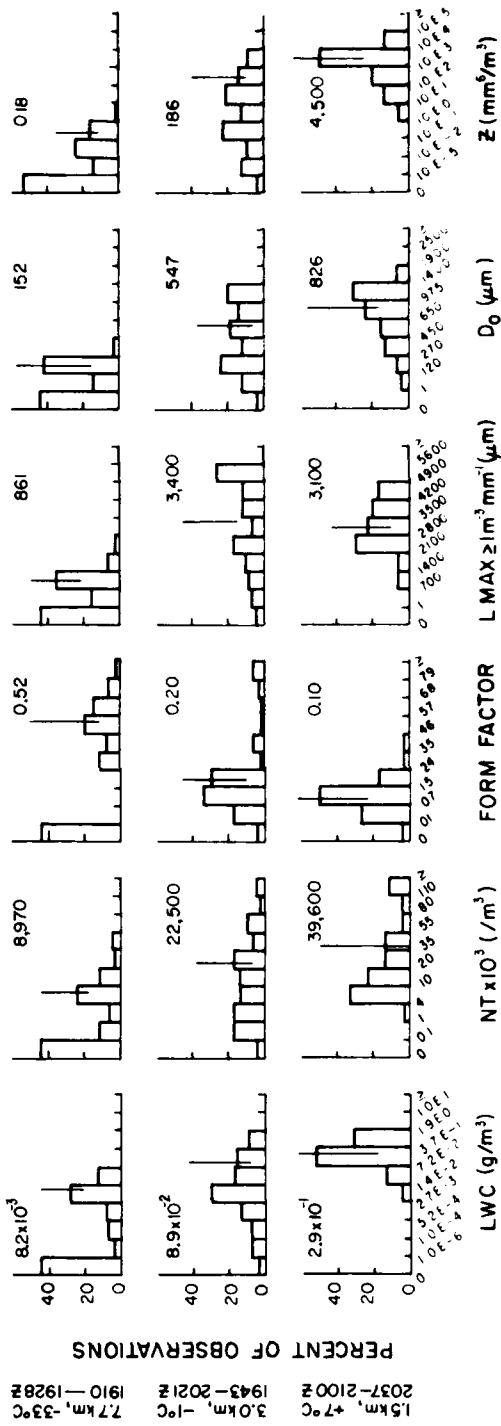


Figure 19. Percent Frequency by Class of Six Measured or Calculated Variables on 2 March 1978 Based on Total Number of 20-sec Mean Values in Overall Pass. Printed numbers and vertical lines are at 50 percentile values. These do not consider data in cloud-free areas

Table 6. Sampling Passes - 2 March

Time (Z)	Duration (min)	Altitude (ft/km)	Ave. Temp (°C)
1910-1928	18	25,000/7.7	-33.4
1943-2021	38	10,000/3.0	- 1.0
2037-2100	23	5,000/1.5	+ 7.0

values are also spread over a wider range at the higher level. At 7.7 km the greatest number of LWC values were in the class between  $2.7 \times 10^{-3}$  and  $1.4 \times 10^{-2}$  g/m<sup>3</sup>. The average LWC at 7.7 km was an order of magnitude less than the corresponding value at 3.0 km.

It is interesting to note the close correspondence of mean LWC values for passes on 1 March and 2 March at roughly corresponding geometric heights. Values at the 7.7 km level were 0.016 and 0.008 g/m<sup>3</sup>, respectively. For the 3.3 km MSL data for 1 March, which was acquired about 1.5 km above ground level, the mean LWC value was 0.30, while the 1.5 km value on 2 March was 0.29 g/m<sup>3</sup>.

The plots of total particle counts, NT, on Figure 19 show that the mean number of particles decreased with altitude from 39,600/m<sup>3</sup> at 1.5 km to 8970/m<sup>3</sup> at 7.7 km. The average values of form factor increased with altitude.

The size of the largest particles, L<sub>max</sub>, on Figure 19 is shown to be slightly larger in the large snow at 3.0 km than in the rain at 1.5 km. Particle mass consolidated in the melting process. The range of recorded maximum sizes is also broader at 3.0 km. On both 1 and 2 March the predominant size range of L<sub>max</sub> at 7.7 km was between 700 and 1400 μm.

The median volume diameter of particles, D<sub>0</sub>, on Figure 19 is less in the snow at 3.0 km than in the rain at 1.5 km. The range of individual samples at both levels, however, is quite broad. The subject of the D<sub>0</sub> and LWC determined near and below the freezing level will be further discussed in Section 7. The mean reflectivity value is much less in the 2.9-km snow region than in the rain at 1.5 km.

### 5.3.3 OBSERVED PARTICLE DISTRIBUTIONS

The figures in this section were selected as being "representative" of typical conditions at the various levels sampled on 2 March 1978 in the Little Rock-Memphis area. They were chosen after reviewing both Figures 18 and 19 in an effort to determine not only mean values, but also modal ones.

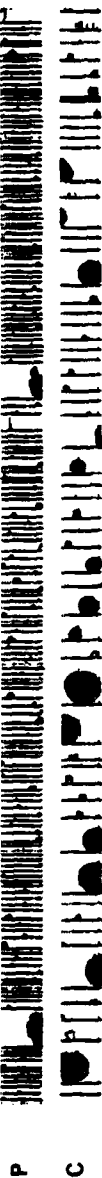
The data and graph on Figure 20 reflect spectral and microphysical conditions in the rain at 1.5 km. The data on this figure were recorded during the 100 seconds

FLT E78-85 02 MAR 78 20 SECOND AVERAGING

START TIME	TEMP C	ALT KM	LWC G/M <sup>3</sup>	Z MM	DW N/M <sup>3</sup>	NT N/M <sup>3</sup>	FF SLOPE /MM	INTERCEPT N/M <sup>3</sup> -MM	C.O.D.	AVE DEPT	LWC X CLD	LMAX UM	PART TYPE
20:40:46	6.7	1.5	.3855	1.3E+03	437	52684	.67	1.88E+04	.9908	1.5565	24	2726	R
20:41:00	6.7	1.4	.1813	8.8E+01	389	31662	.21	7.93E+04	.9894	.4126	34	1835	R
20:41:20	6.8	1.4	.2564	1.4E+03	451	41047	.66	1.52E+04	.9886	1.9109	20	3023	R
20:41:40	6.8	1.4	.2958	1.6E+03	1829	24831	.69	1.43E+04	.9867	.8438	3	3023	R
20:42:00	6.8	1.4	.1882	3.4E+02	619	32648	.11	3.16E+04	.9979	1.8655	14	2132	R

TOT TIME MEAN AND STANDARD DEVIATIONS

TIME	MEAN	STANDARD DEVIATIONS
00:01:46	6.7	1.4
00:01:46	.6	.6523
	6.7	9.8E+02
	6.5E+02	225
	3.6572	.11
	3.19E+04	.9907
	1.1579	19
	.5270	16
	.482	



PARTICLE SIZE DISTRIBUTION (N/M<sup>3</sup>-MM)

SIZE (UM)	SCATTER PROBE	SIZE (UM)	CLOUD PROBE	SIZE (UM)	PRECIP PROBE
2	6.99E+08	23	5.19E+04	485	9.28E+03
4	5.29E+09	43	1.28E+06	648	9.77E+02
6	1.05E+10	63	7.27E+04	945	3.16E+02
7	1.04E+10	83	1.48E+04	1242	6.83E+01
9	7.48E+09	103	1.39E+04	1539	2.87E+01
11	5.47E+09	122	2.18E+04	1836	7.83E+00
13	3.57E+09	142	2.52E+04	2133	2.43E+00
15	3.25E+09	162	2.79E+04	2430	1.47E+00
16	1.77E+09	182	4.88E+04	2727	1.57E+00
18	6.58E+08	202	4.46E+04	3024	1.28E+00
20	2.71E+08	221	4.41E+04	3321	0.
22	8.93E+07	241	5.88E+04	3618	0.
23	5.29E+07	261	3.97E+04	3915	0.
25	3.98E+07	281	3.36E+04	4212	0.
27	6.29E+07	301	2.72E+04	4509	0.

LWC 5.09E-02 4.52E-02 2.89E-01

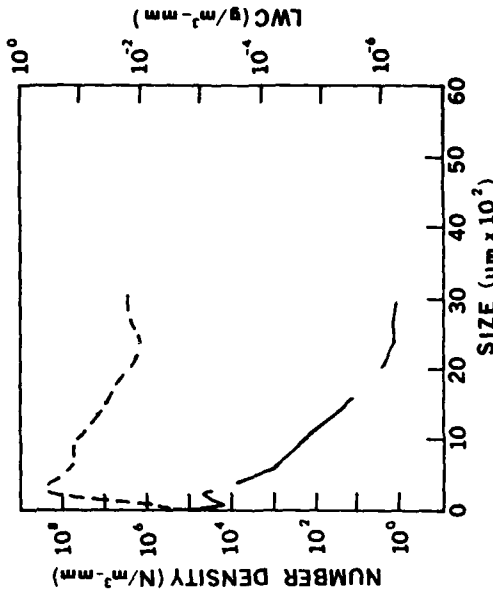


Figure 20. Representative Cloud Data for 5000 ft (1.5 km) MSL Sample on 2 March 1978

beginning at 2040:40Z. The computed slope of the particle distribution was  $-5.0/\text{mm}$  and the  $N_0$  intercept was  $32,000 \text{ m}^{-3} \text{ mm}^{-1}$ . During extended periods of rain, Joss et al<sup>26</sup> found the slope of particle distributions varied from  $-0.6$  to  $-7.0/\text{mm}$  and that  $N_0$  values were between 300 and  $100,000 \text{ m}^{-3} \text{ mm}^{-1}$ . Joss and Waldvogel<sup>38</sup> later indicated that  $N_0$  frequently ranges from 1400 in thunderstorm rain to approximately  $30,000 \text{ m}^{-3} \text{ mm}^{-1}$  in drizzle. Accordingly, the aircraft, at 1.4 km altitude, was in a drizzle type of precipitation, which was precisely that reported by several ground stations in the area. A minimum in the cloud probe portion of the Figure 20 spectrum is present at about  $90 \mu\text{m}$ , and a maximum near  $240 \mu\text{m}$ . These are the same approximate locations where a valley-hill effect was seen in the 25,000 ft (7.7 km) data on Figure 12. This will be discussed in Section 7.

Some 19 percent of the total calculated liquid water content of the Figure 20 spectrum was a result of particles in the 23-301  $\mu\text{m}$  range of the cloud probe. The rest was due to particles as large as 3000  $\mu\text{m}$ .

At 3.0 km the aircraft apparently penetrated at least two different precipitation areas with very few particles recorded between them. The size of particles in the first area was less than in the second, although the number of particles in each was approximately the same or slightly greater for the small sizes. The two different intensities of precipitation are reflected in Figure 19 in the two modal classes in some of the histograms for the 3.0 km data.

Conditions representative of the lighter precipitation area are given in Figure 21 and those for the heavier precipitation in Figure 22. The mean LWC in the first case is 0.006 and in the latter 0.250  $\text{g}/\text{m}^3$ . The mean volume diameter,  $D_v$ , of the light case is less than one-half that of the heavy case. The slopes of the spectral distributions are  $-2.3$  and  $-0.6/\text{mm}$  for the light and heavy precipitation, respectively, while the  $N_0$  intercepts are about 1000 and 700.

The general shape of the heavy precipitation spectrum in Figure 22 resembles the Figure 10 data for the previous day at 3.3 km MSL. One difference, however, is the dip in the spectrum near  $100 \mu\text{m}$  that was not reflected on Figure 10. Both spectra for relatively low levels in the atmosphere display a strong increase in the number of small particles ( $< 1000 \mu\text{m}$  in size) with respect to the larger sizes which have an approximate straight-line distribution. This upturn in the small particle parts of the spectra is reflected in the large "average departure" which is near 4.0 for both figures.

The dashed line on the graph in Figure 21 shows that the number of  $1200 \mu\text{m}$ -sized particles makes the most significant contribution to the total liquid water

38. Joss, J. and Waldvogel, A. (1969) Raindrop size distribution and sampling size errors, *J. Atmos. Sci.* 26:566-569.

FLT E78-85 02 MAR 78 20 SECOND AVERAGING

START TIME	TEMP C	ALT KN	LWC G/M**3	Z	D0	NT	FF SLOPE /MM	INTERCEPT N/M**3-MM	C.O.D.	AVE DEPT	LWC % CLD	LMAX UM	PART TYPE
20:09:40	-7	3.0	.0081	4.4E+00	598	8983	.68	3.44E+02	.9494	3.2892	6	3158	LS
20:10:00	-8	3.0	.0099	5.3E+00	475	7088	.10	1.41E+03	.9479	1.6739	8	3848	LS
20:10:20	-7	3.0	.0043	1.3E+00	450	14301	.06	6.20E+02	.9837	3.2253	17	2813	LS
20:10:40	-7	3.0	.0044	8.0E-01	225	20908	.06	6.35E+02	.9937	2.8903	40	2813	LS
20:11:00	-7	3.0	.0052	7.9E-01	366	26048	.07	2.10E+03	.9992	2.0418	22	2123	LS

TOT TIME MEAN AND STANDARD DEVIATIONS

00:01:40	-7	3.0	.0064	2.5E+00	422	15465	.07	1.02E+03	.9748	2.6241	19	2951	
00:01:40	.0	.0	.0022	1.9E+00	123	7143	.01	6.46E+02	.0219	.6506	12	560	



PARTICLE SIZE DISTRIBUTION (N/M\*\*3-MM)

SIZE (UM)	SCATTER PROBE	SIZE (UM)	CLOUD PROBE	SIZE (UM)	PRECIP PROBE
2	9.49E+08	27	0.	466	3.05E+02
4	6.83E+09	50	5.98E+05	744	1.52E+02
6	1.29E+10	73	2.74E+04	1089	8.71E+01
7	1.33E+10	96	9.17E+03	1434	3.49E+01
9	9.88E+09	119	4.85E+03	1779	1.43E+01
11	6.89E+09	142	4.65E+03	2124	5.76E+00
13	4.15E+09	165	7.33E+03	2469	4.46E+00
15	3.61E+09	188	2.68E+03	2814	1.19E+00
16	2.18E+09	211	2.88E+03	3159	9.58E-01
18	9.35E+08	234	3.55E+03	3504	3.39E-01
20	5.53E+08	257	4.41E+02	3849	3.71E-01
22	2.94E+08	280	1.93E+03	4194	0.
23	1.97E+08	303	1.05E+03	4539	0.
25	1.23E+08	326	5.75E+02	4884	0.
27	1.62E+08	349	4.98E+02	5229	0.

LWC	7.04E-02	1.01E-03	5.36E-03
-----	----------	----------	----------

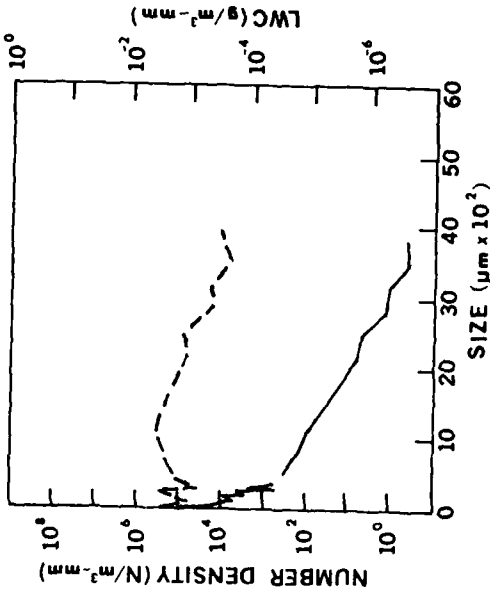


Figure 21. Representative Cloud Data for Light Precipitation Portion of 10,000 ft (3.0 km) MSL. Pass on 2 March 1978

FLT E78-85 #2 MAR 78 20 SECOND AVERAGING

START TIME	TEMP C	ALT MH	LWC G/MH**3	Z MH**6/H**3	D0 MU	NT M/H**3	FF SLOPE /NH	INTERCEPT N/H**3-NH	C.O.D.	AVE DEPT	LWC X CLD	LMAX UH	PART TYPE
20:18:40	-1.0	3.0	.2800	6.9E+02	1044	15930	.16	1.29E+03	.9382	3.6141	3	5228	LS
20:19:00	-0.8	3.0	.2014	5.4E+02	1067	10521	.16	7.53E+02	.8718	3.5851	2	5228	LS
20:19:20	-0.7	3.0	.2178	6.8E+02	1107	10928	.16	5.17E+02	.9754	4.0976	2	5228	LS
20:19:40	-0.8	3.0	.1433	3.8E+02	1092	5557	.19	4.12E+02	.9347	3.5417	2	5228	LS
20:20:00	-1.0	3.0	.1828	5.3E+02	1140	7158	.18	4.22E+02	.8792	3.9003	2	5228	LS

TOT TIME MEAN AND STANDARD DEVIATIONS

00:01:40	-0.8	3.0	.2051	5.5E+02	1089	10018	.17	6.78E+02	.9181	3.7478	2	5228	
00:01:40	.1	.0	.0450	1.0E+02	33	3580	.01	3.29E+02	.0410	.2156	0	0	



PARTICLE SIZE DISTRIBUTION (N/H\*\*3-NH)

SIZE (MU)	SCATTER PROBE	SIZE (MU)	CLOUD PROBE	PRECIP PROBE
2	7.13E+06	27	2.81E+05	466
4	2.72E+07	50	5.19E+04	744
6	2.67E+07	73	6.45E+04	1089
7	3.14E+07	96	1.34E+04	1434
9	3.60E+07	119	2.47E+04	1779
11	3.71E+07	142	2.20E+04	2124
13	3.52E+07	165	3.13E+04	2469
15	4.11E+07	188	3.05E+04	2814
16	4.01E+07	211	2.45E+04	3159
18	3.17E+07	234	2.55E+04	3504
20	3.11E+07	257	2.10E+04	3849
22	2.75E+07	280	1.60E+04	4194
23	2.52E+07	303	1.35E+04	4539
25	2.27E+07	326	1.20E+04	4884
27	2.13E+07	349	1.02E+04	5229
LWC	2.15E-03		5.71E-03	1.99E-01

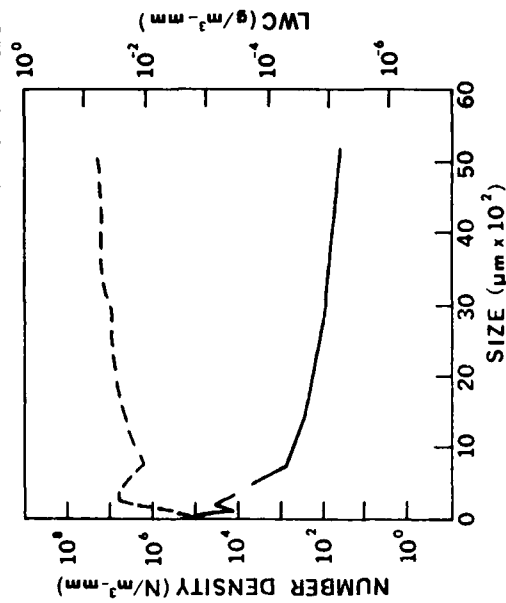


Figure 22. Representative Cloud Data for Heavy Precipitation Portion of 10,000 ft (3.0 km) MSL Pass on 2 March 1978

content. The curve falls toward both smaller and larger sizes from that point. In the heavier precipitation represented on Figure 22, all particle sizes between approximately 1200 and 5200  $\mu\text{m}$  make about equal contributions to the total LWC calculated from the spectrum.

Approximately 40 percent of the flight time at 25,000 ft (7.7 km) MSL was through cloud-free air. While in clouds at that altitude, however, the spectral data on Figure 23 were quite representative according to the modal and mean values shown at the top of Figure 19.

One of the striking features of the graphed data in Figure 23 is the similarity to the data and plot on Figure 12. Both apply to clouds observed at 7.7 km. Both have a mean LWC less than  $1 \times 10^{-2} \text{ g/m}^3$ ,  $D_o$  near 160  $\mu\text{m}$ , and an  $L_{\text{max}}$  near 900  $\mu\text{m}$ . Additionally, both reflect the minimum-maximum points near 100 and 250  $\mu\text{m}$  that have been previously mentioned.

## 6. WEATHER AND FLIGHT DATA -- 3 MARCH 1978

### 6.1 Synoptic Situation

As the area of large-scale cloudiness moved east and northeast, a location off the coast of Delaware was selected for sampling on the third day of this program. Specifically, flying was conducted between two navigation points, Shads and Tunna, which are about 140 miles east of Wallops Island and Cape May, respectively. This coastal area was just east of a stationary front that was shown on the 3 March 1200Z analysis to extend southwestward through northern Florida across into northern Mexico and northward into Colorado and Utah.

By 1800Z there was a low pressure wave on the front along the coastal Carolinas as shown in Figure 24, part a. This wave deepened and continued moving northeastward quite rapidly. By 4 March 00Z it had formed a major low just off the coast of New Jersey. The small low over western Pennsylvania at 1800Z also moved east to consolidate with the New Jersey system by 00Z. Radar data (not shown) indicated strong shower activity in the vicinity of the developing low.

The combined frontal lifting and on-shore flow resulted in moderate precipitation in the eastern and northeastern coastal states as shown in part b of Figure 24. Moderate snow was the rule north and west of central New Jersey while rain was abundant in Delaware, Maryland and coastal Virginia.

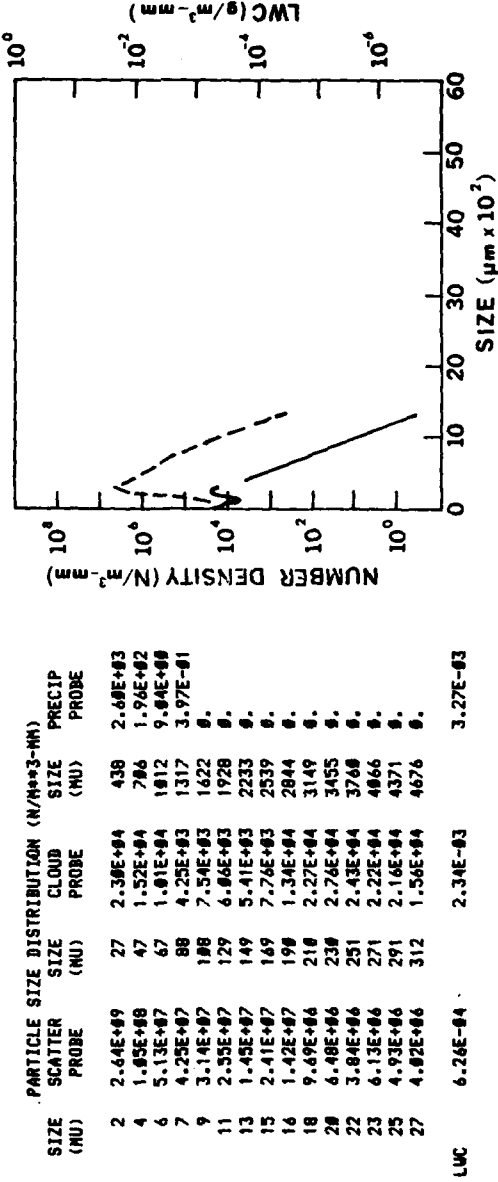
The nephanalysis in Figure 24, part c provides a generalized view of the widespread cloudiness that existed over the entire eastern US on 3 March. Cumulus and stratocumulus were predominant types with widespread higher cirriform clouds.

FLT E78-85 #2 MAR 78 20 SECOND AVERAGING

START TIME	TEMP C	ALT KH	LUC G/M <sup>3</sup>	Z MH <sup>3</sup>	D09 NU	NT N/M <sup>3</sup>	FF /MH	SLOPE /MH	INTERCEPT N/M <sup>3</sup> -MH	C.O.D.	AVE DEPT	LWC X CLD	LMAX UN	PART TYPE
19:26:28	-32.9	7.7	.0035	1.7E-02	114	5791	.68	I	I	I	I	68	786	BR
19:26:48	-32.9	7.7	.0041	2.8E-02	129	4544	.69	I	I	I	I	67	786	BR
19:27:08	-32.9	7.7	.0037	3.7E-02	137	4134	.58	I	I	I	I	54	1811	BR
19:27:28	-32.7	7.7	.0057	5.9E-02	146	4841	.64	I	I	I	I	47	786	BR
19:27:48	-32.5	7.6	.0189	4.3E-01	231	4831	.46	I	I	I	I	11	1316	BR

TOT TIME MEAN AND STANDARD DEVIATIONS

00:01:48	-32.8	7.7	.0056	1.1E-01	151	4816	.61	I	I	I	I	52	889	
00:01:48	.2	.6	.0028	1.6E-01	41	514	.89	I	I	I	I	23	244	



SIZE (MU)	SCATTER PROBE	SIZE (MU)	CLOUD PROBE	SIZE (MU)	PRECIP PROBE
2	2.64E+09	27	2.38E+04	438	2.68E+03
4	1.85E+08	47	1.52E+04	786	1.94E+02
6	5.13E+07	67	1.01E+04	1812	9.84E+00
7	4.25E+07	88	4.25E+03	1317	3.97E-01
9	3.14E+07	108	7.54E+03	1422	0.
11	2.55E+07	129	6.86E+03	1928	0.
13	1.45E+07	149	5.41E+03	2233	0.
15	2.41E+07	169	7.76E+03	2539	0.
16	1.42E+07	199	1.34E+04	2844	0.
18	9.49E+06	218	2.27E+04	3149	0.
20	6.48E+06	238	2.76E+04	3455	0.
22	3.84E+06	251	2.43E+04	3768	0.
23	6.13E+06	271	2.22E+04	4066	0.
25	4.93E+06	291	2.16E+04	4371	0.
27	4.82E+06	312	1.56E+04	4676	0.
LUC	6.26E-04		2.34E-03		3.27E-03

Figure 23. Representative Cloud Data for 25,000 ft (7.7 km) MSL Sample on 2 March 1978

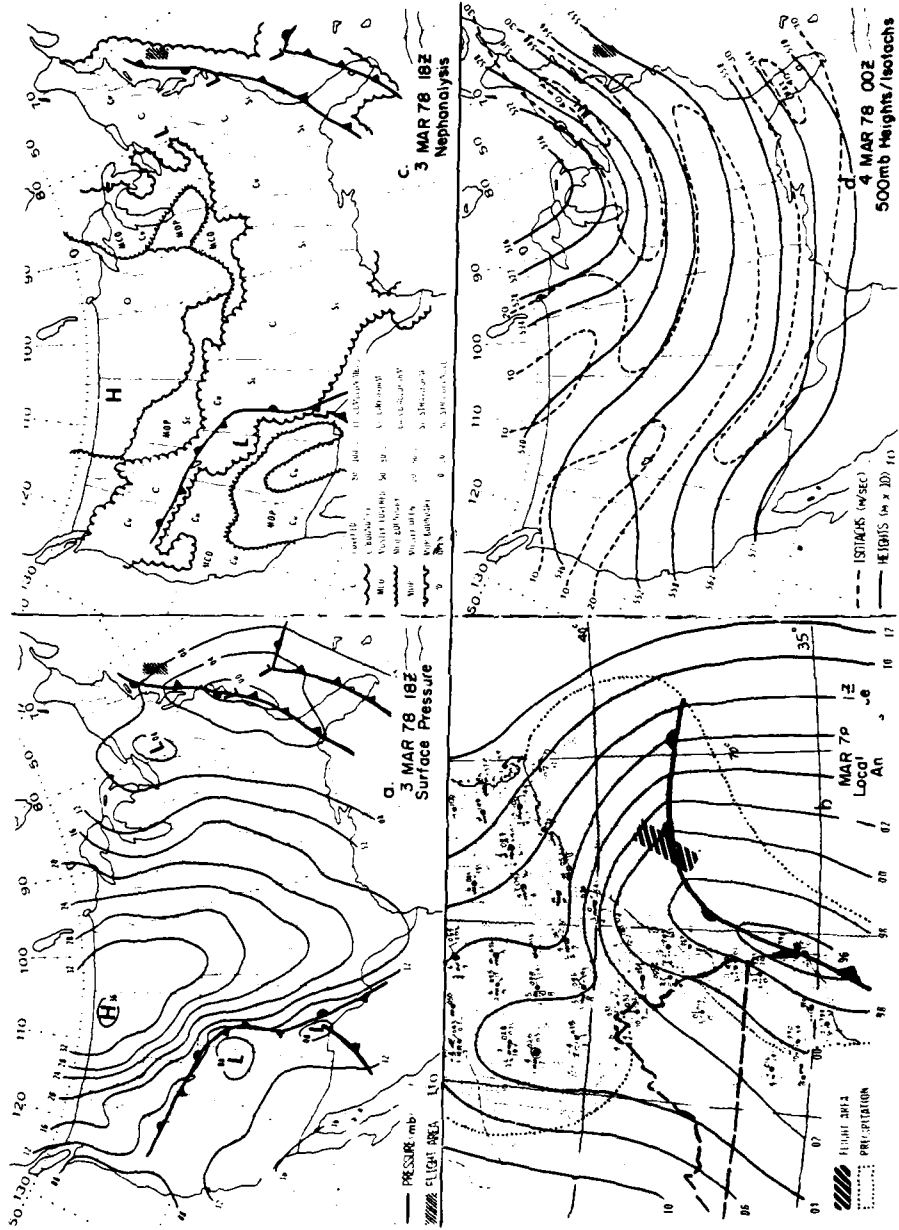


Figure 24. Synoptic Weather Charts for Approximate Time of 3 March Flight. Hatching indicates sampling area

The sampling area selected was generally under the influence of southwesterly winds aloft as shown in part d of Figure 24. The large synoptic-scale trough extending at 500 mb from the Great Lakes to the Gulf of Mexico was responsible for considerable upward motion. This, along with the small temperature-dewpoint spreads all along the East Coast ( $3^{\circ}\text{C}$  or less at 500 mb) contributed to the cloudiness in the middle troposphere.

Other views of the widespread cloudiness are given in the Figure 25a GOES satellite visible picture and in the corresponding infrared picture in Figure 25b. There is little or no indication of curved cloud forms in these pictures that would betray the presence of a classic frontal wave. The frontal clouds were beneath higher layers of cirriform cloudiness. The IR picture shows that the Shads-Tunna sampling area was near the center of a region having the coldest (highest) clouds of any place along the Northeastern Seaboard. The IR cloud top temperatures there were between  $-42$  and  $-52^{\circ}\text{C}$ . These temperatures, according to data on Figure 26 correspond to heights between approximately 8.5 and 10.5 km.

Soundings for Wallops Island before and after the sampling are shown on Figure 26. Conditions were exceptionally moist from the surface to about 8 km at 12Z 3 March. Twelve hours later the volume between 1 and 5 km had become dryer, partially as a result of the surface front moving further east of the location.

Aircraft outside-air temperature data correlated most closely with the 00Z 4 March sounding. The spectral data indicated relatively few particle counts when near 4 km, which agrees with the 00Z sounding showing low humidity (and less cloudiness) at that level.

Both of the Wallops Island soundings are stable in the lowest levels up to about 2 km MSL. Between 5.5 and 8.0 km the stability of the 12Z 3 March sounding decreased to a "potentially neutral" rate where the equivalent wet-bulb temperature curve was parallel to the moist adiabatic rate. The 00Z 4 March sounding was potentially unstable in the dry layer from approximately 2.5 to 4 km. Some degree of instability was actually realized since light turbulence was reported by the C-130.

The freezing level was at the surface at 12Z 3 March, but it rose to near 3 km MSL at 00Z 4 March as a southerly then easterly flow warmed the lowest portion of the atmosphere.

## 6.2 The Flight

The flight mission on 3 March began at Little Rock, Arkansas. The aircraft moved east over Virginia then northeast over coastal waters to the initial sampling point, Shads, at  $37^{\circ}42'\text{N}$ ,  $73^{\circ}00'\text{N}$ . A schematic view of the sampling clouds encountered during the sampling on 3 March is shown in Figure 27.

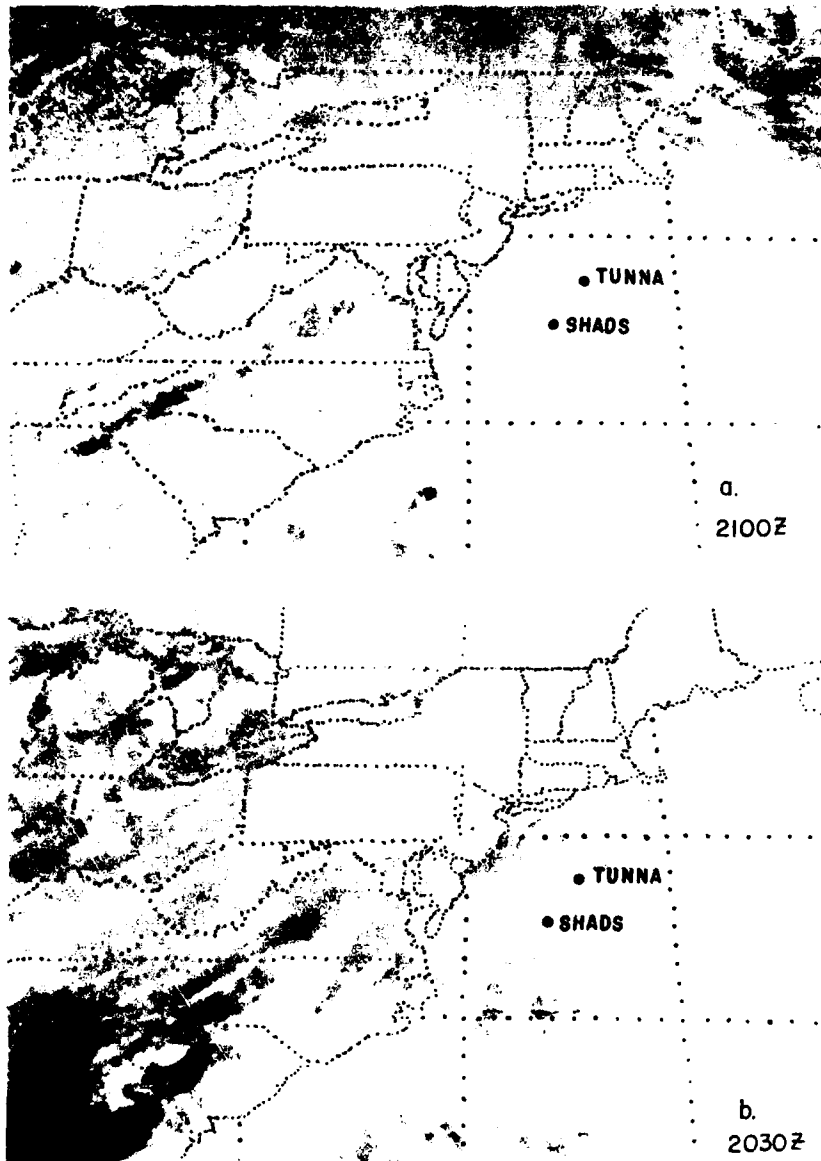


Figure 25. GOES-East Satellite Visible (a) and Infrared (b) Photos of East Coast of U.S. on 3 March 1978. Sampling was conducted between Navigation Points Tunna and Shads

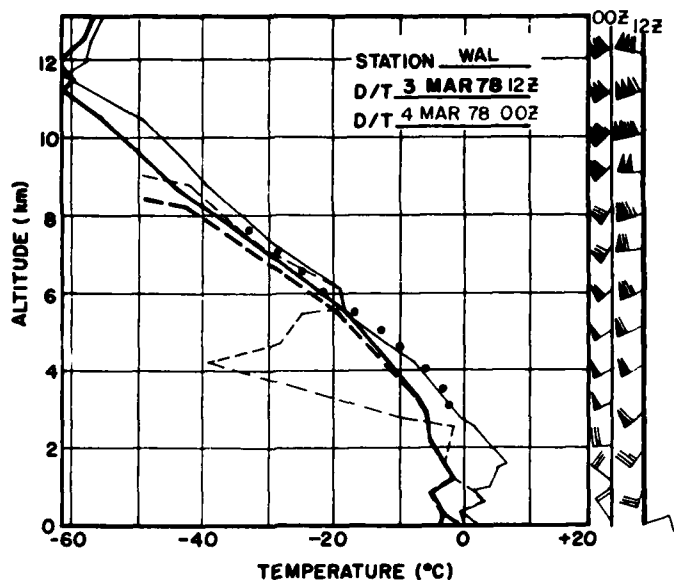


Figure 26. Wallops Island, Virginia Soundings for Times Prior To and After 3 March Sampling Flight. Dots are aircraft-measured temperatures

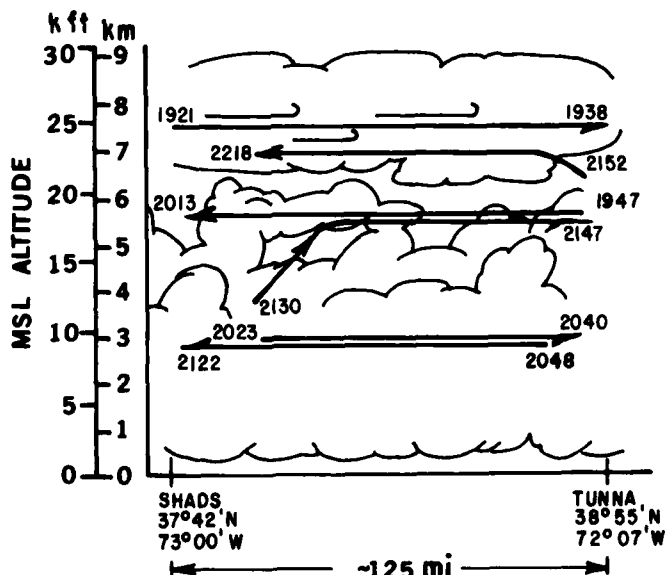


Figure 27. Generalized View of Clouds and Sampling Tracks on 3 March 1978. Main data acquisition was along the passes having the starting and ending times indicated

The first data pass began at Shads at 1921Z (1421L) at 25,000 ft (7.7 km) MSL. As the aircraft flew on a heading of  $020^{\circ}$ , small particles were recorded almost continuously in the cirriform clouds. The sun was moderately bright above, but it was not possible to estimate cloud tops or bases. The mission director commented that the aircraft seemed to be near the base of the cirrus, although this was difficult to judge since there was an undercast of lower clouds. The pass concluded at 1938Z at Tunna at  $38^{\circ}55'N$ ,  $72^{\circ}07'W$ .

The aircraft turned, descended, and began a second pass heading  $235^{\circ}$  from Tunna at 18,300 ft (5.6 km) MSL. Initial clouds encountered were thin with small particles. Occasionally the aircraft appeared to be outside all clouds or moving along the top of a lower layer. Clouds darkened and became more widespread as the flight progressed to the south. After 2003Z the aircraft was in heavy clouds where visibility was very restricted. Cloud conditions were very uniform and no definition of forms or shapes could be seen in any direction. Particle types appeared to be agglomerates. A slight amount of turbulence was noted before the aircraft came out of the cloud at 2012Z. The 5.6 km pass was concluded at 2013Z near Shads where the wind was  $250^{\circ}/50$  kt.

A third horizontal pass to the northeast was begun near Shads at 2023Z at 9900 ft (2.9 km). Particles were mostly large wet snowflakes, but some needles were also observed. The clouds at this level were heavy and uniform. At 2031Z there was 1/4-inch accumulation of particles on the snow stick. Icing also accumulated on the spectrometer-probe cannisters at about this time. This pass was completed at 2040Z near Tunna, where the wind was measured as  $200^{\circ}/56$  kt at flight level.

The aircraft could not obtain air traffic control approval to descend to a lower level, so a turn was made and a fourth pass commenced near Tunna at 2.9 km MSL in a direction approximately opposite to the pass just completed. The heading was  $220^{\circ}$  back toward Shads. The aircraft continued in solid, uniform clouds where an assortment of particle types was noted and light rime icing occurred. At 2051Z both 2-D spectrometer probes were overloaded with a large number of particles.

At 2112Z the recording tape of the 1-D spectrometer system ran out and could not be replaced for a few minutes. This resulted in a gap in the data output which will be noted in Figure 28. Some rain was observed for brief periods, but the predominant particle type was large snow. The fourth pass was concluded at 2122Z a few miles from Shads, and a climbing turn was made to the next level.

A fifth sampling period was begun a few miles north of Shads as the aircraft climbed past 12,000 ft (3.7 km) MSL through large snow flakes. By 2136Z the C-130 began horizontal flight toward Tunna at 18,300 ft (5.6 km). This level was near the top of an altocumulus layer and the aircraft was occasionally outside of most visible clouds, although it concluded the pass at 2147 just after passing through solid, heavy clouds that had LWC values in excess of  $1 \text{ g/m}^3$ .

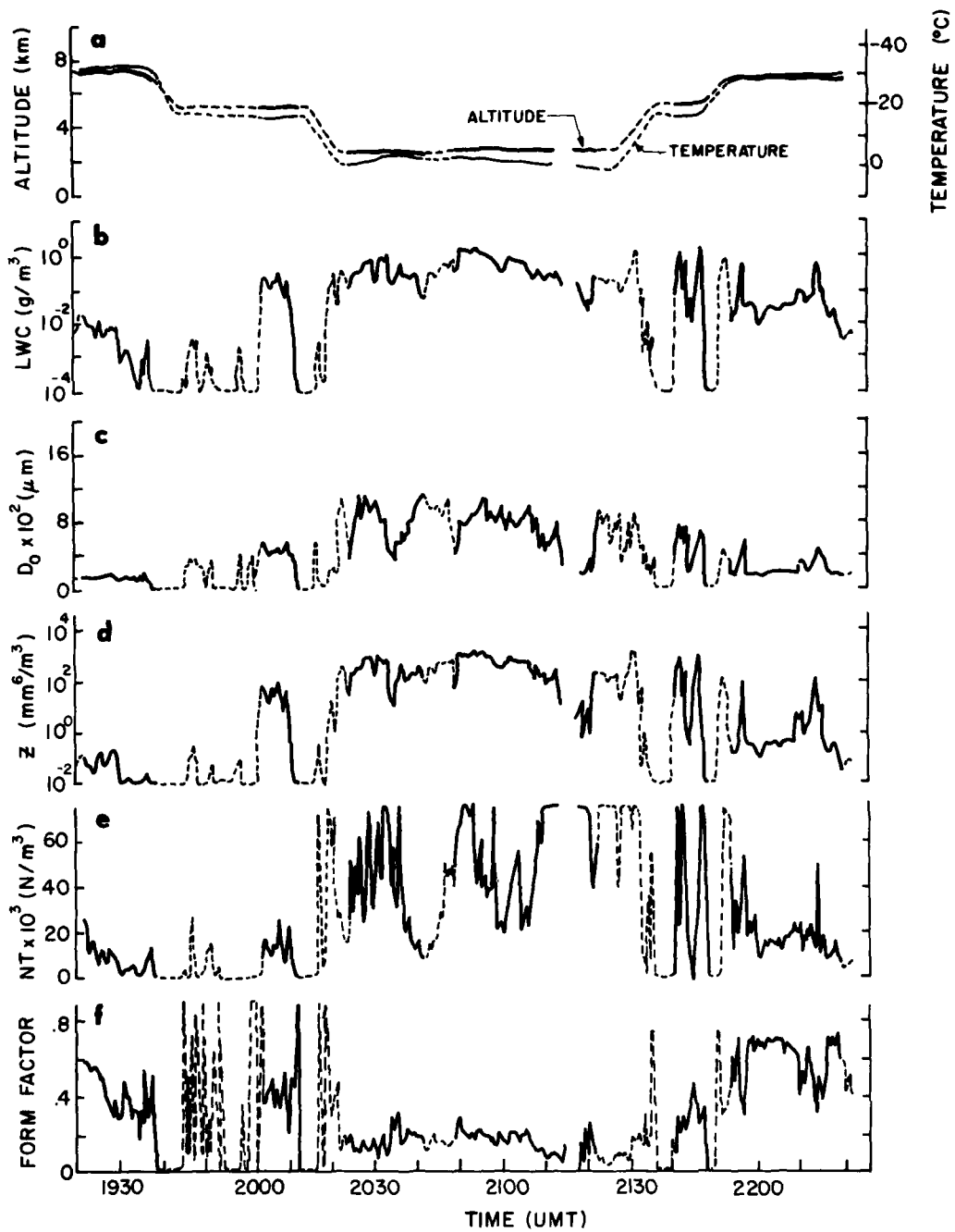


Figure 28. Variation With Time During 3 March 1978 Flight of Several Measured and Calculated Elements Based on Values of Consecutive 20-Second Averages. Solid lines indicate portions of flight for which data on Figure 29 were prepared

The high LWC values and large ice-particle concentrations found in the latter part of the second 5.6-km pass suggested the existence of an intense generating cell. The dry air intrusion, seen in the 4 March 00Z sounding (on Figure 26) at 4 km MSL, may have been responsible for the creation of both turbulence and increased numbers of precipitation particles. This would agree with Wexler and Atlas,<sup>39</sup> who believed some types of generating cells are created when advection of dry air aloft ahead of an upper-level trough forms a convectively unstable layer. This, in turn, can change a uniform, generally stratified cloud area into a more cellular one.

The existence of precipitation generating cells in the 3 March cloud system should perhaps have been anticipated considering the potential for atmospheric instability and the proximity of the frontal system. Houze et al<sup>2</sup> also found what appeared to be small precipitation-generating cells in studying rainbands in an occluded frontal system on the West Coast.

A final sampling pass was begun near Tunna at 2152Z at 22,000 ft. By 2154Z, level flight was attained at 23,600 ft (7.2 km) MSL. The flight continued at this altitude on a heading of 230° in what was believed to have been a uniform, solid cirrus layer. The mission director noted that during the previous 25,000 ft sampling that the cirrus was not this low. The sampling at this level was concluded at 2218Z near Shads and the aircraft continued to the southwest to land at Langley AFB, Virginia at 2326Z (1826L) near sunset.

A transcription of most of the flight comments is given in Appendix C.

### 6.3 Sampling Data: 3 March

#### 6.3.1 TEMPORAL VARIATIONS DURING FLIGHT

The PMS 1-D data tapes for this flight were processed using appropriate melting equations (in Section 3) for the times and particles types in Table 7. The predominant types were determined after a review of both the 2-D shadowgraph data and the mission director's comments.

The variations of the various elements determined from the 1-D probe and other data during the flight are shown in Figure 28. Also shown in part a of that figure are the variations during the flight of altitude and of aircraft-measured outside air temperature. Sampling was conducted primarily on the "plateaus" shown on part a at approximately 7.7 km (25,000 ft), 5.5 km (18,000 ft), 2.9 km (9,900 ft), 5.6 km (18,300 ft) and 7.2 km (23,600 ft).

The b part of Figure 28 indicates values of liquid water content at 7.7 km were fairly consistent in the  $10^{-4}$  to  $10^{-2}$  g/m<sup>3</sup> range. Values at 5.5 km (when in cloud)

39. Wexler, R. and Atlas, D. (1959) Precipitation generating cells, J. of Meteor. 16:327-332.

Table 7. Predominant Particle Types During Periods Indicated on 3 March

Time	Type
1920:00-1939:59	Bullet Rosettes
1940:00-2002:59	Small Snow
2003:00-2032:59	Large Snow
2033:00-2034:39	Needles
2034:40-2047:59	Large Snow
2048:00-2048:59	Needles
2049:00-2132:59	Large Snow
2133:00-2219:59	Small Snow

were near  $10^{-1} \text{ g/m}^3$ . During most of the sampling at 2.9 km the LWC was in the range of  $10^{-1}$  to  $1 \text{ g/m}^3$ , while a maximum of  $1.5 \text{ g/m}^3$  was recorded at 2051Z in large snow.

During the second pass near 5.6 km an unusually high value of  $1.4 \text{ g/m}^3$  was measured in one sample in the tops of the altocumulus layer at 2140Z. Mean values were slightly less than  $0.5 \text{ g/m}^3$  during that pass. At 7.2 km typical LWC calculations were between  $10^{-2}$  and  $10^{-1} \text{ g/m}^3$ .

Median volume diameters, as seen in Figure 28, part c, ranged from 100 to  $200 \mu\text{m}$  at the highest altitudes sampled to approximately  $1100 \mu\text{m}$  in the large snow at 2.9 km. Reflectivity varied from near 0.01 in the small particles at high altitudes to  $2300 \text{ mm}^6/\text{m}^3$  in the large snow near the freezing level.

The total number of particles per  $\text{m}^3$  in part e of Figure 28 was generally in the 2,000-40,000 range at the sampled altitudes above 5 km, although they periodically reached  $75,000/\text{m}^3$  during the second pass in the cloud tops near 5.6 km. Near 3.0 km NT varied considerably between approximately 25,000 and  $100,000/\text{m}^3$  with a few samples in excess of this. However, during a 5-minute period at about 2038Z, NT was less than  $20,000/\text{m}^3$ .

As reflected in part f of Figure 28 the form factor of various spectra ranged from near 0.60 in high altitude ( $> 5 \text{ km}$ ) clouds displaying the minimum-maximum feature below  $300 \mu\text{m}$  to approximately 0.05 in lower altocumulus having a small spectral slope but a large positive departure in the cloud probe range. Values outside this general range are shown in part f, but the data contributing to their computations are not considered to be sufficient or representative.

It is of interest to note that the large fluctuation in particle counts at 2.9 km had very little effect on the form factors determined at that altitude. This is an indication that the general shapes of the particle spectra remained about the same, regardless of number of particles observed at that level.

### 6.3.2 CLASS VALUES OF DATA FROM SIX PASSES

All or selected portions of the data in the six sampling passes were stratified in the histogram classes that are given in Figure 29. Summarized information on the six passes is given in Table 8. In some cases the time periods selected did not encompass the entire period selected by the mission director. A slightly shorter period was chosen in order to concentrate on cloud data, as opposed to times when the pass was continuing through cloud-free air.

Table 8. Sampling Passes - 3 March

Time (Z)	Duration (min)	Altitude (ft/km)	Ave. Temp ( <sup>o</sup> C)
1921:00-1938:00	17	25,000/7.7	-33.3
2152:00-2218:00	26	23,600/7.2	-29.8
2139:00-2147:00	8	18,500/5.6	-17.9
2003:00-2012:00	9	18,500/5.6	-17.5
2048:00-2121:00	33	9,800/2.9	- 2.9
2023:00-2040:00	17	9,800/2.9	- 3.5

The diagrams on Figure 29 are arranged vertically, with data for the lower atmospheric levels below the data for the higher levels. The two lowest rows of histograms reflect data from 2.9 km, the two middle rows represent 5.6 km, and the two upper rows are for 7.2 and 7.7 km.

The Figure 29 pairs of histograms for a given level show considerable diversity in cloud data. For example, the mean NT values for the two samples at 5.6 km are 10,500 and 46,400/m<sup>3</sup>. This is partially the result of data for two passes at the same levels being acquired a few miles apart and partially due to the dynamic movement and generation of the storm itself between two passes.

The left-most column of histograms on Figure 29 generally shows a decrease of liquid water content with altitude. However, the mean value of one of the 5.6 km samples, that taken between 2139 and 2147Z, is only slightly less than one of the 2.9 km samples. The other calculated or recorded values for that 5.6 km pass also appear greater than might be expected from a consideration of other data. They seem to reflect a passage through a generating area or an extended precipitation shaft.

The greatest mean number of particles/m<sup>3</sup> was observed at the lowest level sampled, 2.9 km. About 16 percent of the samples during one of the 2.9 km passes had NTs greater than  $1.1 \times 10^5/m^3$ , but the greatest values in the other

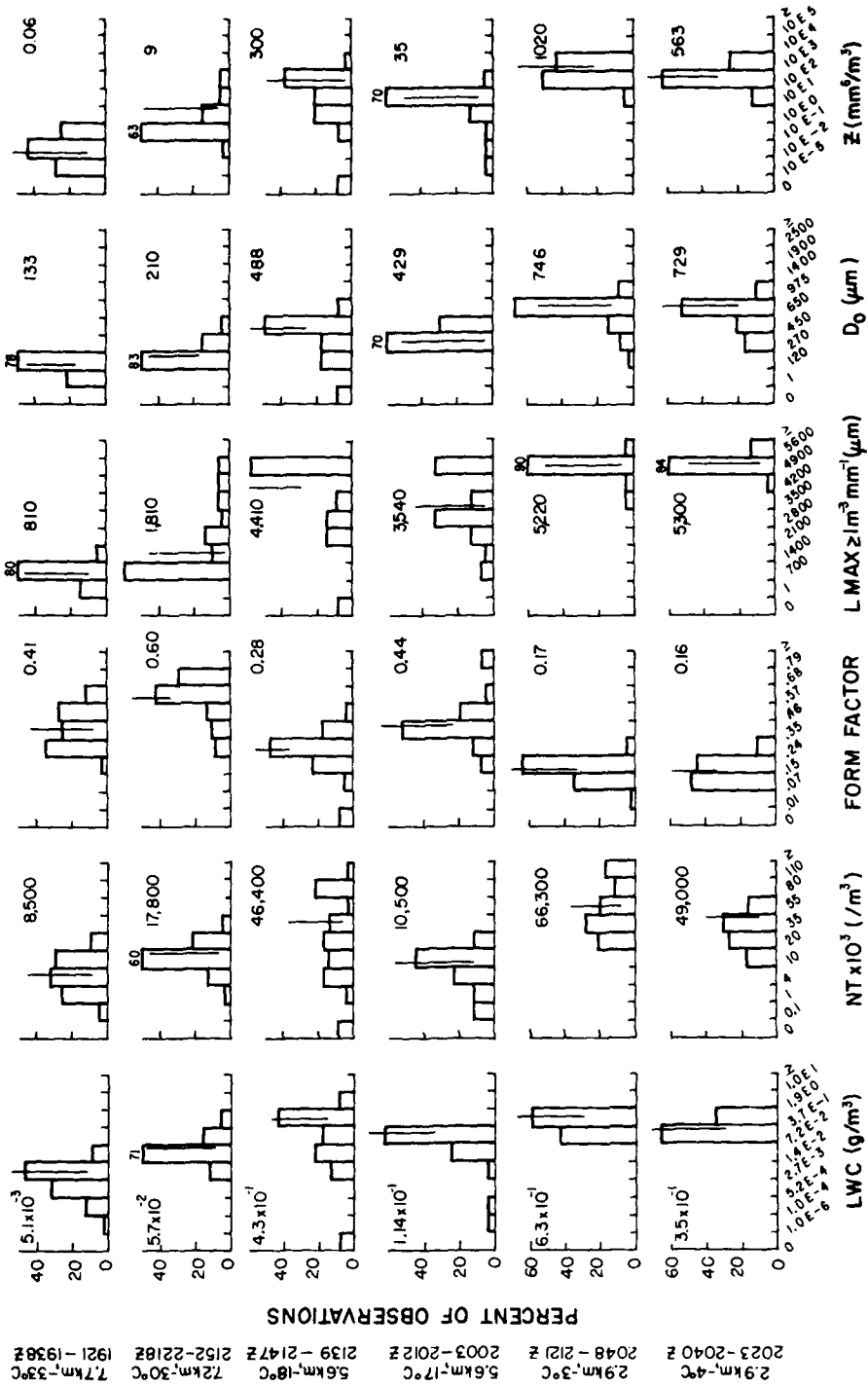


Figure 29. Percent Frequency by Class of Six Measured or Calculated Variables, 3 March 1978 Based on Total Number of 20-sec Mean Values in Overall Pass. Printed numbers and vertical lines are at 50 percentile values. These do not consider data in cloud-free areas

2.9 km pass were less than  $8 \times 10^4/m^3$ . As previously mentioned, there was also considerable difference in the NT spectra between the two passes at 5.6 km. The first pass had a small total and a compact distribution, while the second was larger and spread over a greater number range. The mean NT at 7.2 km was near  $18,000/m^3$  while the smaller mean,  $8500/m^3$  was recorded at the highest level flown, 7.7 km. The mean NT values recorded at 7.7 km varied somewhat on each of 3 days of this flight program, but the modal or predominant number class was the same.

As mentioned in the previous section, and as shown on Figure 29, the form factor calculation did not change significantly at the 2.9 km level. The average value for two samples was 0.16 and 0.17. At 5.6 km, however, the average form factor for the pass through the heavier cloud with larger particles was 0.28 while the average during the pass through the less dense cloud was 0.44. The relatively high 0.60 form factor average at 7.2 km reflects the presence of a maximum in the spectra near 250 to 300  $\mu m$  that was seen previously and will be discussed in a following section. Representative spectra at 7.7 km were similar to those at 7.2 km except that the 250  $\mu m$  peak was less conspicuous. This resulted in a smaller mean form factor at the higher level.

The largest particles recorded during both samples at 2.9 km were 4900  $\mu m$  or larger in at least 84 percent of all cases. Nearly 60 percent were also this large during one of the 5.6 km passes and 30 percent during another. At 7.7 km the mean value of the largest particles was 810  $\mu m$ , while none larger than 2100  $\mu m$  was measured.

The  $D_0$  column of histograms on Figure 29 shows that in general the mean volume diameter increased downward from the highest sampling altitude. The mean value at 7.7 km was approximately 130  $\mu m$ . At 5.6 km the corresponding value was between 430 and 490  $\mu m$ , and at 2.9 km it was between 725 and 750  $\mu m$ .

Reflectivity values again varied considerably from one level to the next with the greatest ones occurring with the greatest precipitable mass. There was also considerable variation in two measurements for the same level. There was an order of magnitude difference, for example, between the mean reflectivities calculated for the two 5.6-km passes. The mean value at 7.7 km was 0.06, which compares to 0.09 and 0.18 for the same level the other 2 days.

### 6.3.3 OBSERVED PARTICLE DISTRIBUTIONS

Based on the histogram plots and mean values on Figure 29, numerous particle size-number spectra and related data were reviewed in a search for "typical" or frequently observed particle distributions on 3 March.

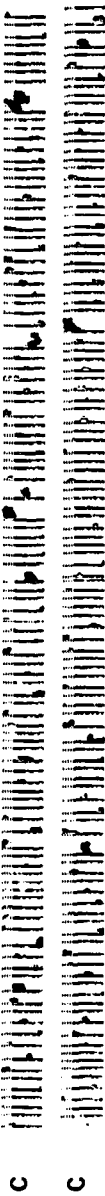
The data on Figure 30 for the 100-sec sample beginning at 1928Z are representative of conditions observed at 7.7 km, the highest level sampled. Approximately

FLI E78-66 03 MAR 78 20 SECOND AVERAGING

START TIME	TEMP C	ALT KH	LUC G/H**3	Z MH**6/H**3	D0 MU	NT N/H**3	FF SLOPE /MH	INTERCEPT N/H**3-MH	C.O.D.	AVE DEPT	LUC X CLD	LMAX UN	PART TYPE
19:28:00	-33.2	7.7	.0071	1.1E-01	159	11184	.38	I	I	I	41	1011	BR
19:28:20	-33.2	7.7	.0082	1.7E-01	166	11446	.36	I	I	I	39	1316	BR
19:28:40	-33.2	7.7	.0087	2.3E-01	172	11461	.32	I	I	I	37	1316	BR
19:29:00	-33.2	7.7	.0064	1.5E-01	172	9948	.31	I	I	I	37	1316	BR
19:29:20	-33.0	7.7	.0086	2.0E-01	175	9326	.38	I	I	I	33	1316	BR

TOT TIME MEAN AND STANDARD DEVIATIONS

00:01:40	-33.2	7.7	.0078	1.7E-01	168	10676	.35	I	I	I	37	1255	
00:01:40	.1	.0	.0009	4.0E-02	5	871	.03	I	I	I	2	122	



PARTICLE SIZE DISTRIBUTION (N/H\*\*3-MH)

SIZE (MU)	SCATTER PROBE	SIZE (MU)	CLOUD PROBE	SIZE (MU)	PRECIP PROBE
2	1.84E+09	27	1.14E+04	438	4.07E+03
4	1.74E+08	47	1.39E+05	706	2.32E+02
6	9.71E+07	67	3.68E+04	1012	1.07E+01
7	7.28E+07	88	2.34E+04	1317	1.16E+00
9	5.04E+07	108	2.40E+04	1622	0.
11	3.49E+07	129	2.08E+04	1928	0.
13	2.19E+07	149	2.40E+04	2233	0.
15	3.04E+07	169	1.54E+04	2539	0.
16	1.71E+07	190	3.12E+04	2844	0.
18	1.21E+07	210	3.34E+04	3149	0.
20	1.22E+07	230	3.07E+04	3455	0.
22	9.28E+06	251	2.93E+04	3760	0.
23	1.16E+07	271	2.38E+04	4066	0.
25	8.01E+06	291	1.97E+04	4371	0.
27	7.02E+06	312	1.58E+04	4676	0.
LUC	9.88E-04		2.94E-03		4.87E-03

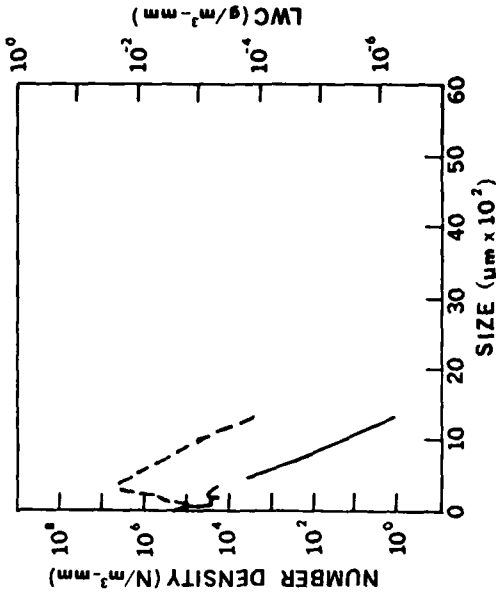


Figure 30. Representative Cloud Data for 25,000 ft (7.7 km) MSL Sampling Pass on 3 March 1978

37 percent of the total calculated water mass of the spectrum in Figure 30 is due to particles in the cloud probe range (27-312  $\mu\text{m}$ ). The greatest contribution to the overall LWC is due to particles approximately 280 to 320  $\mu\text{m}$  in size. The LWC curve falls for sizes both smaller and larger than this range.

The form factor is 0.35 for the Figure 30 spectrum, which is relatively level in particle concentration for sizes from about 100 to 300  $\mu\text{m}$ . The Figure 29 histogram for form factors for the 7.7 km level shows the existence of two modal peaks. About 35 percent of the contributing samples had form factors in excess of 0.46. This is an indication (from experience) that several spectra during the 7.7 km pass had a more pronounced minimum near 100  $\mu\text{m}$  and a maximum near 230  $\mu\text{m}$  than is shown in Figure 30. In other cases, however, when the form factor was less than about 0.40, the slope in the cloud probe range tended to be more an extension of that in the precipitation probe range.

A representative spectrum for the next lower level, 7.2 km, is given in Figure 31. It is similar to the one in the previous figure except that there are now a few more larger sized particles ( $> \sim 1400 \mu\text{m}$ ) and the minimum and maximum phenomena have moved slightly to the right and are centered now near 140  $\mu\text{m}$  and 300  $\mu\text{m}$ , respectively. Aggregation of the smaller sized particles to create larger ones appears to have occurred over a limited portion of the spectrum.

As previously mentioned, there was considerable difference between the data obtained during the two 5.6-km (18,000 ft) passes. A representative sample of data during the second (heaviest) cloud pass is shown in Figure 32. The computed slope of the distribution is a relatively small  $-1.3/\text{mm}$ , while the  $N_0$  intercept value is near 6100. Only 5 percent of the total LWC was determined from cloud probe data, the rest was due to particles larger than about 400  $\mu\text{m}$ .

Figure 33 shows a spectrum of particle data that was recorded during the "light precipitation" pass at 5.6 km. The slope is a steeper  $-2.8/\text{mm}$  and the  $N_0$  intercept is nearly  $58,000/\text{m}^3\text{-mm}$ . The total calculated LWC for this sample is about two-thirds that of the preceding figure.

It is conjectured that the slight peak in particle population on Figure 33 for sizes near 1200  $\mu\text{m}$  is due to the aggregating of smaller crystals. This may be a reflection of the minimum-maximum feature that was seen at smaller crystal sizes at 7.7 and 7.2 km. At the higher levels the maximum was near 280  $\mu\text{m}$ , but as growth continued, the maximum occurred at increasingly larger sizes.

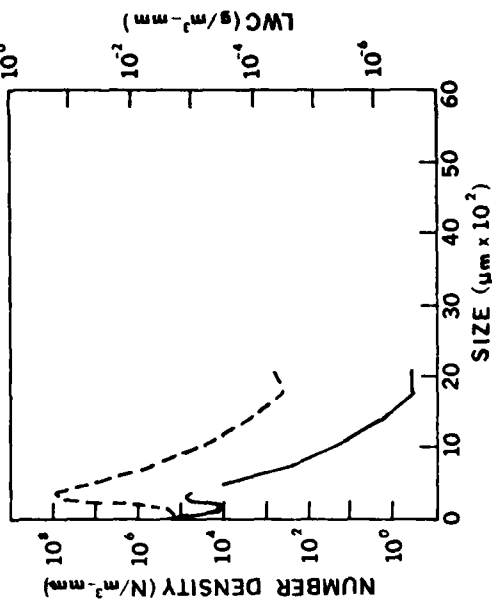
It seems likely that as the aggregation process continues and particles grow larger that the "hump" in the spectrum moves to larger sizes so that the distribution slope becomes smaller with time and distance fallen. If the particles remain at the same level because of strong vertical winds then the change in the distribution with time will occur at that level. The Figure 33 data were recorded in the developing cloud system before those of the Figure 32 data. It is possible then that the

FLT E78-06 03 MAR 78 20 SECOND AVERAGING

START TIME	TEMP C	ALT KM	LUC G/M <sup>3</sup>	Z M/M <sup>3</sup>	D0 M/M <sup>3</sup>	NT N/M <sup>3</sup>	FF /MM	SLOPE N/M <sup>3</sup> -MM	INTERCEPT	C.O.D.	AVE DEPT	LWC % CLD	LMAX UN	PART TYPE
22:00:40	-29.8	7.2	.9388	4.4E-01	168	17560	.67	1	1	1	1	63	2123	SS
22:01:00	-29.7	7.2	.9316	4.9E-01	174	15679	.70	1	1	1	1	57	1433	SS
22:01:20	-29.8	7.2	.9311	4.7E-01	173	15253	.70	1	1	1	1	58	1433	SS
22:01:40	-29.8	7.2	.9288	4.3E-01	172	13684	.72	1	1	1	1	59	1778	SS
22:02:00	-29.7	7.2	.9298	4.4E-01	173	14364	.69	1	1	1	1	58	2123	SS

TOT TIME MEAN AND STANDARD DEVIATIONS

00:01:40	-29.8	7.2	.9303	4.5E-01	171	15388	.70	1	1	1	1	59	1778	
00:03:40	.8	.8	.0012	1.9E-02	2	1322	.02	1	1	1	1	2	308	



SIZE (MU)	SCATTER PROBE	SIZE (MU)	CLOUD PROBE	SIZE (MU)	PRECIP PROBE
2	4.03E+08	27	0.	466	1.14E+04
4	2.05E+08	50	7.36E+04	744	2.85E+02
6	1.60E+08	73	3.18E+04	1089	1.53E+01
7	1.15E+08	96	1.82E+04	1434	1.80E+00
9	8.09E+07	119	1.12E+04	1779	3.82E-01
11	5.95E+07	142	1.11E+04	2124	4.04E-01
13	3.48E+07	165	1.35E+04	2469	0.
15	3.78E+07	188	8.76E+03	2814	0.
16	2.95E+07	211	1.92E+04	3159	0.
18	1.69E+07	234	4.88E+04	3504	0.
20	1.47E+07	257	6.32E+04	3849	0.
22	1.14E+07	280	7.81E+04	4194	0.
23	1.15E+07	303	7.50E+04	4539	0.
25	8.49E+06	326	7.29E+04	4884	0.
27	7.17E+06	349	5.38E+04	5229	0.

LUC 1.23E-03 1.81E-02 1.22E-02

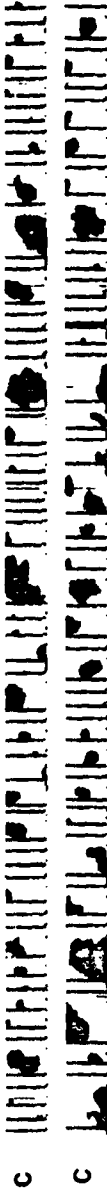
Figure 31. Representative Cloud Data for 23,500 ft (7.2 km) MSL Sampling Pass on 3 March 1978

FLT E78-66 03 MAR 78 20 SECOND AVERAGING

START TIME	TEMP C	ALT KM	LWC G/M <sup>3</sup>	Z M/M <sup>3</sup>	D0 MU	NT N/M <sup>3</sup>	FF SLOPE /MM	INTERCEPT N/M <sup>3</sup> MM	C.O.B.	AVE DEPT	LWC X CLD	LMAX UM	PART TYPE
21:41:00	-18.0	5.6	.6278	4.9E+02	641	52110	.24	-1.0	1.25E+04	.9672	2.0529	2	5228 SS
21:41:20	-18.2	5.6	.1667	5.1E+01	528	9620	.29	-1.5	6.41E+03	.9833	1.0110	2	5228 SS
21:41:40	-18.1	5.6	.4449	3.9E+02	785	33754	.24	-1.9	7.05E+03	.9914	2.3304	2	5228 SS
21:42:00	-18.1	5.6	.0822	5.2E+01	579	7938	.24	-1.2	2.38E+03	.9703	1.5731	3	5228 SS
21:42:20	-17.8	5.6	.0165	3.8E+00	344	4098	.28	-2.1	2.04E+03	.9821	1.7883	19	3848 SS

TOT TIME MEAN AND STANDARD DEVIATIONS

00:01:40	-18.0	5.6	.2556	2.8E+02	559	21503	.26	-1.3	6.08E+03	.9789	1.7511	5	4952
00:01:40	.1	.0	.2382	2.6E+02	122	18520	.02	.4	3.81E+03	.0689	.4489	6	551



SIZE (MU)	SCATTER PROBE		CLOUD PROBE		PRECIP PROBE	
	SIZE (MU)	(MU)	SIZE (MU)	(MU)	SIZE (MU)	(MU)
2	5.51E+07	27	2.15E+05	466	1.68E+04	
4	2.13E+08	50	2.99E+05	744	3.18E+03	
6	2.65E+09	73	9.75E+04	1089	2.82E+03	
7	3.05E+08	96	4.65E+04	1434	1.29E+03	
9	3.33E+08	119	4.12E+04	1779	8.36E+02	
11	3.08E+08	142	3.72E+04	2124	5.66E+02	
13	2.19E+08	165	2.76E+04	2465	3.94E+02	
15	2.44E+08	188	1.74E+04	2814	2.53E+02	
16	1.76E+08	211	2.44E+04	3159	1.85E+02	
18	9.85E+07	234	1.83E+04	3504	1.30E+02	
20	8.99E+07	257	2.47E+04	3849	1.01E+02	
22	6.40E+07	280	1.58E+04	4194	7.51E+01	
23	6.06E+07	303	1.71E+04	4539	3.90E+01	
25	4.94E+07	326	2.63E+04	4884	4.96E+01	
27	4.84E+07	349	1.82E+04	5229	3.85E+01	
LWC	6.85E-03		7.07E-03		2.49E-01	

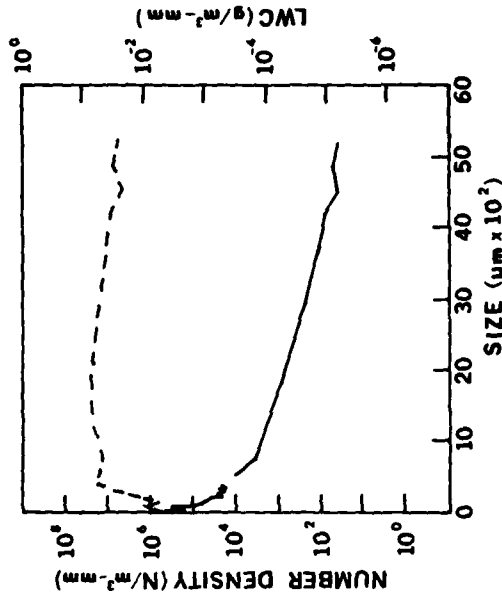


Figure 32. Representative Cloud Data for Large LWC Pass at 18, 500 ft (5.6 km) MSL on 3 March 1978

FLT E78-86 83 MAR 78 20 SECOND AVERAGING

START TIME	TEMP C	ALT KM	LWC g/m <sup>3</sup>	Z	D <sub>0</sub> M	NT	FF SLOPE /MM	INTERCEPT N/1003-MM	C.O.D.	Ave DEPT	LWC	LMAX UM	PART TYPE
20:03:40	-18.2	5.6	.1569	6.2E+01	496	12218	.34	-2.8	5.25E+04	.9782	-6366	2	5228 LS
20:04:00	-18.8	5.6	.2045	8.8E+01	537	15169	.34	-2.4	3.80E+04	.8933	-8264	2	5228 LS
20:04:20	-17.9	5.6	.2072	8.2E+01	488	15189	.36	-2.7	6.10E+04	.9679	-3771	2	5228 LS
20:04:40	-17.7	5.6	.1653	4.8E+01	476	13694	.40	-2.9	6.49E+04	.9653	-5426	2	3848 LS
20:05:00	-17.6	5.6	.1503	3.7E+01	450	11136	.45	-3.1	7.20E+04	.9743	-1.8258	2	3503 LS

TOT TIME MEAN AND STANDARD DEVIATIONS

00:01:40	-17.9	5.6	.1768	6.3E+01	487	13345	.38	-2.8	5.77E+04	.9542	-5112	2	4607
00:01:00	.2	.0	.0242	2.0E+01	28	1590	.04	.2	1.17E+04	.0306	.3431	0	768



SIZE (MU)	PARTICLE SIZE DISTRIBUTION (N/1003-MM)		LWC
	SCATTER PROBE	PRECIP PROBE	
2	3.62E+08	27	2.30E+04
4	6.21E+08	50	7.53E+04
6	5.98E+08	73	6.17E+04
7	4.73E+08	96	2.87E+04
9	3.36E+08	119	4.57E+04
11	2.49E+08	142	3.51E+04
13	1.81E+08	165	2.43E+04
15	1.76E+08	188	1.64E+04
16	1.24E+08	211	2.34E+04
18	6.98E+07	234	2.00E+04
20	5.89E+07	257	1.24E+04
22	4.36E+07	289	1.03E+04
23	4.30E+07	303	8.88E+03
25	3.51E+07	326	7.76E+03
27	3.85E+07	349	7.45E+03
			4.37E-03
			1.72E-01

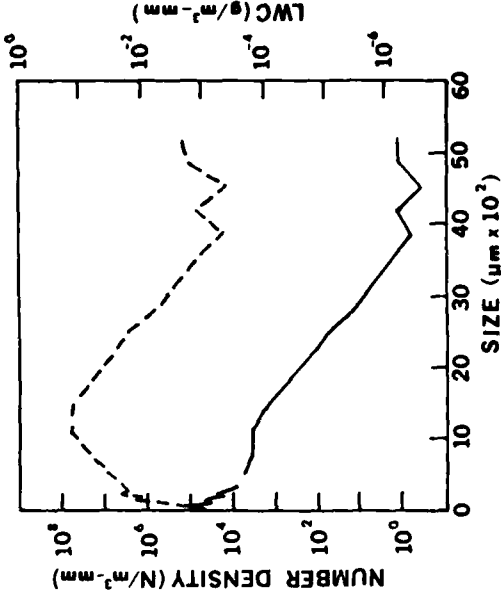


Figure 33. Representative Cloud Data for Small LWC Pass at 18, 500 ft (5.6 km) MSL on 3 March 1978

slight maximum in the particle population for 1200  $\mu\text{m}$  sizes developed into the small-slope distribution of Figure 32 during the 90 or so intervening minutes.

Figure 34 presents data for a 100-sec period when the aircraft was passing through large snow particles at 2.9 km (9900 ft). The LWC for this sample was  $0.7 \text{ g/m}^3$ . The computed best-fit, straight-line slope was  $-0.9/\text{mm}$  and the  $N_0$  intercept was 6960. The dashed line in the spectral graph indicates that all sizes of particles between about 1000 and 5000  $\mu\text{m}$  make equal contributions to the total liquid water content. Only 2 percent of the LWC was determined by cloud probe-sized particles.

Typical data for a second 2.9 km sample are presented in Figure 35. The mean slope and intercept values are  $-0.9/\text{mm}$  and 2480, respectively. The LWC is  $0.29 \text{ g/m}^3$ . Particle population data for the small sizes depart significantly from an extension of the slope line in the precipitation probe range. This seems a common feature in the spectra of storms sampled at 3.0 km altitudes or below. It was also seen in the heavy clouds sampled in Figure 32 at 5.6 km.

The dip, or minimum, in particle density in Figure 35 at sizes near 3000  $\mu\text{m}$  is somewhat unusual for the data in this series. Dingle and Hardy<sup>40</sup> have reported seeing frequent deficits (from a Marshall-Palmer distribution) in the middle-size range ( $\sim 1500\text{-}2000 \mu\text{m}$ ) in rain. They find these represent the first few minutes of showers when the sorting effects of gravity and wind-shear result in big drops coming down first. They believe an excess of small drops is common due to aerodynamic breakup of some of the larger drops. This explanation, however, is not entirely appropriate for the case of falling snowflakes.

Another explanation for the dip in the middle of the Figure 35 particle distribution may be related to the findings of Federer and Waldvogel,<sup>28</sup> Douglas,<sup>41</sup> Smith et al,<sup>42</sup> and Gayet et al,<sup>43</sup> among others. In their work with thunderstorms and Cbs they found changes in the slope of particle distributions differentiated regimes of different particle types. In reviewing the 2-D shadowgraph data for 2025Z on 3 March it appeared many particles on the small end of the spectrum were snowflakes, but there were also some large needle-shaped particles. The

40. Dingle, A.N. and Hardy, K.R. (1962) The description of rain by means of sequential raindrop-size distributions, Quart. Journal Roy. Meteor. Soc. 88:301-314.
41. Douglas, R.H. (1964) Hail size distribution, Preprint 1964 Conf. on Radio Meteorology and Eleventh Weath. Radar Conf., Boulder, CO, 147-149.
42. Smith, P.L. Jr., Musil, D.J., Weber, S.F., Spahn, J.F., Johnson, G.N. and Sand, W.R. (1976) Raindrop and hailstone size distributions inside hailstorms, Preprints International Conf. on Cloud Physics, Boulder, CO, 252-257.
43. Gayet, J.F., Jarmuzynski, M. and Soulage, R.G. (1978) Microstructure of an accumulation zone in a tropical Cb cloud, Preprints Conf. on Cloud Physics and Atmos. Elect., Issaquah, WA, 318-323.

FLT E78-06 03 MAR 78 20 SECOND AVERAGING

START TIME	TEMP C	ALT KM	LUC G/M <sup>3</sup>	Z MM	D0 MU	NT	FF SLOPE /MM	INTERCEPT N/M <sup>3</sup> -MM	C.O.D.	AVE DEPT	LUC % CLD	LMAX UM	PART TYPE
20:55:00	-3.3	2.9	.7587	1.9E+03	1955	39352	.17	3.95E+03	.9174	3.2814	2	5228	LS
20:56:00	-3.2	2.9	.7113	1.5E+03	939	37270	.18	6.26E+03	.9617	2.7745	2	5228	LS
20:56:20	-3.2	2.9	.6727	1.1E+03	891	38943	.19	9.16E+03	.9531	2.5139	2	5228	LS
20:56:40	-3.3	2.9	.7399	1.4E+03	867	56841	.16	7.66E+03	.9524	2.7577	2	5228	LS
20:57:00	-3.8	2.9	.7206	1.3E+03	844	81634	.13	7.77E+03	.9790	2.8960	2	5228	LS

TOT TIME MEAN AND STANDARD DEVIATIONS

00:01:40	-3.4	2.9	.7205	1.4E+03	991	50808	.17	6.96E+03	.9527	2.8447	2	5228	
00:01:40	.2	.0	.0289	2.4E+02	88	16982	.02	1.76E+03	.0201	.2511	0	0	



SIZE (MU)	SCATTER PROBE		CLOUD PROBE		PRECIP PROBE	
	SIZE (MU)	PROBE	SIZE (MU)	PROBE	SIZE (MU)	PROBE
2	1.18E+08	27	8.59E+05	466	1.97E+04	
4	5.72E+08	50	6.91E+05	744	4.94E+03	
6	1.04E+09	73	2.34E+05	1089	3.69E+03	
7	1.25E+09	96	1.05E+05	1434	2.09E+03	
9	1.15E+09	119	9.69E+04	1779	1.16E+03	
11	9.12E+08	142	1.18E+05	2124	7.79E+02	
13	5.75E+08	165	1.20E+05	2469	5.44E+02	
15	5.21E+08	188	6.94E+04	2814	3.65E+02	
16	2.83E+08	211	9.21E+04	3159	2.59E+02	
18	1.51E+08	234	6.87E+04	3504	2.34E+02	
20	1.31E+08	257	7.19E+04	3849	1.90E+02	
22	1.05E+08	280	3.54E+04	4194	1.53E+02	
23	9.71E+07	303	3.70E+04	4539	1.14E+02	
25	8.63E+07	326	3.96E+04	4884	9.78E+01	
27	9.26E+07	349	3.53E+04	5229	8.40E+01	
LWC	1.35E-02		1.86E-02		7.02E-01	

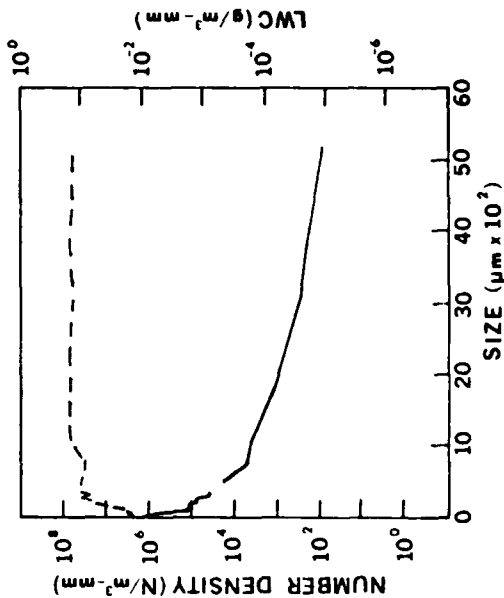


Figure 34. Representative Cloud Data for Large LWC Pass at 9800 ft (2.9 km) MSI, on 3 March 1978

FLT E78-06 03 MAR 78 20 SECOND AVERAGING

START TIME	TEMP C	ALT KM	LUC G/H <sup>0.3</sup>	Z MH <sup>0.6</sup> /H <sup>0.3</sup>	D0 MU	NT N/H <sup>0.3</sup>	FF SLOPE /MM	INTERCEPT N/H <sup>0.3</sup> -MM	C.O.D.	AVE DEPT	LUC % CLD	LMAX UN	PART TYPE
20:25:20	-2.3	2.9	.2656	4.5E+02	721	43559	.11	3.01E+03	.8383	3.3109	5	5228	LS
20:25:40	-2.3	2.9	.3122	5.7E+02	725	35856	.13	3.22E+03	.8079	3.2537	4	5228	LS
20:26:00	-2.3	2.9	.3259	6.9E+02	946	60223	.16	2.34E+03	.7689	3.7791	5	5228	LS
20:26:20	-2.4	2.9	.2706	6.3E+02	1056	25964	.13	1.49E+03	.7057	3.9431	5	5228	LS
20:26:40	-2.5	2.9	.2636	5.1E+02	824	22780	.15	2.29E+03	.9299	3.4320	4	5228	LS

TOT TIME MEAN AND STANDARD DEVIATIONS

00:01:40	-2.4	2.9	.2876	5.7E+02	854	37636	.12	2.48E+03	.8102	3.5438	5	5228	
00:01:40	.1	.0	.0262	8.5E+01	130	13461	.02	6.10E+02	.0745	.2704	0	0	



PARTICLE SIZE DISTRIBUTION (N/H <sup>0.3</sup> -MM)					
SIZE (MU)	SCATTER PROBE	SIZE (MU)	CLOUD PROBE	SIZE (MU)	PRECIP PROBE
2	8.45E+08	27	4.95E+05	464	1.57E+04
4	2.04E+09	50	6.58E+05	744	3.15E+03
6	2.41E+09	73	1.06E+05	1089	1.94E+03
7	2.13E+09	96	6.02E+04	1434	8.69E+02
9	1.29E+09	119	6.85E+04	1779	4.27E+02
11	6.92E+08	142	7.44E+04	2124	2.11E+02
13	2.92E+08	165	7.21E+04	2469	1.12E+02
15	2.22E+08	188	5.26E+04	2814	7.94E+01
16	1.10E+08	211	6.09E+04	3159	6.71E+01
18	5.70E+07	234	5.09E+04	3504	7.03E+01
20	4.94E+07	257	5.59E+04	3849	6.71E+01
22	3.60E+07	280	3.13E+04	4194	6.70E+01
23	4.09E+07	303	3.34E+04	4539	5.65E+01
25	2.81E+07	326	3.62E+04	4884	4.62E+01
27	3.73E+07	349	3.15E+04	5229	3.50E+01
LUC	7.46E-03		1.45E-02		2.73E-01

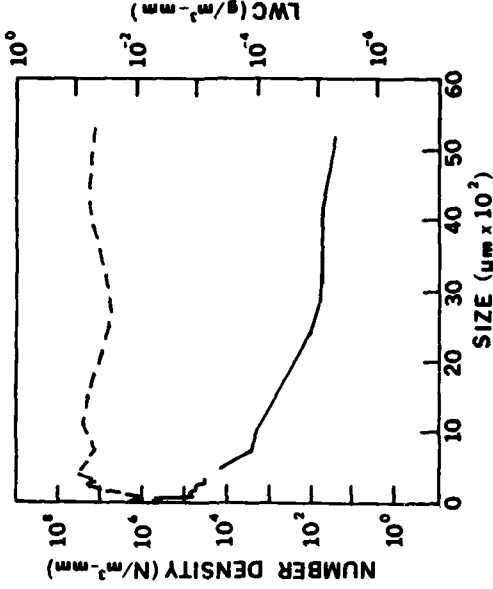


Figure 35. Representative Cloud Data for Small LWC Pass at 9800 ft (2.9 km) MSL on 3 March 1978

dip at about  $3000 \mu\text{m}$  in the Figure 35 spectrum could have been the division between the slope for snowflakes and small needles to the left and the larger needles to the right.

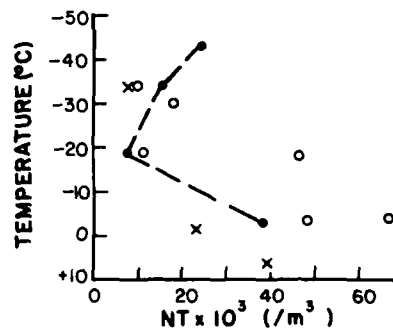
Another possibility is that the steeper portion of the Figure 35 spectrum slope between approximately  $800$  and  $3000 \mu\text{m}$  is a reflection of a large number of growing snow crystals. That is, it would indicate a continuation of the aggregation that has been postulated as occurring in the smaller size particles. If this were the actual situation then the number of larger particles ( $>3000 \mu\text{m}$ ) would be expected to continue to grow and the distribution would become smoother with time. Whether the aggregation process was responsible or not the particle distribution curve did, in fact, become smoother as is shown in the Figure 34 spectrum which was recorded 30 minutes after the one in Figure 35.

## 7. FURTHER OBSERVATIONS

### 7.1 Particle Concentration

Average values of particle concentration, NT, during the various flight passes on 1, 2 and 3 March are plotted as a function of outside air temperature on Figure 36. Individual values are those taken from the histogram plots of Figures 9, 19 and 29.

The difference in average values of the same element during two passes at nearly the same altitude on 3 March obfuscates an overall statement of results. In general, however, it can be seen in Figure 36 that the greatest particle concentrations in the large cloud systems sampled were in the lower levels. The average values during four passes several minutes in duration just above the freezing level varied from  $22,500$  to  $66,300$  particles/ $\text{m}^3$ . Four corresponding values recorded between  $-30$  and  $-35^\circ\text{C}$  were between  $8000$  and  $18,000/\text{m}^3$ . Hobbs and Atkinson<sup>36</sup> similarly found significant variations in NT. For clouds with tops colder than  $-8^\circ\text{C}$  their observations were that ice-crystal concentrations varied over about four orders of magnitude for any given temperature. The greatest concentrations they found in prefrontal clouds were near  $10^5/\text{m}^3$ .



The NT data for 1 March displayed a minimum value near the  $-19^{\circ}\text{C}$  level (5.8 km MSL) with an increase from there to the highest level attained, 9.0 km. This also agrees with Hobbs and Atkinson<sup>36</sup> who found that, for orographic clouds, ice concentrations tend to increase with decreasing temperature. Herzegh and Hobbs<sup>44</sup> documented a study of heavy stratiform clouds over Seattle where the number of ice-particle counts began to increase again at altitudes above approximately 6 km.

The measurements of Heymsfield,<sup>45</sup> however, in a deep cyclonic storm near Medford, Oregon indicated the number of particles  $>100\ \mu\text{m}$  in size decreased relatively smoothly from  $88,000/\text{m}^3$  at 4.4 km to  $76/\text{m}^3$  at 8.9 km and to  $4/\text{m}^3$  at 9.5 km.

At 9.0 km the average ice-particle concentration on 1 March was slightly in excess of  $24,000/\text{m}^3$ , while the modal class extended from 20,000 to  $35,000/\text{m}^3$ . Less than 10 percent of the several 20-sec sample averages at that cirrus altitude had NTs greater than  $55,000/\text{m}^3$ . During flights through cirrus generating cells Heymsfield and Knollenberg<sup>46</sup> found maximum particle concentrations to range from 25,000 to  $50,000/\text{m}^3$ .

The increase of particles in the 2 March data from the  $-1^{\circ}\text{C}$  level to the  $+7^{\circ}\text{C}$  level is to be noted. This may be due to generation of particles near the freezing level, but it is also undoubtedly a result of particle breakup accompanying the melting process. This is in agreement with List and Gillespie<sup>47</sup> who found that, while snowflakes may melt to form large drops, these will rapidly collide and break up. They have indicated that drops larger than 2 to 3 mm break up quite fast and vanish from the population in a short fall. It is likely the relatively steep slope of the rain spectrum in Figure 20 would have become even steeper at lower levels.

A review of all particle concentration data (not just pass averages) indicates the highest values during several passes were near  $10^5/\text{m}^3$ . However, 10 percent of the time during the 1.5-km pass on 2 March and 15 percent of one of the 2.9-km passes on 3 March, the NT was in excess of 110,000 particles/ $\text{m}^3$ . The greatest 20-sec concentration discovered was near  $285,000/\text{m}^3$  at 2117Z on 3 March. The aircraft was in large snow at that time at 2.9 km MSL.

44. Herzegh, P.H. and Hobbs, P.V. (1976) The dynamics and microphysics of a stratiform cloud system, Preprints, 17th AMS Conf. on Radar Meteor., Seattle, WA, 200-205.
45. Heymsfield, A.J. (1976) Particle size distribution measurement: An evaluation of the Knollenberg optical array probes, Atmos. Technology 8:17-24.
46. Heymsfield, A.J. and Knollenberg, R.G. (1972) Properties of cirrus generating cells, J. Atmos. Sci. 29:1358-1366.
47. List, R. and Gillespie, J.R. (1976) Evolution of raindrop spectra with collision-induced breakup, J. Atmos. Sci. 33:2007-2013.

## 7.2 Median Diameter and Form Factor

The computed median volume diameter of particles displays a decided increase with decreasing altitude in Figure 37. At 9 km the  $D_o$  was near  $110 \mu\text{m}$ , while just above the freezing level it ranged from 500 to nearly  $750 \mu\text{m}$ . The increase of  $D_o$  on 2 March from just above the freezing level to the  $+7^\circ\text{C}$  level was not anticipated. It was believed the snow crystals would melt to consolidate their mass in relatively big drops and would then break up in colliding with others to form more numerous small droplets.

It is suspected that this process did occur but that typical snowflakes first grew larger by aggregation than those measured at the 3 km level at  $-1^\circ\text{C}$ . When the measurements at 1.5 km were made on 2 March the melting was not yet complete so that some large crystals were recorded along with the smaller droplets. A few of these crystals can be seen in the Figure 20 2-D particle images along with the more evident round raindrops. These artifact crystals would result in excessive values of  $D_o$  when AFGL equations for raindrops were used. It would have been informative to have data for more sampling passes at more levels near and below the freezing level to further examine the melting process.

The agreement in form factors for the same temperatures during the several passes is shown in Figure 38 to be quite good. In the heaviest precipitation at low levels the small-slope particle spectrum extending to 4000 to 5000  $\mu\text{m}$  sizes typically resulted in form factors near 0.10 to 0.20. At higher levels, where the number of larger particles were fewer, the FF increased considerably. The averages during five passes near the  $-30^\circ\text{C}$  level were between 0.40 and 0.70.

The minimum and maximum features that were so frequently seen in the cloud probe data in the 6 to 8 km MSI altitude range resulted in higher form factors than those associated with more straight-line exponential distributions. The only flight

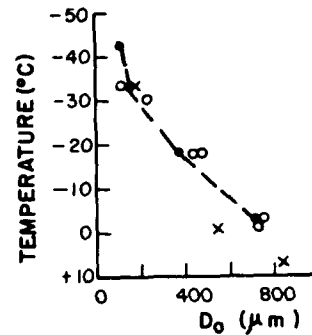


Figure 37. Mean Pass Values of Median Volume Diameter as Function of Temperature. Symbols and line same as on Figure 36

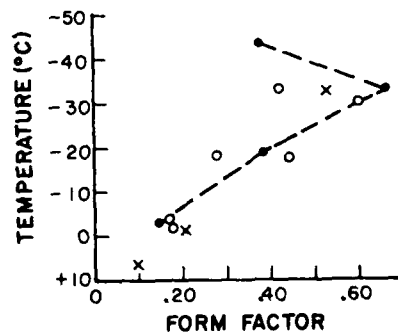


Figure 38. Mean Pass Values of Form Factor as Function of Temperature. Symbols and line same as Figure 36

to get as high as 9.0 km, that on 1 March, found the minimum and maximum phenomena to be less significant, which resulted in a smaller form factor.

At least in this limited study the form factor has been quite useful in providing in a single number considerable insight into the shape of the particle spectrum. The developer of this concept, Plank,<sup>48</sup> has warned, however, that the form factor is ambiguous in that different spectra may have the same or a similar FF. This can be shown by further examining the two spectra shown on Figures 30 and 33, which have form factors of 0.35 and 0.38, respectively. The differences in particle distribution on the figures are apparent; yet, in practice there was little or no confusion in understanding the general distribution a given FF represented as long as the corresponding temperature or altitude was known.

As mentioned in Section 3.2, the particle spectra most closely approaching straight-line exponential distributions have form factors in the 0.25 to 0.35 range. The Figure 13 spectrum, for example, which has a form factor of 0.33, shows relatively minor deviations from a straight-line distribution.

### 7.3 Liquid Water Content

Figure 39 indicates the mean-pass values of liquid water content correlated with temperature. In the large-scale cloud system sampled just above the freezing level the LWC average of four passes varied only from 0.09 to 0.63 g/m<sup>3</sup>. Near the -33°C level, three averages were even more consistent: from 0.005 to 0.016 g/m<sup>3</sup>. The average LWC of the single-pass sample at -43°C (at 9 km) was in the same range: 0.005 g/m<sup>3</sup>. This latter value is considerably less than the 0.25 to 0.40 g/m<sup>3</sup> that Heymsfield and Knollenberg<sup>45</sup> found in cirrus generating cells; however, such cells may typically have greater LWCs than other more frequently observed cirriform types. Maximum LWC values of approximately 0.01 g/m<sup>3</sup> were common in previous Air Force Geophysics Laboratory cirrus flights (for example, Varley and Barnes<sup>25</sup>) at 8 to 10 km altitudes.

The average LWC of the single data pass in rain on 2 March was 0.29 g/m<sup>3</sup>. The corresponding value of the pass made 5000 ft higher that day in the snow region

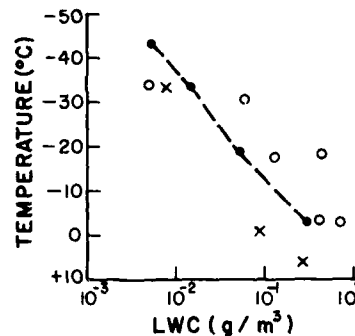


Figure 39. Mean Pass Values of Liquid Water Content as Function of Temperature. Symbols and line same as on Figure 36

48. Plank, V.G. (1979) Private correspondence.

was  $0.09 \text{ g/m}^3$ . This finding does not agree with Herzegh and Hobbs<sup>49</sup> who believe that values of mass in the rain region are generally lower than those in the snow above. They have indicated this is a result of the precipitating particles becoming more widely spaced as their fall speeds increase during melting. As mentioned in Section 7.2, the computed value of the mean-volume diameter at the 1.5 km level on 2 March may be slightly high because "rain" equations were used even though snow remained. This would tend to inflate the corresponding LWC calculations for the same level. Data samples at lower levels where the melting was completed would probably have indicated smaller LWC values. As pointed out by Barnes<sup>50</sup> new instrumentation is required to obtain total LWC values in the melting zone, where snow and rain coexist.

Typical LWCs in the lower levels of the clouds sampled on all 3 days were in the  $0.1$  to  $1.0 \text{ g/m}^3$  range. The highest value for the 3 days for a single 20-sec interval was the previously mentioned  $1.5 \text{ g/m}^3$  near the 2.9 km level on 3 March. For comparison these quantities are close to those reported in hurricanes by Ackerman.<sup>51</sup> She has indicated the bulk of the measurements in hurricane stratiform clouds were a few tenths  $\text{g/m}^3$  and that only a small fraction of the total observations were greater than  $3 \text{ g/m}^3$ . In one hurricane a value of  $9.5 \text{ g/m}^3$  was encountered in the wall cloud. Sissenwine<sup>52</sup> calculated that the 0.5 percent greatest tropical precipitation case would be accompanied by water density in the precipitation and clouds at 4 to 6 km of about  $5.5 \text{ g/m}^{-3}$ .

#### 7.4 Maxima and Minima in Particle Spectra

In the large scale winter storm sampled in this 3-day flight program many data segments displayed a minimum and adjoining maximum feature in the particle concentration-size curves. This has been mentioned in previous sections and is shown, for example, on Figures 12, 23 and 31 in the curves for particles less than  $350 \mu\text{m}$  in size.

It has been suggested that the dips in the spectra that occur in the cloud probe range may be due to evaporation. There are frequently even smaller sized particles

49. Herzegh, P.H. and Hobbs, P.V. (1978) Generating cells and precipitation growth in mesoscale rainbands, Preprints of Conf. on Cloud Physics and Atmos. Elect., Issaquah, WA, 284-291.
50. Barnes, A.A. Jr. (1978) New cloud physics instrumentation requirements, Preprints of Fourth Symposium on Meteorological Observations and Instrumentation, Denver, CO, 264-268. Also AFGL-TR-78-0093, AD A053 235.
51. Ackerman, Bernice (1963) Some observations of water contents in hurricanes, J. of Atmos. Sci. 20:288-298.
52. Sissenwine, N. (1972) Extremes of Hydrometeors at Altitude for MIL-STD-210B, Air Force Cambridge Res. Labs. 72-0369, pp 20.

in the spectra, however, that are not reduced in number, while they would seemingly be the first to disappear.

Another possibility mentioned in a preceding section is that particles observed at the "maximum" point in the spectrum may be aggregating at the expense of smaller particles from the "minimum" point. As the aggregation continues in time or at a lower level the particles become increasingly larger so both the maximum and minimum points move further to the right to form more broadly based spectra. The limited amount of data in this flight program suggests the spectra evolve as in Figure 40.

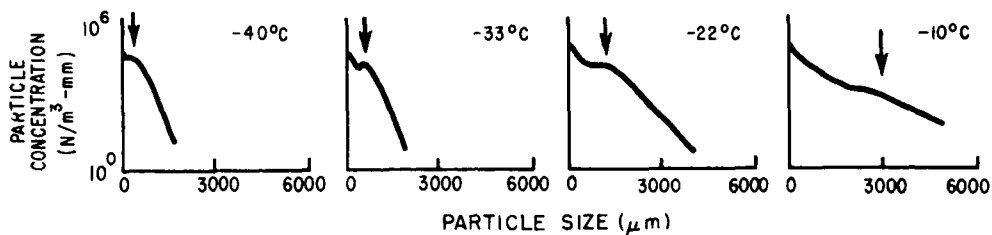


Figure 40. Suggested Changes of Particle Spectra with Temperature Due to Aggregation in Large Cloud Systems. Temperatures and particle sizes are approximations. Arrows point to location of particle "maximum" concentration

The locations of particle concentration shown on Figure 40 are not to be found on all spectra. The aggregation process probably does not proceed in the same manner or intensity throughout a cloud system, and there are undoubtedly cloud areas where it does not occur at all.

The "valley-peak" feature seen in several of the spectra of particles at freezing temperatures may seemingly be explained through an aggregation mechanism, but there is more speculation about such features found in spectra at above-freezing temperatures. The Figure 20 spectrum shows a particle population minimum near 100 μm and a maximum of 240 μm when ambient temperature was almost 7°C. The reason for their existence is open for more conjecture, but they may be related to a process in which both evaporation of small particles and melting of large ones occur.

The 2-D shadowgraph data concurrent with the Figure 20 spectral data showed the predominant particle type was rain, but many small ice crystals had not yet melted. It is suggested that particles near the 240 μm size peak in that figure consisted of the same population of ice crystals as in the Figure 21 spectrum for the 2.9-km level plus numerous recently melted droplets that had become smaller

and moved to the left. As melting continued that peak would move toward smaller sizes until it disappeared entirely or became immeasurable.

### 7.5 Suppressed and Enhanced Spectra

Section 3.4 referred to the "suppressed" and "enhanced" types of particle spectra. These terms, used by Houze et al,<sup>22</sup> apply to distributions that depart significantly in the smallest sizes ( $< \sim 1$  mm) toward smaller (suppressed) or greater (enhanced) numbers than those expected from an extrapolation of the distribution curve for sizes larger than about 1 mm. Figure 41 gives examples of the two types.

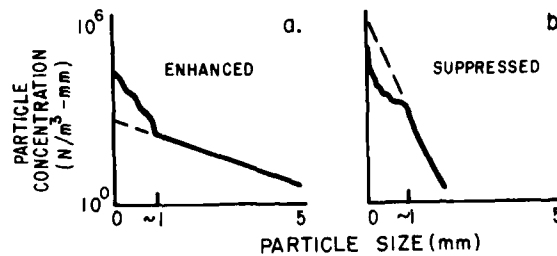


Figure 41. Generalized Examples of Enhanced (a) and Suppressed (b) Particle Distributions

The purposes of this study did not include an effort to determine the frequency of occurrence of these two types of distributions, but it should be pointed out that they were both quite common in the clouds investigated. The enhanced type was frequent in the lower, particle-rich clouds near the freezing level, while the suppressed spectra were seen most often at altitudes above about 20,000 ft (6.1 km) MSL where the number of larger particles was relatively small. The spectra obtained between approximately 5 and 6 km MSL tended to be neither suppressed nor enhanced, but approached a straight-line exponential distribution.

The fact that suppressed spectra were seen primarily at high altitudes with relatively small particles does not agree with the findings of Houze et al,<sup>22</sup> who indicated that suppressed deviations are associated with broad distributions and that the suppression becomes stronger with increasing temperatures. The reason for this difference can not be explained at this time, except by citing differences in basic cloud structures and the fact that we presently have little data at temperatures of  $-5^{\circ}$  to  $-18^{\circ}$ C. Such data might tend to affirm the existence of more suppressed spectra over broad distributions.

Regardless of the frequency of the different types it seems clear that the main determinant of a suppressed, exponential or enhanced distribution is the number of particles in the large-size ( $> \sim 1 \text{ mm}$ ) portion of the spectrum. In Figure 42, which shows spectra from Figures 10 through 13 for 1 March, it can be seen that there is little difference in particle populations in small sizes. The calculated LWCs of particles in the 27 to 350  $\mu\text{m}$  range varied only from 0.003 to 0.019  $\text{g}/\text{m}^3$  for the four Figure 42 spectra.

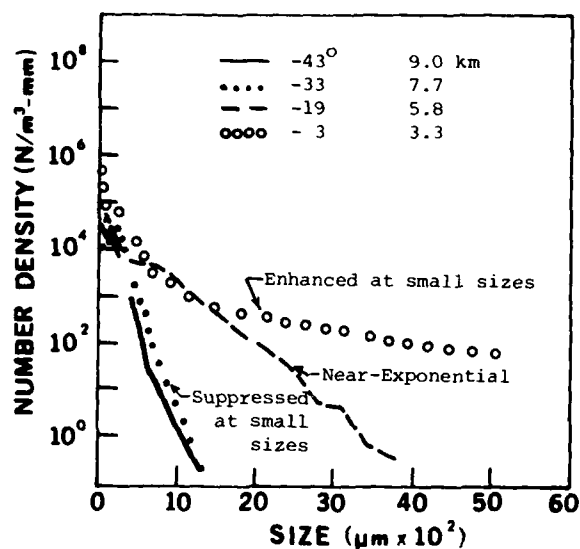


Figure 42. Four 1 March Spectra for 100-sec Periods Replotted From Figures 10 to 13. Populations of small particle sizes remain relatively constant with varying temperature and altitude

The relation of spectra  $N_0$  (N-axis intercept) values to temperature was relatively close for the few values plotted on Figure 43. These have been taken from the various 100-sec data samples presented in preceding figures. In cases where  $N_0$  was not calculated an extrapolation of the existing data was made by eye. The approximated best-fit line is near the slope that was determined for CYCLES data by Houze et al.<sup>22</sup>

The Figure 43 data indicate that in the type clouds sampled, increasing temperature generally results in a smaller  $N_0$ . This, in turn, is an indication that the number of larger sized particles increases so that the spectra slopes decrease.

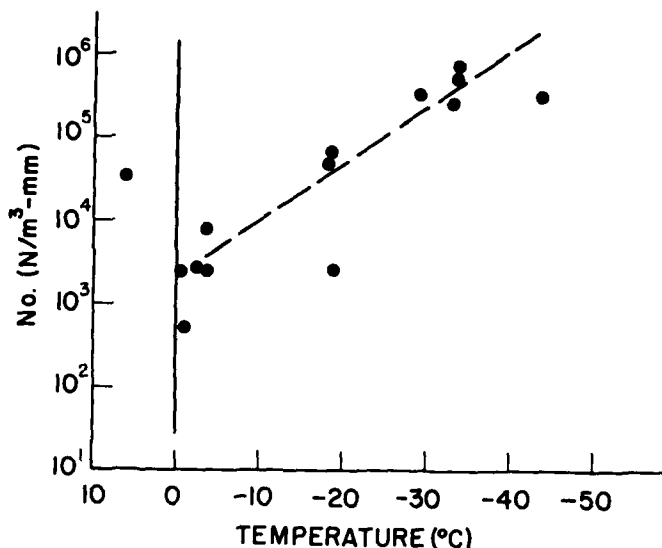


Figure 43. Values of N-Axis Intercept vs Temperature for 14 Data Figures in This Report. Dashed line is approximation to best-fit straight line

The single data point on the figure at above-freezing temperature shows that  $N_0$  increased significantly as particles melted and broke up and the spectrum narrowed.

#### 7.6 Reflectivity Values

The reflectivity-value ( $Z$ ) computation is a routine part of the AFGL particle processing program based on the sixth power of the diameter of "melted" particles. Typical and mean values have been presented in the foregoing data figures. There was no effort made, however, to compare calculated and radar values since radar data were not available.

The greatest mean calculated reflectivity value for a pass during the 3 days was found to be nearly  $4500 \text{ mm}^6/\text{m}^3$  (36.5 dBZ) for the 1.5-km pass in rain on 2 March. The largest mean  $Z$  for any 20-second period during the 3 days was near  $28,900 \text{ mm}^6/\text{m}^3$  (44.6 dBZ) at 2037Z on 2 March in rain. The largest  $Z$  values generally occurred at the lowest levels sampled and the smallest values at the highest levels. There was considerable variation, however, even at one level. For example, on 3 March the mean reflectivity values for two passes at 2.9 km were 1020 and  $563 \text{ mm}^6/\text{m}^3$ . Corresponding values for two 5.6-km passes that day were 300 and  $35 \text{ mm}^6/\text{m}^3$ .

## 8. SUMMARY

The locations selected for aircraft sampling on 1, 2 and 3 March 1978 were each slightly east of the upper-level trough as it moved eastward across the U.S. This generally resulted in abundant clouds to be sampled, although on 2 March the tops of the significant cloudiness, at 14,000 to 18,000 ft (4.2-5.5 km), were lower than desired.

Particles having the smallest average size were recorded at the highest levels sampled each day. At 7.7 km and above the largest particles were near or less than about 2000  $\mu\text{m}$  and the median volume diameter (of melted particles) was between 100 and 200  $\mu\text{m}$ . The calculated water content at this level on all 3 days was approximately 0.01  $\text{g}/\text{m}^3$ , and the total particle count was between 8000 and 18,000/ $\text{m}^3$  over Arkansas and coastal Delaware, but near 24,000 over the mountains of New Mexico.

Values of mass and mean-particle sizes both increased with distance fallen, indicating growth of particles was by collectional means. Typical particle spectra also broadened to the largest sizes recordable as ice crystals fell toward the freezing level.

The largest water contents were found in the layers within a few Celsius degrees of the freezing level. During passes of at least 8 minutes duration mean water contents near the  $-1$  to  $-3^\circ\text{C}$  level were between 0.09 and 0.63  $\text{g}/\text{m}^3$ . The greatest pass average of particle counts was approximately 66,000/ $\text{m}^3$  which was also recorded near the  $-3^\circ\text{C}$  level.

The single sampling pass made below the freezing level recorded a greater number of particles than the pass made the same day 1.5 km higher (above the freezing level). The calculated mean water content for the low (warm) pass was 0.29  $\text{g}/\text{m}^3$  while that for the higher one was 0.09  $\text{g}/\text{m}^3$ . It is believed there were many unmelted crystals in the warmer sample that resulted in slightly high calculations of LWC. As the melting continued the calculated LWC values would probably decrease in magnitude. Cunningham,<sup>7</sup> however, has previously reported higher LWC values below the melting level than above it. He indicates this is the result of scavenging of small droplets as larger ones fall through heavy low cloud.

The form factor, a mathematical parameter, was found useful in studying particle spectra. Low values were found to be associated with broad distributions at low altitudes. The maximum form factors on all 3 sampling days resulted from spectra observed in the 7.2 to 7.7 km altitude range where slight concentration minima near the 100  $\mu\text{m}$  size and maxima near the 240  $\mu\text{m}$  size were common. Form factors between 0.25 and 0.35 were usually related to approximately straight-line exponential distributions.

It is suggested that the slight "maximum" points in the distribution seen in several spectra in this study are evidence of aggregation of small particles. These peaks occur at progressively larger particle sizes as the particles fall toward the freezing level.

The data in this study have been useful in expanding our knowledge of the microphysics of large cloud systems. Other similar sampling has been completed and it will be informative to compare results with those presented here. In future flights efforts will be directed toward obtaining more samples at more levels so that particle changes with height and temperature may be better documented.

## References

1. Hobbs, P. V. (1978) The University of Washington's CYCLES Project: An Overview, Preprints of Conference on Cloud Physics and Atmospheric Electricity, Issaquah, WA, 271-276.
2. Houze, R. A. Jr., Locatelli, J. D. and Hobbs, P. V. (1976) Dynamics and cloud microphysics of the rainbands in an occluded frontal system, J. of Atmos. Sci. 33:1921-1936.
3. Harper, W. G. (1957) Variation with height of rainfall below the melting level, Quart. J. Roy. Meteor. Soc. 83:368-371.
4. Hardy, K. R. (1963) The development of raindrop-size distributions and implications related to the physics of precipitation, J. of Atmos. Sci. 20:299-312.
5. Ohtake, T. (1969) Observations of size distributions of hydrometeors through the melting layer, J. of Atmos. Sci. 26:545-557.
6. Ohtake, T. (1970) Factors affecting the size distribution of raindrops and snowflakes, J. of Atmos. Sci. 27:804-813.
7. Cunningham, R. M. (1952) The Distribution and Growth of Hydrometeors Around a Deep Cyclone. Ph.D Thesis, Mass. Institute of Techn., pp 59. Also M.I.T. Dept. of Meteor. Tech. Report No. 18.
8. Marwitz, J. D. and Stewart, R. E. (1978) Dynamical and microphysical characteristics of winter storms over the Sierra Nevadas, Preprints of Conf. on Cloud Physics and Atmospheric Electr., Issaquah, WA, 244-246.
9. Lamb, D., Nielson, K. W., Klieforth, H. E. and Hallett, J. (1976) Measurements of liquid water content in winter cloud systems over the Sierra Nevadas, J. Appl. Meteor. 15:763-775.
10. Hobbs, P. V. (1975) The nature of winter clouds and precipitation in the Cascade Mountains and their modification by artificial seeding. Part 1: Natural conditions, J. Meteor. 14:783-804.
11. Marwitz, J. D. (1974) An airflow case study over the San Juan Mountains of Colorado, J. of Meteor. 13:450-458.

12. Waldvogel, A. (1974) The  $N_0$  jump of raindrop spectra, J. of Atmos. Sci. 31:1067-1078.
13. Browning, K. A. (1974) Mesoscale structure of rain systems in the British Isles, J. of Meteor. Soc. Japan 52:314-327.
14. Hobbs, P. V. and Locatelli, J. D. (1978) Rainbands, precipitation cores and generating cells in a cyclonic storm, Jour. Atmos. Sci. 35:230-241.
15. Plank, V. G., Atlas, D. and Paulsen, W. H. (1955) The nature and detectability of clouds and precipitation as determined by 1.25 cm radar, J. Meteor. 12:358-377.
16. Braham, R. R. Jr. (1967) Cirrus cloud seeding as a trigger for storm development, J. Atmos. Sci. 24:311-312.
17. Knollenberg, R. G. (1972) Measurements of the growth of the ice budget in a persisting contrail, J. Atmos. Sci. 29:1367-1374.
18. Marshall, J. S. and Palmer, W. McK. (1948) The distribution of raindrops with size, J. Meteor. 5:165-166.
19. Gunn, K. L. S. and Marshall, J. S. (1958) The distribution with size of aggregate snowflakes, J. of Meteor. 15:452-461.
20. Douglas, R. H. (1964) Hail size distribution, Preprints of World Conf on Radio Meteor. and Eleventh Weath. Radar Conf., Boulder, CO, 147-149.
21. Smith, P. L. Jr., Musil, D. J., Weber, S. F., Spahn, J. F., Johnson, G. N., and Sand, W. R. (1967) Raindrop and hailstone size distributions inside hailstorms, Preprints Intnatl. Conf. on Cld. Physics, Boulder, CO, 252-257.
22. Houze, R. A. Jr., Hobbs, P. V., Herzegh, P. H., and Parsons, D. B. (1979) Size distributions of precipitation particles in frontal clouds, J. Atmos. Sci. 36:156-162.
23. Hardy, K. R. (1963) The development of raindrop-size distributions and implications related to the physics of precipitation, J. Atmos. Sci. 20:299-312.
24. Blanchard, D. C. (1953) Raindrop size distributions in Hawaiian rains, J. of Meteor. 10:457-473.
25. Varley, D. J. and Barnes, A. A. Jr. (1979) Cirrus Particle Distribution Study, Part 4, Air Force Geophysics Lab TR-79-0134, Air Force Surveys in Geophysics, No. 413, 91 pp.
26. Joss, J., Thams, J. C. and Waldvogel, A. (1968) The variation of raindrop size distributions at Locarno, Proceedings Intnatl. Conf. on Cld. Phy., Toronto, Ontario, 369-373.
27. Waldvogel, A. and Joss, J. (1970) The influence of a cold front on the drop size distribution, Preprints Conf. on Cld. Physics, Ft Collins, Amer. Meteor. Soc., 195-196.
28. Federer, B. and Waldvogel, A. (1975) Hail and raindrop size distributions from a Swiss multicell storm, J. Appl. Meteor. 14:91-97.
29. Knollenberg, R. G. (1975) The response of optical array spectrometers to ice and snow: A study of probe size to crystal mass relations, AFCRL-TR-75-0494. Air Force Cambridge Research Laboratories, 69 pp.
30. Cunningham, R. M. (1978) Analysis of particle spectral data from optical array (PMS) 1-D and 2-D sensors, Preprints of Fourth Symposium on Meteorological Observations and Instrumentation, Amer. Meteor. Soc., 345-350. Also, AFGL-TR-78-0102.

31. Plank, V.G. (1977) Hydrometeor Data and Analytical-Theoretical Investigations Pertaining to the SAMS Rain Erosion Program of the 1972-73 Season at Wallops Island, Virginia, Air Force Geophysics Laboratory TR-77-0149, pp 239.
32. Plank, V.G. and Barnes, A.A. Jr. (1978) An improvement in obtaining real-time water content values from radar reflectivity, Preprints of 18th Conf. Radar Meteor., Atlanta, Amer. Meteor. Soc., 426-431.
33. Smith, P.L. Jr. and Iaco, C. P. (1978) Techniques for fitting size distribution functions to observed particle size data, Preprints of 18th Conf. on Radar Meteor., Atlanta, GA, 129-133.
34. Chin, D. and Hamilton, H.D. (1978) Synoptic Analysis Case 1, 1 March 1978-4 March 1978, Systems and Applied Sciences Corporation Scientific Report No. 1, AFGL-TR-78-0294, AD A065 486.
35. AWS-USAF (1969) Use of the Skew T, Log p Diagram in Analysis and Forecasting, Air Weather Service Manual, 105-124.
36. Hobbs, P.V. and Atkinson, D.G. (1976) The concentrations of ice particles in orographic clouds and cyclonic storms over the Cascade Mountains, J. Atmos. Sci. 33:1362-1374.
37. Plank, V.G. (1974) Hydrometeor Parameters Determined From the Radar Data of the SAMS Rain Erosion Program, AFCRL/SAMS Report No. 2. AFCRL-TR-74-0249, pp 86.
38. Joss, J. and Waldvogel, A. (1969) Raindrop size distribution and sampling size errors, J. Atmos. Sci. 26:566-569.
39. Wexler, R. and Atlas, D. (1959) Precipitation generating cells, J. of Meteor. 16:327-332.
40. Dingle, A.N. and Hardy, K.R. (1962) The description of rain by means of sequential raindrop-size distributions, Quart. Journal Roy. Meteor. Soc. 88:301-314.
41. Douglas, R.H. (1964) Hail size distribution, Preprint 1964 Conf. on Radio Meteorology and Eleventh Weath. Radar Conf., Boulder, CO, 147-149.
42. Smith, P.L. Jr., Musil, D.J., Weber, S.F., Spahn, J.F., Johnson, G.N. and Sand, W.R. (1976) Raindrop and hailstone size distributions inside hailstorms, Preprints International Conf. on Cloud Physics, Boulder, CO, 252-257.
43. Gayet, J.F., Jarmuzynski, M. and Soulage, R.G. (1978) Microstructure of an accumulation zone in a tropical Cb cloud, Preprints Conf. on Cloud Physics and Atmos. Elect., Issaquah, WA, 318-323.
44. Herzegh, P.H. and Hobbs, P.V. (1976) The dynamics and microphysics of a stratiform cloud system, Preprints, 17th AMS Conf. on Radar Meteor., Seattle, WA, 200-205.
45. Heymsfield, A.J. (1976) Particle size distribution measurement: An evaluation of the Knollenberg optical array probes, Atmos. Technology 8:17-24.
46. Heymsfield, A.J. and Knollenberg, R.G. (1972) Properties of cirrus generating cells, J. Atmos. Sci. 29:1358-1366.
47. List, R. and Gillespie, J.R. (1976) Evolution of raindrop spectra with collision-induced breakup, J. Atmos. Sci. 33:2007-2013.
48. Plank, V.G. (1979) Private correspondence.
49. Herzegh, P.H. and Hobbs, P.V. (1978) Generating cells and precipitation growth in mesoscale rainbands, Preprints of Conf. on Cloud Physics and Atmos. Elect., Issaquah, WA, 284-291.

50. Barnes, A.A. Jr. (1978) New cloud physics instrumentation requirements, Preprints of Fourth Symposium on Meteorological Observations and Instrumentation, Denver, CO, 264-268. Also AFGL-TR-78-0093.
51. Ackerman, Bernice (1963) Some observations of water contents in hurricanes, J. of Atmos. Sci. 20:288-298.
52. Sissenwine, N. (1972) Extremes of Hydrometeors at Altitude for MIL-STD-210B, Air Force Cambridge Res. Labs. 72-0369, pp 20.

## Appendix A

Mission Director Comments (1 March 1978)

<u>TIME (Z)</u>	<u>COMMENTS</u>
(To obtain local time subtract 7 hours)	
1740	Takeoff from Albuquerque (ABQ).
1749	Broken clouds below, tops 7000.
1751	Entering cloud at 11,000. Bases about 9500 ft, tops about 15,000 ft.
1754	In cloud, no structure.
1756	Noticeably darker. Snow stick is riming up.
1757	Can see lower clouds occasionally.
1800	Very big crystals.
1802	Generally heavy cloud; occasionally can see downward.
1807	Very large crystals. Are near freezing level.
1809	Can see ground now.
1810	Very solid cloud above.
1811	Back into cloud.
1814	Multiple layers above. Tops to about 18,000 ft.
1816	Entered and exited small cumulus.
1818	End 11,000 ft MSL pass. 14 mi SW of Farmington. Begin climb to 19,000 ft.
1827	Fairly bright sun. At 16,000 ft. No optical phenomena.
1828	Passing 17,000 ft. Cloud bases here.
1829	Opening in clouds ahead.
1835	High stratified clouds over Farmington. Lower ones appear convective.
1838	Begin pass at 19,000 ft toward ABQ.
1839	Bright sun above. 65 mi NW of ABQ. In clearing.
1841	Getting hazier. May be getting fallout particles from above.
1842	Ground is disappearing as we enter cloud.
1845	Ground dimly visible. Gray uniform cloud above.
1846	Uniform cloud, bases at 17,000 ft. No estimate of tops possible.
1849	Still in uniform cloud. Sun only dimly visible.

<u>TIME (Z)</u>	<u>COMMENTS</u>
1852	Sun getting bright.
1856	Broke out of cloud. But may be getting fallout from above.
1857	End 19,000 ft MSL pass. 7 mi NW of ABQ.
1904	Bright sun above, in and out of cloud.
1905	Cumulus tops near 12,000 ft. Thin cirrus above.
1909	Begin 25,000 ft data pass. 30 mi NW of ABQ, heading 305°. Sun is bright, but hazy. May be in thin cirrus now. Ci above too.
1912	In thin cirrus, tops 4000-5000 ft above aircraft. Occasional hint of blue sky.
1914	Bright sun, no optical phenomena.
1915	In very uniform cirrus now.
1917	Cirrus thickening now.
1918	Visibility about 3 mi in uniform cirrus.
1920	Cirrus tops about 4000-5000 ft above aircraft. No halos.
1922	Cirrus bases about 2000 ft below aircraft.
1924	Sun moderately bright through cirrus.
1925	Continuous light turbulence along this pass.
1930	Uniform cirrus all directions. End 25,000 ft MSL data pass at 110 mi NW of ABQ.
1933	Climbing and turning back toward ABQ.
1937	In uniform cirrus at about 27,000 ft.
1940	In uniform cirrus, getting thinner. 28,300 ft and climbing.
1941	Leveling off near 29,000 ft. Light intensity, uniform crystals.
1943	Very small crystals on snowstick (~500 μm). Cirrus tops approx 36,000 ft.
1944	85 mi from ABQ, heading about 160°.
1945	Still uniform cirrus, visibility approximately 1 mile. Sun fairly bright. Wind at 29,000 ft 224° 62 kt.
1948	No structure in the thin cloud.
1954	In a cloud-free area temporarily.
1956	Sun fairly bright through thin cirrus.
1959	Clouds below have more structure now.
2004	END 29,000 ft pass. Wind 222° 65 kt, 15 mi NW ABQ.

## Appendix B

Mission Director Comments (2 March 1978)

<u>TIME (Z)</u>	<u>COMMENTS</u>
	(To obtain local time subtract 6 hours)
1634	Take off from Kirtland AFB at Albuquerque.
1856	Uniform cirrus near flight altitude (~25,000 ft).
1900	Cumuliform buildups all around. Tops of most Sc near 18,000 ft.
1902	Begin official pass over Little Rock at 25,000 ft. Flying on 060 radial from Little Rock. No definition of cloud form the aircraft is in. Wind: 240°/54 kt.
1904	Have broken out of cloud but heading toward more. Heading is now 080°.
1905	Cirrus is above us now. Base at about 34,000 ft.
1906	Next deck coming soon. 31 nm out of Memphis on J-66.
1910	In hazy cirrus layer. Quite bright from sun.
1911	Now out of cloud. Bright blue sky above.
1914	Any cirrus at this level is thin, hard to locate.
1915	Mostly blue sky. Have had very little good cloud data so far.
1919	Coming up to large cumuliform cloud with tops near 30,000 ft (9.1 km).
1920	Entering large cumuliform cloud. 91 nm E of Little Rock.
1923	Wind 230°/52 kt, true air speed (TAS) - 230 kt, heading = 080°.
1924	110 nm E of Little Rock.
1928	End 25,000 ft pass. Tops of patchy cirrus extend to about 30,000 ft. Wind - 240°/45 kt.
1929	15 nm E of Memphis. Turning west toward Memphis.
1930	Descending through uniform cloud. Ten miles NE of Memphis.
1932	Descending through 19,000 ft.
1934	In clear with A <sub>c</sub> undercast, thin cirrus above.
1938	103 nm E of Little Rock.
1940	Descending into cumuliform tops. Heavy cloud. 96 nm E of Little Rock.

<u>TIME (Z)</u>	<u>COMMENTS</u>
1941	Getting good data now. A little turbulence.
1943	Begin a pass at 10,000 ft (3.0 km) MSL. Particles are large snow-flakes. Wind - 255 <sup>0</sup> /32 kt.
1944	Heavy cloud. Both crystals and water. Tops extend about 4000 ft above this altitude.
1949	Particle type seems to change from crystal to drops and back.
1952	In heavy cloud. Visibility low all directions. No turbulence.
1957	Clouds slightly brighter here.
1958	55 nm E of Little Rock on 080 Little Rock radial. Wind = 242 <sup>0</sup> /36 kt.
1959	Visibility near zero in all directions. Clouds slightly lighter than a few minutes ago. No turbulence.
2000	Particles seem to be mostly rain.
2002	Solid, uniform cloud. Large crystals.
2008	On Little Rock 080 <sup>0</sup> radial, 32 nm, out.
2009	Very uniform cloud. Much water.
2010	Cloud is slightly lighter now.
2012	Many large crystals, but water drops too.
2015	Big mushy snow. Light turbulence.
2017	Very dark cloud. Big agglomerates. 10 nm E of Little Rock.
2021	End 10,000 ft pass. About 3 mi W of Little Rock.
2025	Descending for next pass. All water now. Can see cloud texture. Much of previous clouds believed to extend from about 9000 to 12,000 ft.
2029	Seven nm E of Little Rock.
2037	Begin sampling at 5000 ft in rain 35 nm E of Little Rock flying east. Wind - 240 <sup>0</sup> /55 kt. TAS = 164 kt.
2040	In rain, big drops.
2047	Uniform rain, light to moderate.
2054	Little Rock AFB reports 600 ft ceiling.
2055	In uniform, stratified cloud. Can't see up or down.
2102	End 5000 ft pass. Over Memphis. Completely in cloud.
2105	Solid cloud at 5000 ft, climbing to 14,000 ft.
2110	At 12,500. Beginning to break out of lower cloud. Base of another layer at 16,000 ft, and cirrus higher still.
2141	Land at Little Rock AFB, Arkansas.

AD-A083 140

AIR FORCE GEOPHYSICS LAB HANSCOM AFB MA  
MICROPHYSICAL PROPERTIES OF A LARGE SCALE CLOUD SYSTEM, 1-3 MAR--ETC(U)  
JAN 80 D J VARLEY

F/G 4/2

MAR--ETC(U)

UNCLASSIFIED

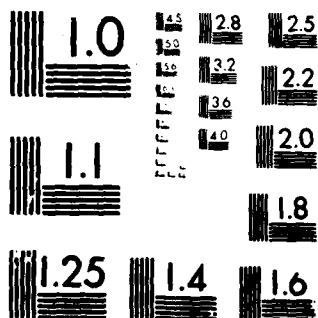
AFGL-TR-80-0002

NL

2 of 2  
AF  
NO. 1000



END  
DATE  
FILMED  
5-80  
DTIC



MICROCOPY RESOLUTION TEST CHART  
NATIONAL BUREAU OF STANDARDS-1963-A

## Appendix C

Mission Director Comments (3 March 1978)

TIME (Z)      COMMENTS  
(To obtain local time subtract 5 hours)

1916	At Shads, 24,000 ft (7.3 km) MSL. Completely in cloud.
1921	<u>Begin Pass #1</u> at 25,000 ft (7.6 km). Heading 020°.
1922	At 37°54'N, 72°45'W. Radar altitude 24,980 ft.
1925	Continuous light intensity particles. Sun moderately bright through cirrus above. Light rime icing on spinners, light turbulence.
1928	Visibility low. In continuous thin cirrus. Can't estimate tops.
1931	TAS 225 kt, IAS 152 kt, 25,000 ft, wind 245°/83 kt.
1934	Continuous light intensity particles. Seem to be in base of cirrus now.
1935	Very hazy ahead. Probably in cirrus base now. Undercast below.
1938	<u>End Pass #1.</u> At 38°58'N, 72°02'W. Near base of cirrus.
1943	Have turned around and are going south.
1947	<u>Begin Pass #2</u> near Tunna (38°43'N, 72°15'W). Heading 235°, wind 256°/63. Light rime. Sun moderately bright. Flight level 18,300 ft (5.6 km).
1950	In thin cloud.
1951	Entering cloud bank, near top of IFR layer.
1953	Near top of cloud layer.
1958	Reentering cloud. Position 38°22'N, 72°32'W, FL 18,000 ft. Snow stick is iced up.
2001	Between layers. Some fallout from above.
2003	Cloud getting heavier as we go south.
2004	Can't see up or down. Heavy cloud. Wind 252°/57 kt.
2007	Solid cloud. Can't see any cloud texture.
2009	Uniform cloud. Very little turbulence. Agglomerates.
2012	Exit cloud.
2013	<u>End Pass #2.</u> 37°47'N, 72°56'W (near Shads). Heading 230°. Sun moderately bright.

<u>TIME (Z)</u>	<u>COMMENTS</u>
2022	Descending through 12,800 ft (3.9 km). Particle size is larger here.
2023	<u>Begin Pass #3</u> at 37°58'N, 72°48'W at 9900 ft (3.0 km). Particles are very large agglomerates. Heading is 040°.
2025	Large snow. Changing to wet snow. Wind 220°/57.
2028	Very uniform heavy cloud, picking up light rime icing.
2030	Very dark, heavy cloud. Many different types of particles.
2032	Light turbulence.
2033	Icing on probe cannisters.
2040	<u>End Pass #3</u> in uniform, heavy cloud. 9800 ft. Heading 046°.
2048	<u>Begin Pass #4</u> at 9800 ft heading 220° at 38°45'N, 72°14'W. Particle type seems to be "Wet Snow."
2051	2-D probes are both in overload. Different types of particles.
2102	In uniform heavy cloud still. Ground speed 112 kt. Heading 225°.
2111	Plates, dendrites, needles. Light icing.
2112	At 10,000 ft, IAS 152 kt. 1-D tape ran out.
2114	Starting new 1-D tape.
2117	Smaller particles and rain.
2121	Back into wet snow. The rain area was small. Light rime.
2122	<u>End Pass #4</u> at 37°46'N, 72°57'W, heading 230°.
2125	Still IFR conditions in cloud, light turbulence, big particles.
2130	<u>Begin Pass #5</u> as aircraft climbs through 12,000 ft (3.7 km) IAS 154 kt. 37°55'N, 72°51'W, wind 240°/70 kt.
2132	Cloud tops near 15,000 ft. No large particles now.
2134	Between layers, but can barely tell. Go through occasional clouds.
2136	At 18,300 ft (5.6 km) and leveling off.
2138	Getting into light intensity cloud tops.
2140	Flight level 18,300 ft. In large snow regime. Heading 030°.
2143	In cloud. No structure visible.
2147	<u>End Pass #5</u> at 38°57'N, 72°05'W (near Tunna).
2149	Climbing. Still hazy. Thick Ci above. Ac tops were near 15,000 ft, with some reaching 18,000 ft.
2152	<u>Begin Pass #6</u> at 38°51'N, 72°06'W, heading 240°. At 22,000 ft (6.7 km) and climbing. Light intensity particles.
2154	Level at 23,600 ft (7.2 km). In solid cloud.
2159	Wind 246°/72 kt. Hdg 230°. IAS 150 kt, TAS 220 kt, IFR.
2202	At 23,600 ft. In solid cloud layer. The cloud during Pass #1 was not this low.
2205	Continue to have light rime. Wind 245°/60 kt.
2212	Still uniform cloud, light icing. Light turbulence.
2218	<u>End Pass #6</u> near 37°54'N, 72°51'W. FL 23,600 ft, heading 235°.
2326	Uniform cloud, thick above. Can't see below. Land at Langley AFB, Virginia.

## Appendix D

### List of Abbreviations

1. AFB - Air Force Base
2. AFGL - Air Force Geophysics Laboratory
3. AGL - Above ground level
4. ASSP - Axial Scattering Spectrometer Probe
5. AVE DEPT - Average departure of cloud probe data from an extension of slope line
6. °C - Degrees Celsius
7. C. O. D. - Coefficient of determination
8. DMSP - Defense Meteorological Satellite Program
9.  $D_o$  - Median volume diameter (of melted particle)
10. FF - Form factor
11. GT - Greater than
12. LE - Less than or equal to
13. LWC - Liquid water content (used synonymously with ice water content)
14.  $L_{MAX}$  - Maximum size of particles in spectra that number  $\geq 1 \text{ m}^{-3} \text{ mm}^{-1}$
15.  $\Lambda$  - Slope of particle spectra distribution ( $\text{mm}^{-1}$ )
16. MSL - Mean sea level
17. MU - Micrometers (used in data listings)
18. N - Number of particles ( $\text{m}^{-3}$ )
19.  $N_o$  - N-axis intercept of spectra straight-line slope
20. NT - Total number of particle  $\text{m}^{-3}$  in 50-5300  $\mu\text{m}$  range

- 21. P, C - Used in references to precipitation and cloud probe 2-D data
- 22. PMS - Particle Measuring Systems, Inc.
- 23. UMT - Universal Mean Time
- 24. Z - Used after numerals to indicate UMT
- 25. Z - Equivalent Reflectivity ( $\text{mm}^6 \text{m}^{-3}$ )
- 26.  $\mu\text{m}$  - Micrometer (=  $10^{-6}$  meter)
- 27. 1-D - 1-Dimensional PMS probe
- 28. 2-D - 2-Dimensional PMS probe

\*U.S. GOVERNMENT PRINTING OFFICE: 1980-600-039/14